

JCEEA

Czasopismo
Inżynierii Lądowej,
Środowiska
i Architektury

Journal of Civil
Engineering,
Environment
and Architecture

Kwartalnik
tom XXXV
zeszyt 65 (nr 1/2018)
styczeń-marzec

(e-ISSN 2300-8903)

Czasopismo Inżynierii Lądowej, Środowiska i Architektury jest kontynuacją
Zeszytów Naukowych Politechniki Rzeszowskiej - Budownictwo i Inżynieria Środowiska.

Issued with the consent of the Rector

Editor in Chief Publishing House of Rzeszow University of Technology
Professor Grzegorz OSTASZ, DSc, PhD

Scientific Council

prof. Hasan Arman (United Arab Emirates), prof. Zinoviy Blikharskyy (Ukraine)
prof. Antonio João Carvalho de Albuquerque (Portugal), prof. Marina Ciuna (Italy)
prof. Volodymyr V. Cherniuk (Ukraine), prof. Maurizio d'Amato (Italy)
prof. Endre Domokos (Węgry), prof. Mohamed Eid (Francja), prof. Maria Elektorowicz (Canada),
prof. Haritha Malladi (USA), prof. Samuel Hudson (USA), prof. Dušan Katunsky (Slovakia)
prof. Krzysztof Knapik (Poland), prof. Ryszard L. Kowalczyk (Australia)
prof. Jozef Kriš (Slovakia), prof. Vincent Kvočák (Slovakia), prof. Stanisław Kuś (Poland)
prof. Mladen Radujkovic (Croatia), prof. Czesława Rosik-Dulewska (Poland)
prof. Francesca Salvo (Italy), prof. João Antonio Saraiva Pires da Fonseca (Portugal)
prof. Marco Simonotti (Italy), prof. Nadežda Številová (Slovakia),
prof. Janusz A. Tomaszek (Polska), prof. David Valis (Czech Republic)
prof. António Avelino Batista Vieira (Portugal), prof. Oksana Vovk (Ukraine)
prof. Tomasz Winnicki (Poland), prof. Jerzy Ziółko (Poland)

Editorial Board

(affiliation: Poland)

Editor-in-Chief

Piotr KOSZELNIK, DSc, PhD, Eng., Professor

Editorial Committee (Thematic editors)

Bartosz MILLER, DSc, PhD, Eng., Professor

Professor Janusz RAK, DSc, PhD, Eng.

Statistical Editor

Szczepan WOLIŃSKI, DSc, PhD, Eng., Professor

Editorial Assistant

Katarzyna PIETRUCHA-URBANIK, PhD, Eng.

Members

Renata GRUCA-ROKOSZ, DSc, PhD, Eng., Professor;

Anna SIKORA, PhD, Arch, Eng.; Michał JUREK, PhD, Arch, Eng.;

Lucjan ŚLĘCZKA, DSc, PhD, Eng., Professor; Artur SZALACHA, MSc, Eng.

Language Editors

Barbara OLEKSIEWICZ, Msc

James RICHARDS, PhD – native English speaker (UK)

Volume Editor

Artur SZALACHA

e-ISSN 2300-8903

p-ISSN 2300-5130

The electronic version of the Journal is an original version.

Editorial Office: Rzeszow University of Technology, Faculty of Civil and Environmental Engineering
and Architecture, St. Poznańska, 35-084 Rzeszów, Poland, www.oficyna.prz.edu.pl/pl/zeszyty-naukowe/czasopismo-inzynierii-ladowej-s/ (e-mail: jceea_bud@prz.edu.pl)

Publisher: Publishing House of Rzeszow University of Technology, 12 Powstanców Warszawy Ave.,
35-959 Rzeszow, www.oficyna.prz.edu.pl (e-mail: oficyna@prz.edu.pl)

Additional information and an imprint – p. 177

SPIS TREŚCI

Peter CAUNER, Stanislav KMEŤ: Analysis of Cable Dome under Various Initial Conditions	5
Magdalena WARZYBOK, Jolanta WARCHOŁ: Synthesis of Kaolin-Based Zeolite Y and Its Application for Adsorption of Two Carbonyl Compound Gases.....	13
Volodymir KORNIICHUK, Mykola KHLAPUK, Olexander BEZUSYAK, Liubov YASINSKA: Sharp-Crested Weir Head Losses Investigation	27
Anna BOCHENEK, Katarzyna KLEMM: Evaluation of Thermal Comfort of the City's Public Spaces By the Use of Numerical Simulations ..	35
Zuzana VRANAYOVA, Daniela KAPOSZTASOVA, Zuzana POOROVA: Water Management of "Smart" Buildings and Cities	45
Maria MRÓWCZYŃSKA, Elżbieta GROCHOWSKA, Sławomir GIBOWSKI: Monitoring Vertical Displacements of an Engineering Object with Masonry Walls	53
Dominika KUŚNIERZ-KRUPA: Moret-Sur-Loing – Cultural Heritage, Its Value and Protection	63
Agata ZDYB, Piotr DRAGAN, Arkadiusz JAREMEK: The Analysis of the Solar Power Plant Performance in Temperate Climate	73
Jakub JURA, Małgorzata ULEWICZ: Impact of Glass and Ceramic Waste on Selected Properties of Materials with a Cement.....	81
Wojciech RADWAŃSKI, Tomasz PYTLOWANY, Izabela SKRZPCZAK: The Analysis of Road Building Technology with a Data Normalization Method	89
Tadeusz NOCH: The Use of a Heat Pump and Solar Energy in the Heat Demand	99
Piotr KONCA: The Effect of Pozzolans Addition on Cement Mortars.....	109

Marek JABŁOŃSKI, Iwona SZER, Jacek SZER: Risk Analysis on Scaffoldings Exposed to Noise.....	117
Alicja TAMA, Katarzyna ADAMEK, Karolina PARGIEŁA, Agnieszka OCHAŁEK, Artur KRAWCZYK, Michał LUPA: Monitoring of Historical Land Use Changes Caused by Underground Mining in Miedzianka Town, Based on a Webgis Tool and Insar Observations	127
Magdalena SEP, Anna SIKORA: The Validity of the BDOT10K Database on the Example of the Town of Tarnobrzeg.....	141
Karol KRUPA, Piotr GLEŃ: The Complex of St. Florian and St. Catherine Church in Gołęb as a Unique Example of Military Art of Lublin Voivodeship.....	151
Iveta BULLOVÁ: Analysis of the Air Flow in Selected Buildings.....	161
Irena ICKIEWICZ, Piotr KODA: The Influence of the Environment on Objects of Historical Value	167

Peter CAUNER¹
Stanislav KMEŤ²

ANALYSIS OF CABLE DOME UNDER VARIOUS INITIAL CONDITIONS

The paper focuses on the numerical analysis of Levy cable dome under two various initial conditions. Experimental device of cable dome is equipped with 7×7 wire ropes with diameter ϕ 6 mm. Nevertheless, it is completely changed for 1×19 wire ropes single strand with diameter ϕ 4 mm. The interchange could lead to creation of more adaptive structure for further static and dynamic analyses. Furthermore, it is essential to stress out that force gauges will improve accordingly.

Keywords: cable dome, active member, stiffness, tensegrity

1. Introduction

Cable domes have been employed as lightweight, large span roofs. Cable domes belong to hybrid tensegrity systems to a class of free-standing jointed structures where stability is provided by the self-stressed state in tensioned and compressed elements [1, 3]. The cable-strut structural system is statically and kinematically indeterminate. The initial pre-stress is a key factor for determining the shape and load carrying capacity. The stiffness of cable domes is determined by their states of prestress [1, 4, 5].

2. Model of cable dome

Laboratory of Excellent Research in Technical University of Košice is equipped with experimental device of Levy cable dome. The Levy cable dome is on Figure 1. Model of the cable dome consists of 7 compression members and 42 tension members. Nevertheless, one of the 7 struts is designed as an hydraulic actuator (active member – AM). Cable dome is created above circular plan with diameter 3,000 mm and it is fixed in 6 nodes. Geometry of the cable dome with individual sets of members is on Figure 2. Regarding the model of Levy cable

¹ Corresponding author: Peter Cauner, Technical University of Košice, Faculty of Civil Engineering, Institute of Structural Engineering, Vysokoškolská 4, Košice, 04200, Slovakia, peter.cauner@tuke.sk

² Stanislav Kmeť, stanislav.kmet@tuke.sk

dome, vertical struts are Set 6, active member is Set 7, diagonal cables are Set 3 and Set 4, ridge cables are Set 1 and Set 2 and hoop cables are Set 5. Load cylinder (LC), force gauges (FG) and construction details (CD) are on the Figure 1 [2, 3].

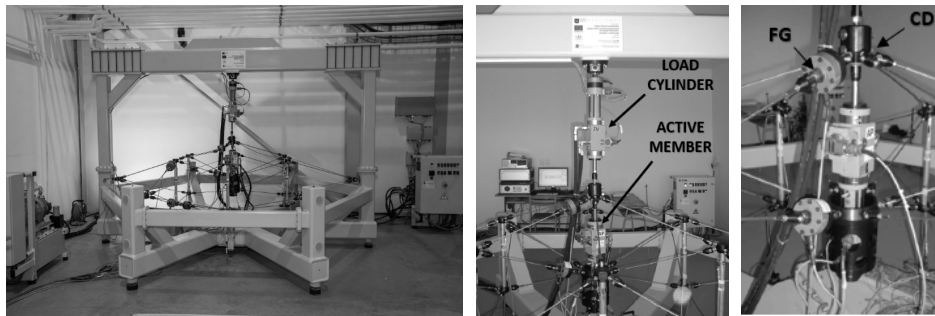


Fig. 1. Experimental device of Levy cable dome

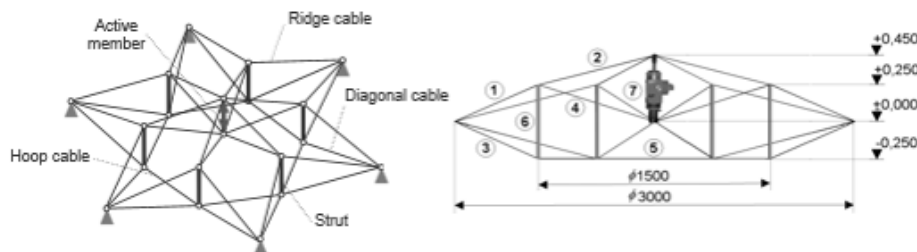


Fig. 2. Geometry of Levy cable dome

3. Analysis

The analysis was carried out with 7x7 wire ropes with diameter $\phi 6$ mm and 1x19 wire ropes single strand with diameter $\phi 4$ mm. The stiffness of cable domes is conditioned by their states of prestress.

3.1. Dynamic relaxation method

The cable domes belong to a class of truss structures that cannot attain a stable equilibrium configuration without introducing prestress to some members. The stable equilibrium state is achieved by form-finding. Whereas, the efficient method for achieve stable equilibrium state is dynamic relaxation method [2, 6]. At any time t the residual force R_{ix}^t in the x coordinate R_{ix}^t direction at node i , as the difference between external and internal forces in the corresponding direction, is expressed as:

$$R_{ix}^t = M_{ix} \dot{v}_{ix}^t + C_{ix} v_{ix}^t \quad (1)$$

where: M_{ix} – fictitious mass at node i in the x direction,

C_{ix} – viscous damping factor for node i in the x direction,

v_{ix}^t – velocity at time t in the x direction at node i ,

\dot{v}_{ix}^t – acceleration at time t in the x direction at node i .

Due to damping, nodal velocities and acceleration decay to zero as the solution is approached. The static equilibrium is thus attained and residual forces come to zero [3].

3.2. Initial pre-stress of the Levy cable dome

Equilibrium state is determined by geometry of the structure and value of prestress of its members. However, form-finding was carried out by dynamic relaxation method in order to achieve stable equilibrium state.

Table 1. Element properties

Element	Cross-section	E	Material	Tensile strength	Breaking load
Cable	φ 6 mm	120 GPa	7x(1+6)	1 770 MPa	24.72 kN
Cable	φ 4 mm	130 GPa	1x19	1 770 MPa	14.88 kN
Strut	φ 30/5 mm	210 GPa	S235	-	-

Table 2. Initial pre-stress

	φ 6 mm		φ 4 mm
Element	Initial prestress [N]	Member	Initial prestress [N]
Set 1	1 572.7	Set 1	1 579.9
Set 2	811.2	Set 2	816.5
Set 3	1 989.8	Set 3	1 993.5
Set 4	1 064.6	Set 4	1 067.8
Set 5	2 269.4	Set 5	2 273.6
Set 6	-989.6	Set 6	-992.3
Set 7	-1 378.8	Set 7	-1 386.0

Nevertheless, initial force 5 kN was applied to diagonal cables Set 3. Initial geometry has been approached after 4 approximations. The maximum nodal displacement (in cables ϕ 6 mm) is $-1.6 \cdot 10^{-3}$ mm and $-1.2 \cdot 10^{-3}$ mm (in cables ϕ 4 mm). Element properties and initial pre-stress forces are shown in the Table 1 and Table 2.

3.3. Static analysis with symmetric load

Numerical model contains symmetrical vertical load which is applied on the structure with various initial conditions. First model consists of cables with diameter ϕ 6 mm a next model contains cables with diameter ϕ 4 mm. Load is applied on the top of every vertical strut where cables and struts are connected. This symmetrical load is applied on the both cable domes. In the Figure 3 and Figure 4 are compared internal forces in every Set. Conversely maximum of nodal displacements of both structures are shown in the Figure 5. Nevertheless, maximal nodal displacement is in the bottom point of active member i.e. in the middle of span of Levy cable dome. The difference between internal forces is minimal although value of difference of nodal displacements is nearly 1.2 mm. Stiffness of structure with cables ϕ 4 mm is lower, moreover, added mass of construction details and force gauges is lower as well. Based on these conditions interchanges of cables could lead to creation of better prototype of Levy cable dome for further dynamic analyses and optimization process.

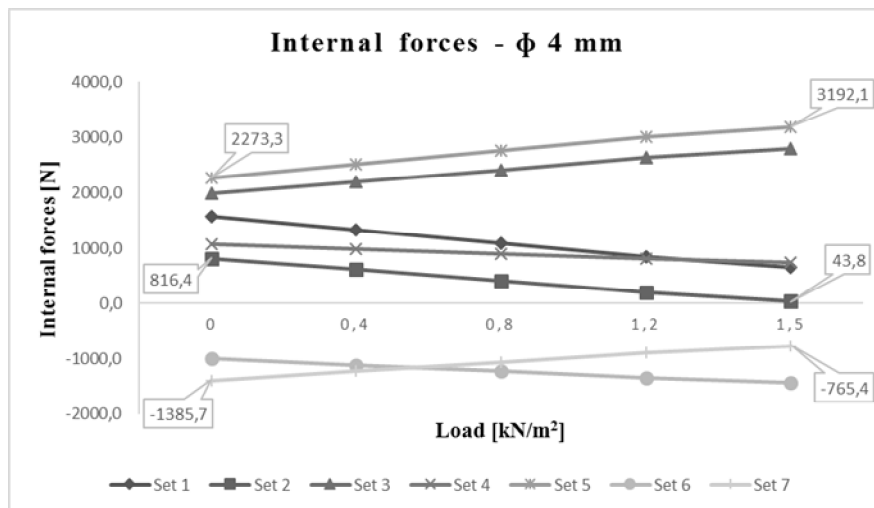


Fig. 3. Internal forces – ϕ 4 mm

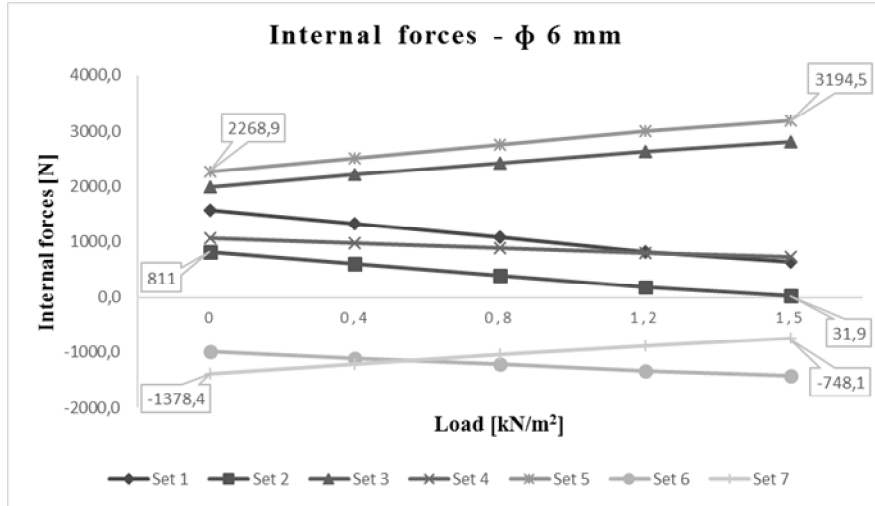


Fig. 4. Internal forces – φ 6 mm

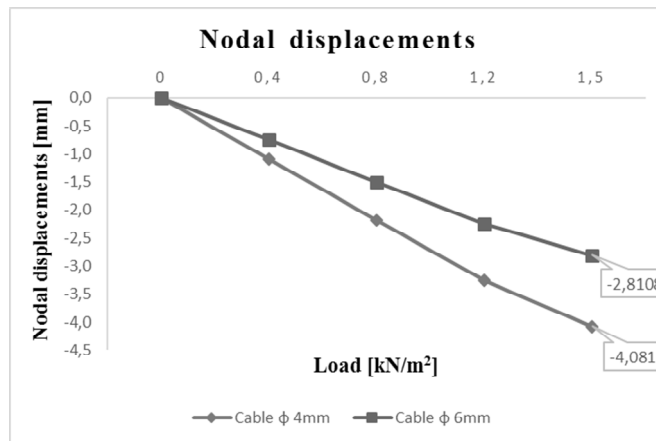
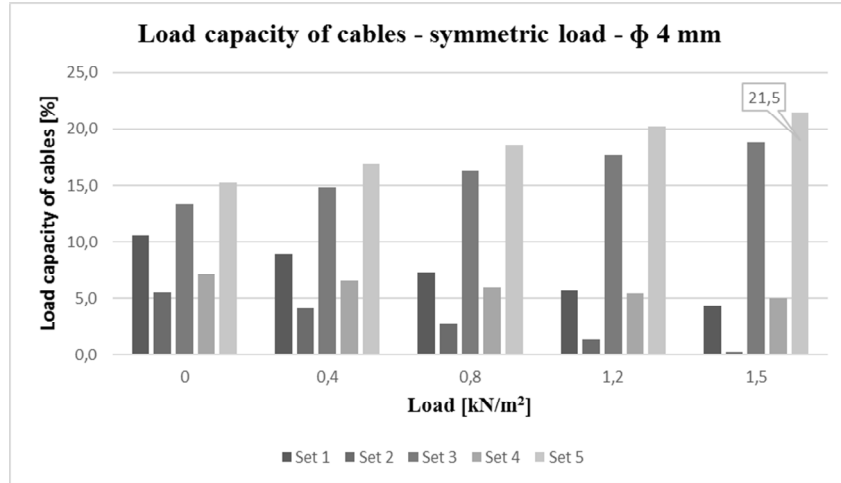
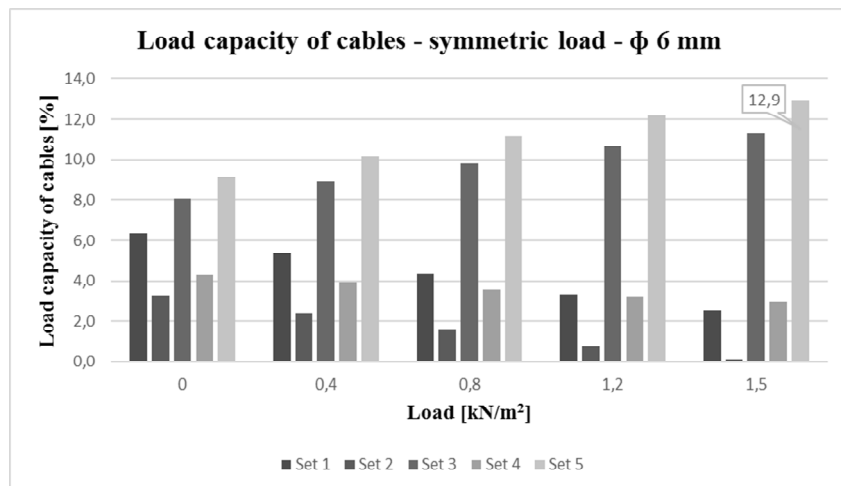


Fig. 5. Nodal displacements

Load capacity of cables is on the Figure 6 and Figure 7. Naturally, cables with diameter φ 4 mm are more efficient than cables with diameter φ 6 mm. The value of maximum load capacity is 21.5% when 1.5 kN/m² of vertical symmetric load is applied.

Fig. 6. Load capacity of cables – ϕ 4 mmFig. 7. Load capacity of cables – ϕ 6 mm

3.4. Active cable dome

Next analysis provides some other view on analysis of Levy cable dome focused on load capacity of cables. Adaptive cable dome is equipped with active member. Active member has ability to prolong its length about 100 mm. Levy cable dome was loaded by load cylinder. Load cylinder generate force to active member. Maximal force generated by load cylinder is 7 kN. Set 5 is most important group of cables which includes the maximal tensioned forces in the Levy cable dome. Load capacity of Set 5 cables with diameter ϕ 4mm is on the

Figure 8. Main axis contains force in load cylinder. Force in active member is on the Figure 9. Chain-dotted columns represent situation beyond limits. Force in load cylinder and active member cannot extend 7 kN (black chain-dotted) and axial forces in tensioned members cannot be lower than 0 kN (red chain-dotted - forces lower than 0 kN in group of cables Set 2). The value of load capacity of cables extended 41% in this type of analysis.

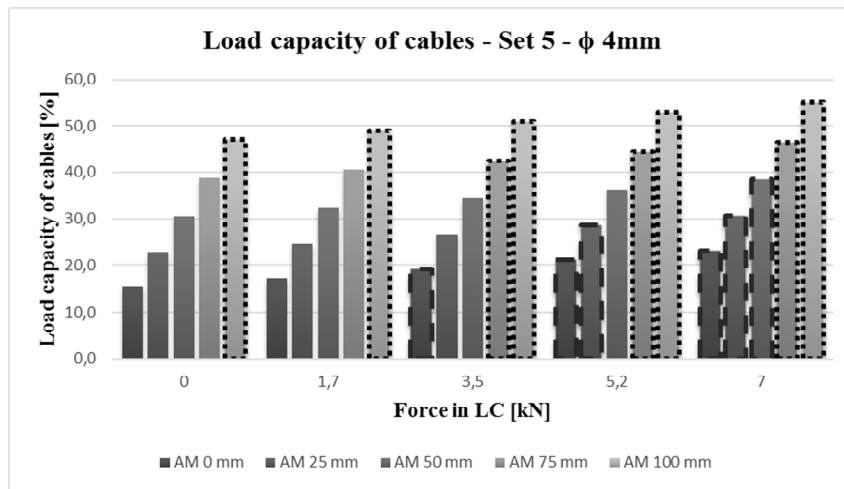


Fig. 8. Load capacity of cables – Set 5

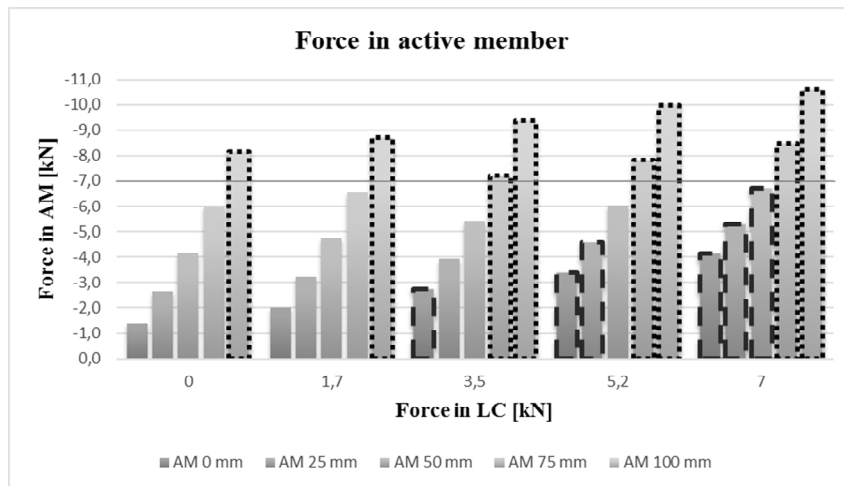


Fig. 9. Force in active member – φ 4 mm

4. Conclusion

Above is presented analysis of Levy cable dome under various initial conditions. Results lead to creation of better conditions for further static and dynamic analysis of cable dome. Cables with diameter ϕ 4 mm are more suitable than ϕ 6 mm. Given the above, load capacity of cables extended 41%. Added mass of construction details and associated force gauges is lower. It provides the improvement of dynamic properties of structure. Analyses were carried out by software Ansys – LS DYNA.

Acknowledgements: The paper is carried out within the project No. 1/0302/16, partially founded by the Science Grant Agency of the Ministry of Education of Slovak Republic and the Slovak Academy of Sciences. Paper is the result of the Project implementation: University Science Park TECHNICOM for Innovation Applications Supported by Knowledge Technology, ITMS: 26220220182, supported by the Research & Development Operational Programme funded by the ERDF.

References

- [1] Yuan, X. F., Chen, L. M., Dong, S. L.: Prestress design of cable domes with new forms. In: International Journal of Solids and Structures. Vol. 44, 2007, no. 9, p. 2773–2782.
- [2] Mojdis, M: Analysis of adaptive cable domes. PhD thesis, Technical University of Kosice, 2011, Slovakia (in Slovak).
- [3] Kmet, S., Mojdis, M. Time-dependent analysis of cable domes using a modified dynamic relaxation method and creep theory, Computers & Structures, Volume 125, September 2013, Pages 11–22, ISSN 0045-7949.
- [4] Kmet, S., Platko, P., Mojdis, M. Analysis of Adaptive Light-Weight Structures, Procedia Engineering, Volume 40, 2012, Pages 199–204, ISSN 1877-7058.
- [5] Motro, R. 2003. Tensegrity: Structural system of future. Published in Great Britain and the United States by Kogan Page Science, an imprint of Kogan Page Limited. ISBN 1-903996-37-6.
- [6] Ohsaki, M, Kanno, Y.: Form-finding of cable domes with specified stresses by using nonlinear programming, Kyoto University, Sakyo, Kyoto 606-8501, Japan. <http://www.se-lab.archi.kyoto-u.ac.jp/ohsaki/pdf/c0302.pdf>.

Przesłano do redakcji: 24.09.2017 r.

Przyjęto do druku: 31.03.2018 r.

Magdalena WARZYBOK¹
Jolanta WARCHOŁ²

SYNTHESIS OF KAOLIN-BASED ZEOLITE Y AND ITS APPLICATION FOR ADSORPTION OF TWO CARBONYL COMPOUND GASES

The aim of the study was to synthesize zeolite Y based on natural clay mineral and to determine its potential for adsorption of carbonyl compounds. The synthesis route consisted of four steps: thermal activation of kaolin into metakaolin; aging of reaction mixtures at ambient temperature; crystallization of the reaction mixture; washing and drying of the final product. The reaction mixture consisted of metakaolin silica gel (SiO₂), sodium chloride (NaCl) and sodium hydroxide (NaOH). All substrates were used at an intended molar ratio. The physicochemical properties of the synthesized adsorbent were attained through the advanced instrumental analysis. The adsorption of acetone and methyl ethyl ketone (MEK) on synthesized zeolite as well as on four commercially available adsorbents and three natural materials was examined in a dedicated home-made installation. The results showed, that the synthesized zeolite Y has the highest affinity for acetone over other adsorbents, while its affinity for MEK is only a little lower than AC. Additionally, adsorption isotherms of acetone and MEK on zeolite Y were measured on a gravimetric balance. Experimental binding isotherms were fitted by a non-linear regression to five empirical equations. In both acetone and MEK cases, the best results of statistical tests were obtained for the Marczewski-Jaroniec model.

Keywords: adsorption, acetone, methyl ethyl ketone, Y zeolites

1. Introduction

Carbonyl compounds are one of the most common volatile organics (VOCs) emitted by industrial processes into the atmosphere [19, 21]. Their primary emission sources are vehicle exhausts, industrial processes, cook stoves, household commodities and solvent evaporation. Other source of carbonyl compounds is

¹ Corresponding author: Magdalena Warzybok, Rzeszów University of Technology, Department of Water Purification and Protection, al. Powstańców Warszawy 6, 35-959 Rzeszów, Poland or Otto Engineering Polska Sp. z o. o., ul. Połonińska 15, 35-082 Rzeszów, Poland, 726-104-604, e-mail: magdalena.warzybok@ottoindustries.com.pl

² Jolanta Warchoła, Wrocław University of Science and Technology, Department of Chemical Technologies and Processes, Wybrzeże Wyspiańskiego 42, 50-370 Wrocław, Poland, 713203839, jolanta.warchol@pwr.edu.pl

photochemical oxidation of atmospheric hydrocarbons [13, 41]. Ketone group of VOCs are usually toxic or carcinogenic and their elimination, at a reasonable cost, is a serious challenge for many industrial processes [6, 35]. To meet the stringent regulations of pollutants emission two methods have been mainly investigated in industrial applications (95%): thermal and catalytic oxidation. Both processes are highly energy consuming and produce huge amount of combustion by-products (NO_x, CO₂). In the contrary adsorption based processes are considered as an effective and low-cost technique. Activated carbons (AC) are the most abundantly used adsorbents in industry mainly due to their high surface area and high adsorption capacity. However, the application of AC has some obstacles. AC is flammable, difficult to regenerate for high boiling point solvents, requires humidity control and promotes polymerization or oxidation of some solvents to toxic or insoluble compounds. One should also keep in mind that ACs has low affinity for polar organics.

Hydrophobic, thermo-stable zeolites are considered as an effective alternative to active carbons, essentially because they possess a large range of surface polarities [21, 28, 34]. Their first definitive synthesis was reported in 1948, when an analog of natural zeolite mineral, mordenite, was synthesized by R.M. Barrer [13]. A little later, Milton and Breck discovered a number of zeolites, types A, X and Y [40] which next, in 1954, the Union Carbide commercialized as a new class of industrial materials for separation and purification processes [22]. Currently more than 600 zeolites have been identified and more than 119 types of zeolitic structures have been cataloged by the Structure Committee of the International Zeolite Association [5, 37].

Faujasitic zeolite has gained immense popularity within the research community and in industry [3]. Its basic structural units are sodalite cages which form supercages and can accommodate spheres up to 1.2 nm in diameter [12]. The synthesis of faujasite is quite expensive if it is based on pure silica and alumina sources, i.e. colloidal silica and aluminium isopropoxide [2, 31] or water glass and sodium aluminate [26]. To reduce the production cost, it is possible to use for its synthesis a natural clay mineral [20, 30]. Among the clays, several investigators have studied the preparation of zeolite from kaolin and have been successful in the synthesis of zeolites [15]. Kaolin has unique properties and can be easily transformed into amorphous phase. The present study was therefore undertaken aiming at synthesis of zeolite Y from metakaolin. The obtained zeolitic product was characterized by some instrumental techniques and was applied for adsorption of acetone and methyl ethyl ketone (MEK) gases.

2. Experimental

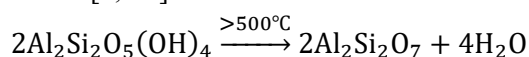
2.1. Reagents

NaOH was purchased from Polskie Odczynniki Chemiczne (analytical grade), NaCl and silica gel were supplied by Chempur (analytical grade). The starting material of kaolin was purchased from BioDrain, Poland. Two gaseous mixtures,

acetone in nitrogen and methylethylketone (MEK) in nitrogen, at a concentrations of 0.48 and 0.6 mg/m³ respectively, were supplied by AirLiquide.

2.2. Synthesis of the zeolite

The Y zeolite precursor (metakaolin) was obtained by thermal activation of kaolin at 800°C for 6h (muffle furnace SNOL 8:2/1000). During this process crystalline kaolin was converted to chemically reactive amorphous metakaolin according to the reaction [4, 36]:



Metakaolin was mixed with appropriate volume of NaOH (20%) solution and mass of SiO₂ to keep molar composition of the mixture as follow: SiO₂/Al₂O₃ = 10, Na₂O/SiO₂ = 1, H₂O/Na₂O = 20 [7]. Reaction mixture was aged at ambient temperature for 10 days and then kept in laboratory dryer (POLEKO SLW32 EKO) at 100°C for 24 h for crystallization [20]. After that, the mixture was washed with distilled water until pH was equal 7. Finally the sample was filtrated by laboratory filters and dried at 120°C for 2 h [38].

2.3. Characterization of the synthesized material

2.3.1. Chemical composition

The chemical composition was determined by Wavelength Dispersive X-Ray Fluorescence Spectroscopy (WDXRF), using the AxiosMAX PANalytical spectrometer. Measurements were made from the pellet (diameter of 32 mm) pressed from the ground, dried and homogenised material. Elemental analysis (measurement of average concentration of elements in the bulk phase) was made using a semi-quantitative method.

2.3.2. Phase composition

Zeolite sample was analyzed by X-ray powder diffraction (XRD) using an Empyrean PANalytical diffractometer with Cu K α radiation. The tube voltage was 40 kV and the current was 25 mA. The diffractograms were recorded in 0.0263° 2 θ . The diffraction data were analyzed by Rietveld method using HighScore Plus 3.0 software.

2.3.3. Specific surface area

The specific surface area, pore volume and pore size distribution of the synthesized zeolite were determined by N₂ adsorption/desorption at -196°C, on a Micromeritics ASAP 2420M instrument. Zeolite was outgassed at 200°C before analysis. The specific surface area was calculated using BET model (Brunauer-Emmett-Teller). The external surface area and micropore volume were determined

from t -plot analysis. The total volumes of mesopores and micropores were calculated from the amounts of N_2 adsorbed at $P/P_0=1$. The pore size distribution of the zeolite was calculated using the BJH method (Barrett-Joyner-Halenda).

2.3.4. Thermal analysis

TG, DTG and DTA analyses were done by using a Derivatograph-C (Paulik-Paulik & Erdey) thermal analyzer where the samples of about 10 mg in silica crucibles were heated starting from 20°C up to 1,200°C at a heating rate of 10°C min⁻¹ under an air atmosphere.

2.4. Adsorption study in home-made installation

The efficiency of acetone and MEK adsorption on synthesized zeolite Y as well as on other commercially available adsorbents was performed in dedicated home-made installation provided by the Otto Engineering Poland Sp. o.o. company, shown in Fig. 1 [27]. The adsorbent sample was at first dried in an oven at 473 K, weighted out (0.25 g) and located in the middle of the column (3) of 1 cm inner diameter. A thin layer of glass wool was placed at both ends of the bed to hold packing in a right position. Gas flow rate equal to 0.0001 m³/min at p 0.04 MPa and T 393 K were regulated by using a Defender flow controller (2) supplied by MassLabs. Nitrogen was used as a carrier gas for both carbon contaminants (CC). About 200 ppm of CC was passed through the column. Its concentration in the outlet of the column was monitored on-line by using gas chromatograph (Thermo Scientific 1300 TRACE GC) and recorded by a computer to obtain the breakthrough curves. The experiment ended when the outlet concentration equaled the inlet concentration.

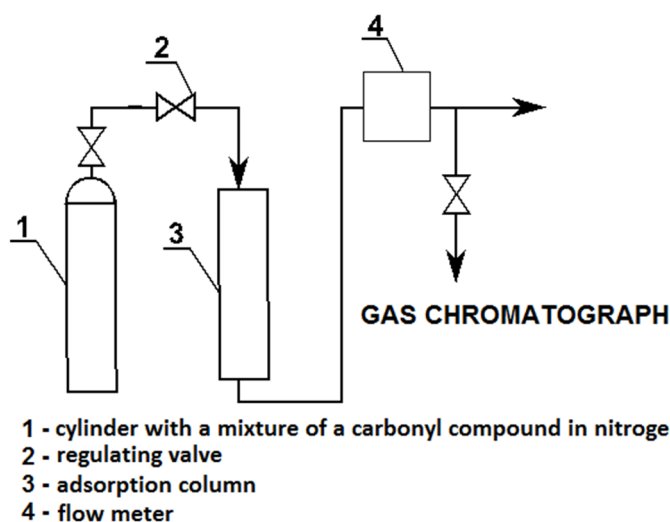


Fig. 1. Scheme of the installation for adsorption of acetone and MEK

The adsorption loading of gases was obtained by integration of the area behind the breakthrough curve. The amount of carbonyl compound adsorbed, q_e [mg/g] was calculated from Eq. (1). and Eq. (2).

$$m = \left[\frac{\max(\dot{m}_{i=0}; \dot{m}_n) - (\dot{m}_i + \dot{m}_{i+1})}{2} \right] \cdot (t_{i+1} - t_i) \quad (1)$$

$$q_e = \frac{\sum_{i=0}^n m}{m_{zeolite}} \quad (2)$$

where: $\dot{m}_{i=0}$, \dot{m}_n , \dot{m}_i , \dot{m}_{i+1} is the mass flow rate of CC in the outlet stream, respectively, at the time $t=0$, $t=n$, $t=i$, $t=i+1$ [mg/min]; t_i , t_{i+1} – is the duration of the adsorption process; and $m_{zeolite}$ is the mass of zeolite packed in column.

2.5. Determination of adsorption isotherms

The adsorption isotherms of acetone and MEK on zeolite Y were estimated on an IGA-002 gravimetric instrument (Hiden-Isochema) at 293°C and pressure up to 0.902 atm. The apparatus possesses an ultra-high vacuum system and can accurately control the subtle weight changes of the samples by changing the pressure [40]. Prior to the measurements, the sample of approximately 75 mg of zeolite was degassed in high vacuum (10^{-6} Pa) at 180°C by 2 hours to remove the excess water and impurities adsorbed in the pores. During adsorption measurements, the pressure was altered with the set pressure points and the mass uptake was measured in real time using the Real Time Processor (RTP).

The determined isotherms were examined by fitting the experimental data to the following isotherms models:

Langmuir:
$$q_e = \frac{q_m \cdot K \cdot (C_e)}{1 + K \cdot (C_e)} \quad (3)$$

Freundlich:
$$q_e = K \cdot (C_e)^{\frac{1}{n}} \quad (4)$$

Dubinin-Radushkevich:
$$q_e = 10^{\log_{10} q - n \cdot \log_{10} [K \cdot (C_e)]^2} \quad (5)$$

Aranovich and Donohue:
$$q_e = \frac{q_m \cdot K \cdot (C_e)^n}{(1 + K) \cdot [1 - (C_e)]^n} \quad (6)$$

Marczewski-Jaroniec:
$$q_e = \frac{q_m \cdot [K \cdot (C_e)]^m}{1 + [K \cdot (C_e)]^n} \quad (7)$$

where: q_e [mmol/g] is the solid phase adsorption quantity of carbonyl compound (acetone or MEK) at equilibrium; q_m [mmol/g] is the carbonyl compound

adsorption capacity; K is the isotherm constant; n is the empirical constant; C_e is the equilibrium concentration in the gaseous phase.

The parameters of isotherm models were calculated by nonlinear regression based on the Levenberg-Marquardt algorithm. The accuracy of determination of the model's parameters was assessed for the 95% confidence interval of Student's test. The following statistical criteria were used for the assessment of the proposed model accuracy:

$$\text{The Fisher test: } TF = \frac{(n-l) \sum_{i=1}^n \left(q_{e,i} - \frac{1}{n} \sum_{i=1}^n q_{e,i} \right)^2}{(n-1) \sum_{i=1}^n (q_{e,i} - q_{cal,i})^2} \quad (8)$$

$$\text{Approximation of the standard deviation: } \sigma = \sqrt{\frac{\sum_{i=1}^n (q_{e,i} - q_{cal,i})^2}{n-l}} \quad (9)$$

$$\text{Mean error: } ME(\%) = \frac{1}{n} \sum_{i=1}^n \left| \frac{q_{cal,i} \cdot 100}{q_{e,i}} - 100 \right| \quad (10)$$

where: $q_{e,i}$ and $q_{cal,i}$ are designated and calculated solid phase adsorption quantities at equilibrium, respectively; n is a number of experimental points, l is a number of estimated parameters.

3. Results and discussion

3.1. Chemical and structural properties of the synthesized materials

Chemical composition of the starting material, kaolin, and the synthesized zeolite Y are shown in Table 1. The content (%) of SiO_2 in both zeolite Y and kaolin, is almost equal while the content of Al_2O_3 is approximately 10% bigger in kaolin. Consequently, the zeolite has higher $\text{SiO}_2/\text{Al}_2\text{O}_3$ ratio. The zeolite contains sodium, which is not found in the substrate. The content (%) of other marked components increased (Fe_2O_3 , TiO_2 and K_2O) or decreased (CaO and MgO) slightly.

Table 1. Chemical characterization of the zeolite (mass%)

Component		SiO_2	Al_2O_3	Fe_2O_3	CaO	MgO	K_2O	Na_2O	$\text{SiO}_2/\text{Al}_2\text{O}_3$
Content [%]	Kaolin	52.5	34.5	0.8	0.1	0.1	0.6	0.0	2.57
	Zeolite	52.2	23.9	0.51	0.24	0.14	0.33	12.8	3.80

The results of XRDP analysis together with the results of the fitting operation of the phase with diffraction database ICDD PDF4+, of the synthesized zeolite are depicted in Table 2 and Fig. 2, respectively. The data presented reveal that the

main product of the synthesis is faujasite (77%) and the minor by-products are unreacted quartz (10%) and zeolite P (12%).

Depending on the $\text{SiO}_2/\text{Al}_2\text{O}_3$ molar ratio, faujasites can be considered as a zeolites X if $\text{SiO}_2/\text{Al}_2\text{O}_3 = 2-3$ or zeolite Y if $\text{SiO}_2/\text{Al}_2\text{O}_3 > 3$ [10]. The obtained molar ratio of $\text{SiO}_2/\text{Al}_2\text{O}_3$ is 3.80 (Tab. 1), thus the final product is zeolite Y. It is worth to emphasized that zeolite Y, in opposite to zeolite X, can have hydrophobic properties, because zeolites are hydrophobic when molar ratio $\text{SiO}_2/\text{Al}_2\text{O}_3$ is bigger then 20 [18].

Table 2. Phase characterization of the zeolite (mass %)

Chemical formula	Substance	Mineral	Standard deviation
$\text{Na}_{1.84}\text{Al}_2\text{Si}_4\text{O}_{11.92} \cdot 7\text{H}_2\text{O}$	Sodium Aluminium Silicate Hydrate	Faujasite	$77 \pm 3\%$
SiO_2	Silicon Oxide	Quartz	$10 \pm 1\%$
$\text{Na}_4\text{Al}_4\text{Si}_{12}\text{O}_{32}(\text{H}_2\text{O})_{14}$	Sodium Aluminium Silicate Hydrate	-	$12 \pm 2\%$

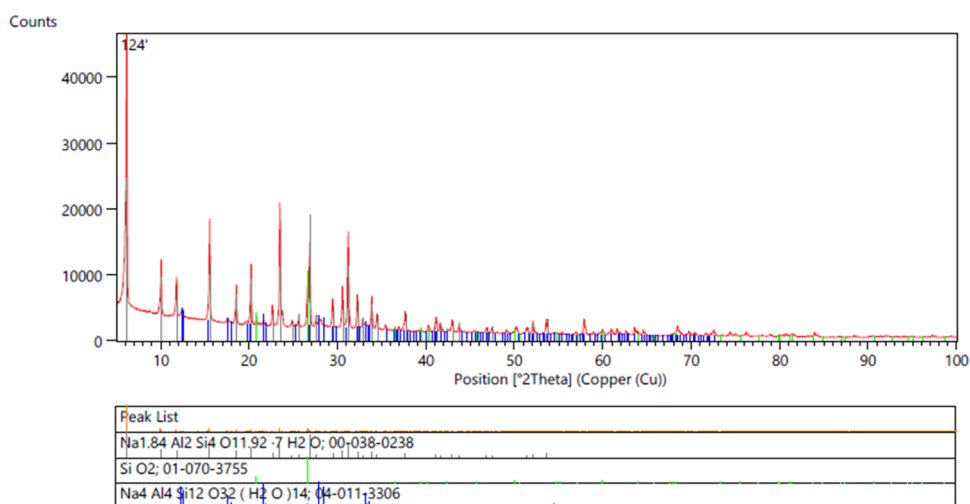


Fig. 2. Diffractogram of zeolite along with the alignment results against the diffraction ICDD PDF4+ database

3.2. Thermal analysis

Thermal analysis of the obtained zeolite, presented in Fig. 3A, reveals a little more than 10% loss of weight associated with the dehydration of the zeolite sample during heating from room temperature up to 200°C. It is worth to mention that a maximum temperature of 200°C is used for desorption of pollutants under real conditions. Further loss of weight observed in the range 400–700°C corresponds to the dehydroxylation of the structural -OH groups [2, 14]. The results of DTA analysis (Fig. 3B) identified the presence of

endothermic peak having maximum effect at temperature 200°C (due to the loss of adsorbed water), and exothermic peak at 900°C indicating recrystallization of zeolite.

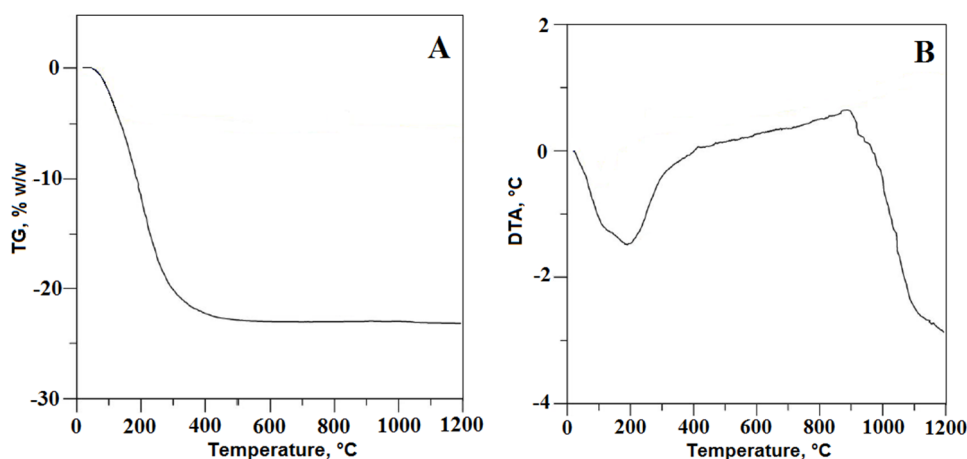


Fig. 3. (A) TG and (B) DTA curves of the zeolite Y

3.3. Textural properties analysis

The estimated specific surface areas (BET areas), pore volume and diameter of the zeolite sample are depicted in Table 3. Additionally, N₂ adsorption-desorption isotherm of the zeolite is shown in Fig. 4. At $P/P_0 = 0.8$, the sample shows substantial increase of nitrogen adsorption. The zeolite Y exhibited type IV isotherms, which is characteristic for mesoporous materials with H-IV hysteresis loops [17, 33]. This type of loop is usually attributed to the slip-shaped pores [24]. As shown in Fig. 4, the pore size distribution of zeolite exhibits a bimodal distribution; two peaks appear at ca. 2 and 90 nm., which indicates the presence of meso- and microporous structure. Thus, no molecular sieve effect affects adsorption of acetone (4.3 Å) and MEK (5.2 Å).

Table 3. Textural parameters of the zeolite

Surface area (m ² /g)			Pore volume (cm ³ /g)		D _{mean} ^b (nm)
S _{BET}	S _{micro} ^a	S _{ext} ^a	V _{total}	V _{micro} ^a	
685,85	590,59	35,26	0,30	0,26	1,76

^a Calculated from *t*-plot curve

^b Adsorption average pore width (4V/A by BET)

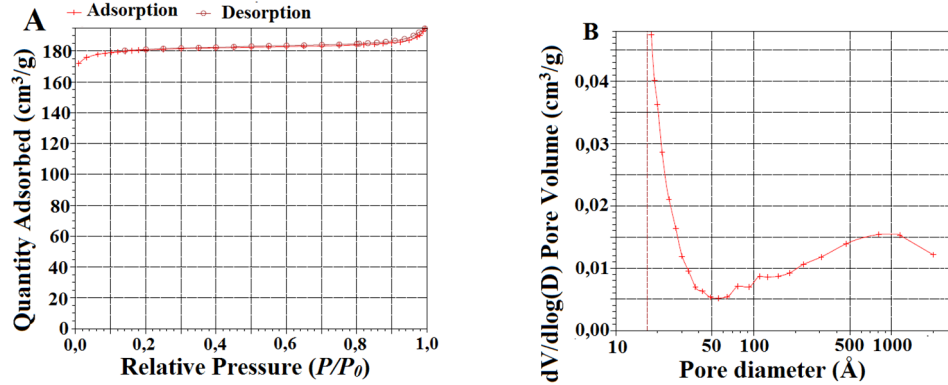


Fig. 4. (A) N₂ adsorption-desorption isotherm and (B) Pore size distribution of the zeolite

3.4. Adsorption isotherms

The adsorption isotherms of acetone and MEK are given in Figs. 5 and 6, respectively. Both depicted isotherms have long horizontal plateau, which extends up to relatively high P/P_0 ratio. This characteristic shape of the isotherms allows for their allocation to the type-I of the IUPAC classification [32]. Type I of isotherm proves microporosity of the zeolite and suggests micropole filling mechanism of adsorption [42]. It is partially confirmed by the best approximation of the value of maximum adsorption capacity ($q_{m,exp}$) obtained for the Dubinin-Radushkevich model (Table 4). Slightly worse approximation of $q_{m,exp}$ was obtained for the Langmuir model but with a better result of statistical tests. Nevertheless, in both acetone and MEK cases, the best results of statistical tests were obtained for the Marczewski-Jaroniec model. It probably results from the biggest number ($p = 4$) of estimated parameters.

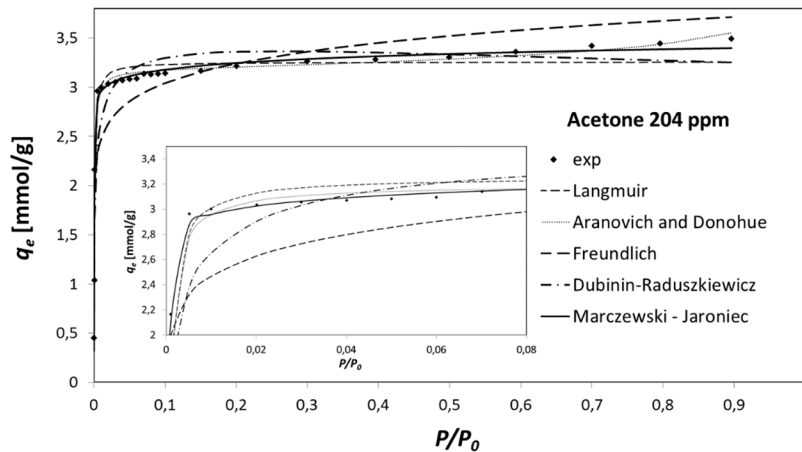


Fig. 5. Comparison of models prediction and experimental data obtained for acetone adsorption on zeolite

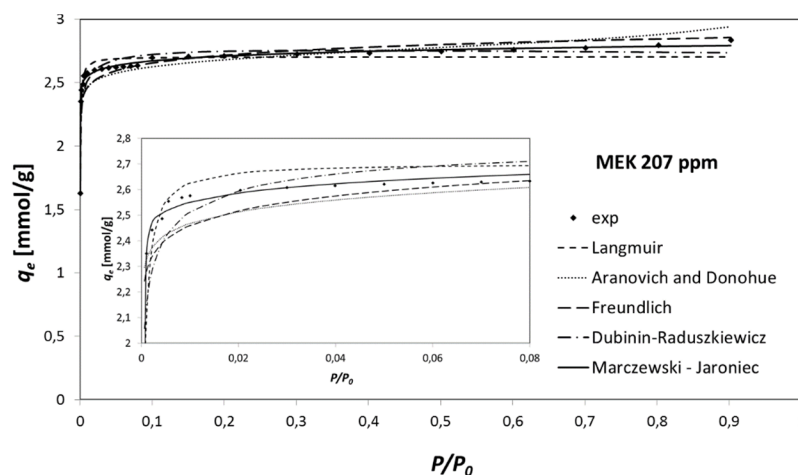


Fig. 6. Comparison of models prediction and experimental data obtained for MEK adsorption on zeolite

Table 4. Models parameters and statistical tests results for acetone and MEK adsorption on zeolite Y

Model	Parameters				Statistical tests		
	K	q_m [mmol/g]	N	m	TF	ME	σ
acetone $q_{m,exp}=3.50$ (mmol/g)							
Langmuir	1 207	3.257	-	-	21.52	7.001	0.160
Freundlich	3.751	-	10.99	-	2.949	22.59	0.432
Dubinin-Radushkevich	3.832	3.366	0.052	-	7.031	13.01	0.280
Aranovich Donohue	1 295	3.182	0.049	-	31.53	5.806	0.132
Marczewski-Jaroniec	1 691	2.720	2.181	2.212	144.1	2.860	0.062
MEK $q_{m,exp}=2.83$ (mmol/g)							
Langmuir	3 336	2.704	-	-	6.807	2.720	0.091
Freundlich	2.865	-	30.16	-	2.549	3.598	0.148
Dubinin-Radushkevich	2.840	2.754	0.018	-	3.623	3.380	0.124
Aranovich Donohue	9 174	2.778	0.026	-	2.122	3.888	0.162
Marczewski-Jaroniec	1 864	2.405	5.038	5.058	128.9	0.590	0.021

The comparison of the efficiency of acetone and MEK adsorption onto: synthesized zeolite Y, four commercial adsorbents (X13 India, AC Desotec, AC Norit and zeolite ZSM-5) and three natural clay minerals (montmorillonite, bentonite, haloizyte) are shown in Fig. 7. The ZSM-5 based zeolite is widely used as adsorbent in zeolite concentrators (temperature swing adsorbers) for continuous VOCs adsorption and desorption [8]. 13X zeolite has been studied to

adsorb various VOCs with pressure swing adsorption (PSA) [11, 39]. Natural minerals are cost-effective alternative adsorbents to widely used ACs [9, 29]. As can be seen, the synthesized zeolite Y has the highest affinity for acetone over other adsorbents, while its affinity for MEK is only a little lower than AC. Both organics have similar polarity (acetone 2.76 D, MEK 2.78 D), thus the observed difference in their adsorption can stem from different molar volume of both molecules (acetone 70.4 cm³/mol, MEK 90.1 cm³/mol at 25°C [23]).

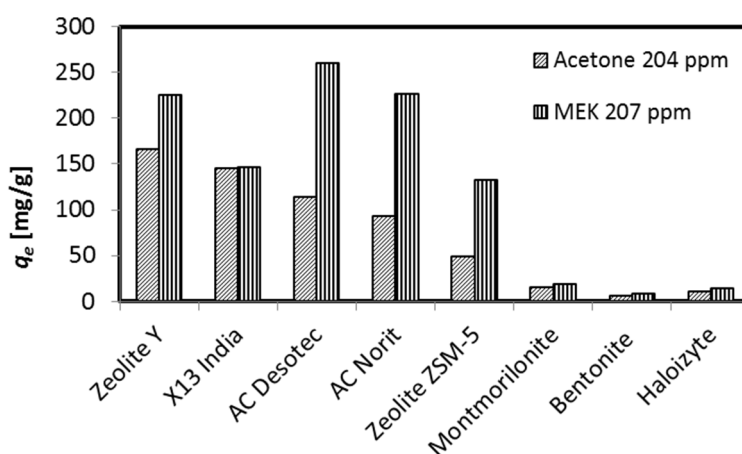


Fig. 7. Comparison of acetone and MEK adsorption efficiency of different adsorbents

4. Conclusions

The use of kaolin as an aluminum and silica source for the synthesis of Y-type zeolite allows obtaining an effective adsorbent of polar organics. The relatively big dimension of the aperture of the zeolite channels can favor the entrance of the small organics molecules. Thus, their adsorption can follow a micropore filling what was further confirm by characteristic shape of isotherm curves and by the results of model calculations. The determined adsorption capacity of the two tested carbonyl compounds reached about 170 mg_{acetone}/g and about 225 mg_{MEK}/g.

Despite the fact that the synthesized zeolite Y has relatively low specific surface area (380–750 m²/g) in comparison to ACs (800–1,500 m²/g), its affinity for polar acetone is higher than any other commercially available adsorbent. Furthermore, its high thermal stability up to 200°C allows safety thermal regeneration and zeolite reuse. Thus, the synthesized zeolite Y comprises attractive and competitive solution for cleaning of wasted gases towards commercially available adsorbents.

References

- [1] Adeoye J. B., Omoleye J. A., Ojewumi M. E., Babalola R.: Synthesis of Zeolite Y from Kaolin Using Novel Method of Dealumination, *International Journal of Applied Engineering Research*, 5/12, 2017, 755–760.
- [2] Ahmedzeki N.S., Yilmaz S., Al-Tabbakh B.A.: Synthesis and Characterization of Nanocrystalline Zeolite Y, *Al-Khwarizmi Engineering Journal*, 1/12, 2016, 79–89.
- [3] Alaba P.A., Sani Y.M., Daud W.M.A.W.: Synthesis and characterization of hierarchical nanoporous HY zeolites from acid-activated kaolin, *Chinese Journal of Catalysis*, 36, 2015, 1846–1851.
- [4] Ayele L., Perez-Pariente J., Chebude Y., Diaz I.: Synthesis of zeolite A from Ethiopian kaolin, *Microporous and Mesoporous Materials*, 215, 2015, 29–36.
- [5] Bortolatto L.B., Boca Santa R.A.A., Moreira J.C., Machado D.B., Martins M.A.P.M., Fiori M.A., Kuhnen N.C., Riella H.G.: Synthesis and characterization of Y zeolites from alternative silicon and aluminium sources, *Microporous and Mesoporous Materials*, 248, 2017, 214–221.
- [6] Bradberry S.: Acetone, *Medicine*, 3/44, 2016, 127.
- [7] Chandrasekhar S., Pramada P.N.: Kaolin-based zeolite Y, a precursor for cordierite ceramics, *Applied Clay Science*, 27, 2004, 187–198.
- [8] Chang F.T., Lin Y.C., Bai H.L., Pei B.S.: Adsorption and desorption characteristic of semiconductor volatile organic compounds on the thermal swing honeycomb zeolite concentrator, *Journal of Air & Waste Management Association*, 53, 2003, 1384–1390.
- [9] Dobre T., Parvulescu O.C., Iavorschi G., Stroescu M., Stoica A.: EXPERIMENTAL STUDY OF VOCs ADSORPTION ONTO FIXED BED ACTIVATED CARBON, *Analele Universităţii din Oradea Fascicula: Ecotoxicologie, Zootehnie si Tehnologii de Industrie Alimentară*, 2010, 1241 – 1246.
- [10] Falth L., Hakansson U., Hansen S.: Structure of synthetic zeolite Na-P2, *Acta Crystallographica Section C: Crystal Structure Communications*, 46, 1990, 1361–1362.
- [11] Gangil S., Mewar Ch., Jha R., Kumar J., Malviya L., Modhera B.: Performance of 13X Zeolite for Volatile Organic Compound Adsorption by Pressure Swing Adsorption, *Int. Conf. on Advances in Chemical Engineering and Technology, ICACE TKMCE*, 2014, 41–44.
- [12] Garcia G., Cardenas E., Cabrera S., Hedlund J., Mouzon J.: Synthesis of zeolite Y from diatomite as silica source, *Microporous and Mesoporous Materials*, 219, 2016, 29–37.
- [13] Hellen H., Hakola H., Reissell A., Ruuskanen T.M.: Corbonyl compounds in boreal coniferous forest air in Hyytiala, Southern Finland, *Atmospheric Chemistry and Physics*, 4, 2004, 1771–1780.
- [14] Hilal G.: Liquid Phase Hydrogenation of Citral on Zeolite Supported Monometallic (Ni,Pt) and Bimetallic (Ni, Sn), (Pt-Sn) Catalysts, *MSc Thesis, Izmir Institute of Technology*, 2005.
- [15] Hildebrando E.A., Bastos Andrade Ch.G., Ferreira da Rocha Junior C.A., Angélica R.S., Valenzuela-Diaz F.R., de Freitas Neves R.: Synthesis and Characterization of Zeolite NaP Using Kaolin Waste as a Source of Silicon and Aluminum, *Materials Research*, 17(1), 2014, 174–179.

- [16] Htay M.M., Oo M.M.: Preparation of Zeolite Y Catalyst for Petroleum Cracking. *World Academy of Science, Engineering and Technology*, 48, 2008, 114–120.
- [17] Huang W.L., Liu B.J., Sun F.M., Zhang Z.H., Bao X.J.: Synthesis and characterization of thermally stable MCM-41/ γ -Al₂O₃ composite materials, *Microporous and Mesoporous Materials*, 94, 2006, 254.
- [18] Jha B., Singh D.N.: Fly Ash Zeolites, *Advanced Structured Materials*, 78, 2015, 5–31.
- [19] Jiang Ch., Li S., Zhang P., Wang J.: Pollution level and seasonal variations of carbonyl compounds, aromatic hydrocarbons and TVOC in a furniture mall in Beijing, China, *Building and Environment*, 69, 2013, 227–232.
- [20] Kazemimoghdam M., Mohammadi T.: Preparation of nano pore hydroxysodalite zeolite membranes using of kaolin clay and chemical sources, *Desalination*, 278, 2011, 438–442.
- [21] Khan F.I., Ghoshal A.Kr.: Removal of Volatile Organic Compounds from polluted air, *Journal of Loss Prevention in the Process Industries*, 13, 2000, 527–545.
- [22] Kulprathipanja S., Flanigen E.M., Broach R.W., Wilson S.T.: *Zeolites in Industrial Separation and Catalysis*, Chapter 1. Introduction. Wiley-VCH Verlag GmbH & Co. KGaA, 2010, 1–26.
- [23] Mark J.E.: *Physical Properties of Polymers Handbook: Edition*, Springer Science & Business Media, Berlin, 2007, 296–298.
- [24] Meng Q., Liu B., Piao J., Liu Q.: Synthesis of the composite material Y/ASA and its catalytic performance for the cracking of n-decane. *Journal of Catalysis*, 290, 2012, 55–64.
- [25] Omoleye J. A., Hymore F.K., Babalola R., Adefila S. S., Ajayi O.A.: Comparative Analysis of Zeolite Y From Nigerian Clay and Standard Grade. *International Conference on African Development Issues (CU-ICADI) 2015: Materials Technology Track*, 2015, 179–182.
- [26] Penkaj S., Su-Jung J., Moon-Hee H., Churl-Hee Ch.: Influence of the silica precursors on octahedron shaped nano NaY zeolite crystal synthesis, *Journal of the Taiwan Institute of Chemical Engineers*, 000, 2015, 1–7.
- [27] Pliś I., Prokop W., Petrus R., Warchoł J.: Sorption of acetone onto clay materials, *12 Scientific Conference POL-EMIS, Karpacz 4-7 June 2014*.
- [28] Qi J., Li J., Li Y., Fang X., Sun X., Shen J., Han W., Wang L.: Synthesis of porous carbon beds with controllable pore structure for volatile organic compounds removal, *Chemical Engineering Journal*, 307, 2017, 989–998.
- [29] Qiu W., Dou K., Zhou Y., Huang H., Chen Y., Lu H.: Accepted Manuscript. Hierarchical pore structure of activated carbon fabricated by CO₂/microwave for VOCs adsorption, *Chinese Journal of Chemical Engineering*, 2017.
- [30] San Cristobal A.G., Castello R., Martin Luengo M.A., Vizcayno C.: Zeolites prepared from calcined and mechanically modified kaolins. A comparative study, *Applied Clay Science*, 49, 2010, 239–246.
- [31] Sang S., Liu Z., Tian P., Liu Z., Qu L., Zhang Y.: Synthesis of small crystals zeolite NaY, *Material Letters*, 60, 2006, 1131–1133.
- [32] Sing K.S.W., Everett D.H., Haul R.A.W., Moscou L., Pierotti R.A., Rouquerol J., Siemieniewska T.: Reporting Physisorption Data for Gas/Solid Systems with Special Reference to the Determination of Surface Area and Porosity, *Pure and Applied Chemistry*, Vol. 57, No. 4, 1985, 603–619.

- [33] Tan Q.F., Bao X.J., Song T.C., Fan Y., Shi G., Shen B.J., Liu C.H., Gao X.H.: Synthesis, characterization, and *catalytic* properties of hydrothermally stable macro-meso-micro-porous composite materials synthesized via in situ assembly of preformed zeolite *Y* nanoclusters on kaolin, *Journal of Catalysis*, 251, 2007, 69.
- [34] Tang L., Li L., Chen R., Wang Ch., Ma W., Ma X.: Adsorption of acetone and isopropanol on organic acid modified activated carbons, *Journal of Environmental Chemical Engineering*, 4, 2016, 2045–2051.
- [35] Tittarelli F., Giosue C., Mobili A., Ruello M.L.: Influence of binders and aggregates on VOCs adsorption and moisture buffering activity of mortars for indoor applications, *Cement and Concrete Composites*, 57, 2015, 75–83.
- [36] Ugal J.R., Hassan K.H., Ali I.H.: Preparation of type 4A zeolite from Iraqi kaolin: Characterization and properties measurements, *Journal of the Association of Arab Universities for Basic and Applied Sciences*, 9, 2010, 2–5.
- [37] United States Environmental Agency, Office of Air Quality, Technical bulletin, Zeolite a versatile air pollutant adsorber, 1998, <http://www.epa.gov/ttn/catc>.
- [38] Warzybok M., Chverenchuk A., Warchoł J.: Acetone adsorption on synthesized zeolite from natural clay material, *Czasopismo Inżynierii Łądowej, Środowiska i Architektury – Journal of Civil Engineering, Environment and Architecture, JCEEA*, z. 62, t. XXXII (3/I/15), 2015, 487–495, DOI:10.7862/rb.2015.132.
- [39] White D.H.: Compressed Air and Gas Purification and Fractionation for High Purity Applications by Improved PSA Processes, *Separation Science and Technology*, 43, 2008, 2298–2306.
- [40] Yuan W., Yuan P., Liu D., Deng L., Zhou J., Yu W., Chen F.: A hierarchically porous diatomite/silicalite-1 composite for benzene adsorption/desorption fabricated a facile pre-modification in situ synthesis route, *Chemical Engineering Journal*, 294, 2016, 333–342.
- [41] Zhang M., An T., Fu J., Sheng G., Wang X., Hu X., Ding X.: Photocatalytic degradation of mixed gaseous carbonyl compounds at low level on adsorptive TiO₂/SiO₂ photocatalyst using a fluidized bed reactor, *Chemosphere*, 64, 2006, 423–431.
- [42] Zhang P.: Adsorption and Desorption Isotherms, KE Group, 2016.

Przesłano do redakcji: 10.03.2018 r.

Przyjęto do druku: 31.03.2018 r.

Volodymir KORNIICHUK¹
Mykola KHLAPUK²
Olexander BEZUSYAK³
Liubov YASINSKA⁴

SHARP-CRESTED WEIR HEAD LOSSES INVESTIGATION

The work is devoted to the rectangular sharp-crested weir calculation methods improvement. This can be realized by using mathematical model developed on energy and momentum conservation principles. In order to get energy conservation equation within sharp-crested weir we have to know weir head losses. This article presents theoretical and experimental investigations of the sharp-crested weir head losses. The height of the weir plate p_w and weir head H are estimated as main operating factors that determine hydraulic weir outbound parameters: threshold depth h and the specific weir flow q . The flow moving over sharp-crested weir suffers sudden vertical contraction and transforms from the uniform flow to a jet. Mentioned above, causes sharp-crested weir head losses. To determine these losses, we propose to use Hind's formula that describes similar contraction losses in the channel. Experimental investigations proved Hind's formula application adequacy to evaluate these losses. Sharp-crested weir energy conservation equation that includes head losses is determined. Graphs set out in the article disclose the influence of the main operating factors and their ratio on the relative head losses.

Keywords: flow energy, total head, head losses, nappe, jet flow

¹ Corresponding author: Volodymir Korniiichuk, National University of Water and Environmental Engineering, Department of Hydraulic Engineering and Hydraulics, Soborna 11, 33028 Rivne, Ukraine, phone: 38 068 568 4430, v.i.korniichuk@nuwm.edu.ua

² Mykola Khlapak, NUWEE, Department of Hydraulic Engineering and Hydraulics, Soborna 11, 33028 Rivne, Ukraine, phone: 38 067 362 1115, m.m.khlapak@nuwm.edu.ua

³ Olexander Bezusyak, NUWEE, Department of Hydraulic Engineering and Hydraulics, Soborna 11, 33028 Rivne, Ukraine, phone: 38 097 483 3863, o.v.bezusyak@nuwm.edu.ua

⁴ Liubov Yasinska, NUWEE, Department of Hydraulic Engineering and Hydraulics, Soborna 11, 33028 Rivne, Ukraine, phone: 38 096 737 3627, l.r.yasinska@nuwm.edu.ua

1. Introduction

Sharp-crested weir or thin-plate weir is hydrotechnical structure over which the fluid must flow. Such weirs are commonly used as means of flow measurements because they are less sensitive to the downstream conditions, the channel roughness and the influence of backwater than the velocity-area method, for example [1].

Famous scientists have made significant contribution to sharp-crested weirs theory development. A.R. Berezinskij, D.I. Kumin, F.I. Pikalov, R.R. Chugaev, V.V. Smyslov, M. Castel, P. Boileau, H. Bazin, James B. Francis, A. Fteley & F. Stearns, T. Rehbock, K. Kindsvoter, R. Carter, A. Ramamurthy, N. Rajaratnam and others are among them. However, we have to admit, that in spite of large amount of carried out theoretical and experimental investigations and large bulk of obtained data, weirs calculation, in most cases, comes down to determination of flow discharge capacity by using empirically obtained weir discharge coefficients. These coefficients are obtained for small-scale weirs models with minor change of operating factors and don't take into consideration peculiarities of the weir in each specific case as well as scale factor. As a result, calculation data by different equations for the same conditions can significantly differ. Studies carried out by different scientists have shown that existing theories do not reflect with sufficient accuracy and completeness phenomena typical for sharp-crested weirs. To produce more specific and accurate solutions, a mathematical model that can link up all operating factors to solve a weir flow problem should be developed. This mathematical model can be based on the fundamental laws of conservation of mechanical energy in the form of energy and momentum equations. To get energy conservation equation for sharp-crested weir head losses should be determined.

2. Theoretical studies of sharp-crested weir head losses

To determine head losses, we consider the simplest form of weir, consisting of a plate set perpendicular to the flow in a rectangular horizontal channel with vertical upper edge running the full width of the channel b . The design circuit of such weir is shown on the figure 1.

Section 1–1 is located in the channel upstream at a sufficient distance from the weir, where dropping curve doesn't influence the stream line surface and the flow can be suggested as uniform. Flow depth in this section is $p_w + H$, where p_w is the height of the weir plate in cm , H is the weir head in cm . Section 2–2 is accepted through weir plate where flow depth above the crest of the weir is h in cm .

According to Bernoulli equation [2] total flow energy in section 1–1 towards datum plane 0–0 passing through the bottom of the channel, supposing that the flow is uniform, can be find in the following form

$$E_1 = p_w + H + \frac{\alpha_1 q^2}{2g(p_w + H)^2} \quad (1)$$

where α_1 is kinetic energy coefficient in section 1–1; q is a specific weir flow that can be calculated as $q = Q/b$ in cm^2/s , where Q is total discharge over sharp-crested weir.

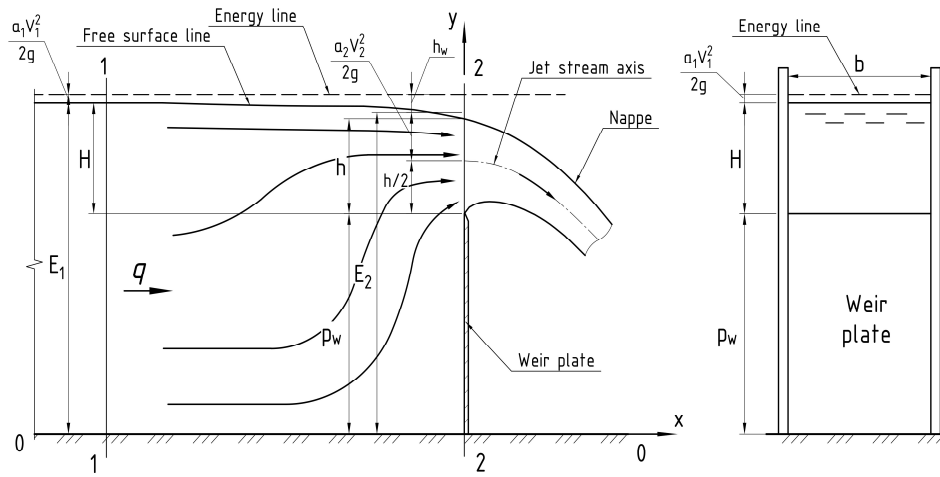


Fig. 1. Rectangular sharp-crested weir geometry

The flow moving over sharp-crested weir suffers sudden vertical contraction and transforms from the uniform flow to the nappe. As the pressure above and under the nappe is atmospheric, we consider it, with some assumptions, as jet stream flow. Hence, flow energy in section 2–2, according to Bernoulli equation, can be calculated as following [2]

$$E_2 = p_w + \frac{h}{2} + \frac{\alpha_2 q^2}{2gh^2} \quad (2)$$

where $p_w + h/2$ is high-altitude position of the jet stream axis in cm; $(\alpha_2 q^2)/2gh^2$ is the jet stream kinetic energy in cm; α_2 is kinetic energy coefficient in section 2–2.

To determine head losses h_w we accepted a hypothesis that they can be evaluated with Hind's formula [3], which describes similar head losses caused by sudden flow contraction in the channel

$$h_w = \zeta \frac{q^2}{2g} \left(\frac{\alpha_2}{h^2} - \frac{\alpha_1}{(p_w + H)^2} \right) \quad (3)$$

where ζ is the loss coefficient, that is determined experimentally.

Utilizing equation (3) energy conservation equation for sharp-crested weir can be given in following form

$$H + \frac{\alpha_1 q^2}{2g(p_w + H)^2} = \frac{h}{2} + \frac{\alpha_2 q^2}{2gh^2} + \zeta \frac{q^2}{2g} \left(\frac{\alpha_2}{h^2} - \frac{\alpha_1}{(p_w + H)^2} \right) \quad (4)$$

3. Mathematical processing of experimental data

In order to determine loss coefficient ζ special experimental investigations were conducted in the hydrotechnical laboratory at National University of Water Management and Environmental Engineering [4]. The height of the weir plate p_w and weir head H were estimated as main operating factors that determine weir head losses h_w . Experimental conditions are shown in table 1.

Table 1. Hydraulic experimental conditions

Factors		Levels of variation									Int. of var.
natural view	code view	-1	-0.75	-0.5	-0.25	0	0.25	0.5	0.75	1	
p_w, cm	X_1	5				25				45	20
H, cm	X_2	5	10	15	20	25	30	35	40	45	5
Experimental order for each X_i		7	21	1	2	26	15	27	5	22	
		12	3	13	18	9	20	25	14	19	
		8	6	10	16	11	23	24	17	4	

In experiments the relation between main operating factors H/p_w ranged from 0.11 to 9.0; Reynold number Re from 17 954 to 764 797 that corresponds to wholly turbulent flow and Froude number Fr from 0.003 to 0.930 that corresponds to lower flow regime.

In experiments weir plate height p_w was changing according to experimental conditions (table 1). Required weir head H was provided by changing input sharp-crested flow rate. The matrix to study the influence of the

main operating factors on the average hydraulic weir outbound parameters, for example for the weir plate height $p_w = 25 \text{ cm}$, is shown in Table 2.

Table 2. Influence of the main operating factors on the weir head losses h_w

Factors				Averaged experimental values		Calculated values			
code view		natural view		specific weir flow q	threshold depth h	weir head losses h_w		relative weir head losses h_w/E_f	
X_1	X_2	p_w	H			exp. (5)	theor. (3)	exp.	theor.
		<i>cm</i>	<i>cm</i>	<i>cm²/s</i>	<i>cm</i>	<i>cm</i>	<i>cm</i>		
0	-1	25	5	205.76	4.29	1.63	1.64	0.054	0.055
	-0.75		10	596.65	8.63	3.25	3.26	0.093	0.093
	-0.50		15	1134.68	13.05	4.89	4.88	0.121	0.121
	-0.25		20	1777.11	17.34	6.47	6.49	0.141	0.142
	0		25	2570.96	21.84	8.12	8.10	0.158	0.158
	0.25		30	3457.50	26.22	9.73	9.72	0.170	0.170
	0.50		35	4449.69	30.59	11.34	11.33	0.180	0.180
	0.75		40	5562.86	35.02	12.98	12.95	0.188	0.188
	1		45	6705.77	39.19	14.52	14.56	0.194	0.194
Statistical parameters									
Error mean square $\bar{S}_e^2 \cdot 10^4$ for $f_e = 54, \text{cm}^2$							285.52		
PRESS statistic $\bar{S}_a^2 \cdot 10^4$ for $f_a = 26, \text{cm}^2$							292.50		
Calculated F-test \bar{F}_p							1.025		
Table F-test F_m							1.70		
Error $\pm \bar{\varepsilon}$, % reporting to $\zeta = 1.35$							± 1.70		

Experimental weir head losses h_w for each point of experiment plan according to obtained experimental values of specific weir flow q and threshold depth h were determined by equation (4), that is given in the following form

$$h_w = H - \frac{h}{2} + \frac{q^2}{2g} \left(\frac{\alpha_1}{(p_w + H)^2} - \frac{\alpha_2}{h^2} \right) \quad (5)$$

For verification accepted hypothesis, weir head losses computed with Hind's equation (4) were compared with experimental values calculated with equation (6). Unknown loss coefficient ζ in equation (4) was determined according to statistical experimental data processing, with probability of 95%, and assumed equal to $\zeta = 1.35$.

The influences of main operating factors: height of the weir plate p_w , weir head H and their ratio H/p_w on the weir head losses h_w were made by relative head losses h_w/E_1 – ratio of the weir head losses to total flow energy in section 1–1 calculated with equation (1).

$$h_w/E_1 = h_w / \left(p_w + H + \frac{\alpha_1 q^2}{2g(p_w + H)^2} \right) \quad (6)$$

Relative head losses h_w/E_1 were calculated for experimental weir head losses h_w obtained by equation (5) and for theoretical values by the Hind's formula (6). Calculation data is shown in table 2.

Figures 2–4 displays experimental points of the relative weir head losses, depending of main operating factors: height of the weir plate p_w , weir head H (fig. 2, 3) and their ratio H/p_w (fig. 4). Experimental points in this diagrams are approximated by solid lines obtained by Hind's formula.

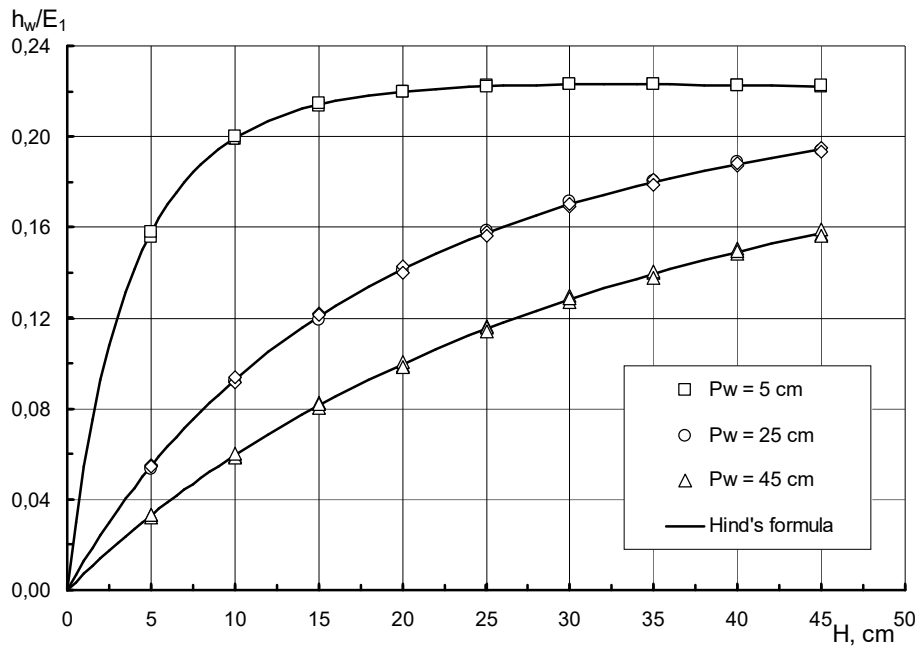


Fig. 2. Dependency graph $h_w/E_1 = f(H, p_w)$

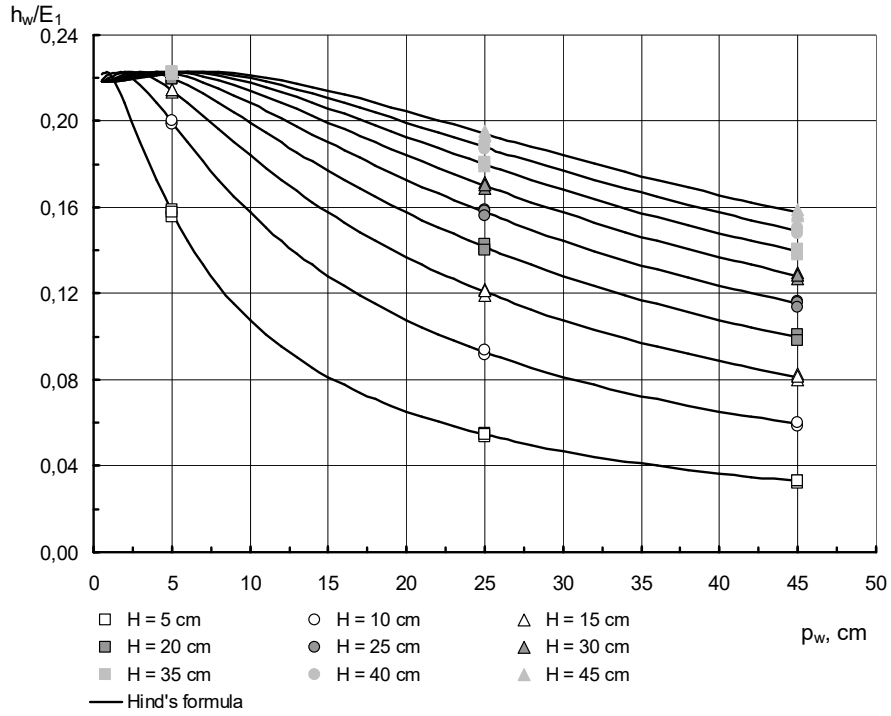


Fig. 3. Dependency graph $h_w/E_1 = f(p_w, H)$

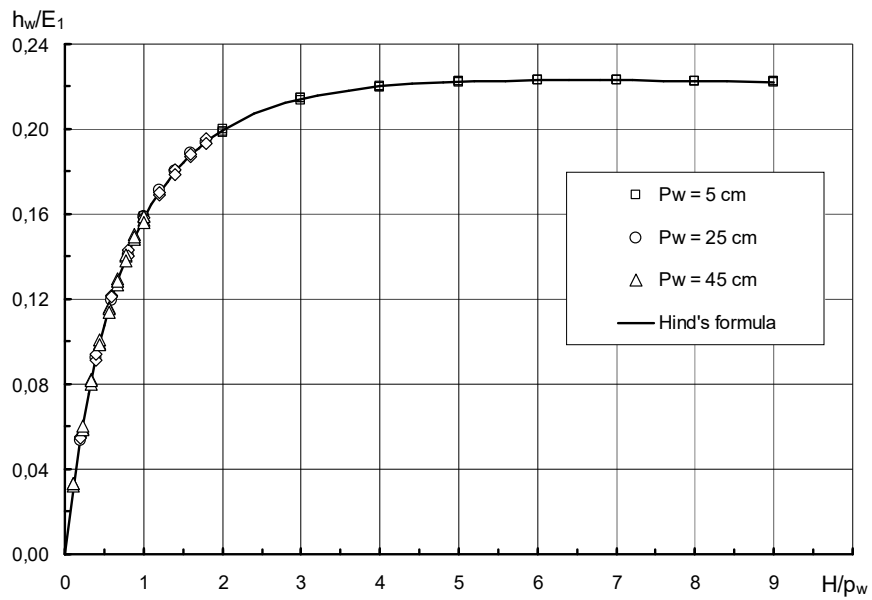


Fig. 4. Dependency graph $h_w/E_1 = f(H/p_w)$

Obtained graphs analysis in figure 2 has shown, that with weir head H rising relative weir head losses h_w/E_1 increase monotonically. Behavior of the relative weir head losses change is strongly pronounced at low weir plate height ($p_w = 5\text{ cm}$), at this time, they rise sharply in low heads and with further increase they asymptotically tend to their maximum.

Obtained graphs analysis in figure 3 has shown, that for small values of the weir plate height p_w relative weir head losses h_w/E_1 go up and under certain weir plate height they reach their maximum value, then these losses are reduced. Behavior of the relative weir head losses change is strongly pronounced in low heads.

Obtained graphs analysis in figure 4 has shown, that experimental relative weir head losses h_w/E_1 are approximated in dimensionless coordinates with universal graph $h_w/E_1 = f(H/p_w)$ that is calculated by Hind's formula and it does not depend on the weir plate height. Within the range $0 < H/p_w \leq 2$ relative head losses rise sharply, with further ratio increase they asymptotically tend to maximum $h_w/E_1 \approx 22\%$.

4. Conclusions

Based on theoretical and experimental investigations an energy equation for sharp-crested weir that considers head losses is determined. Adequacy of Hind's formula usage to determine weir head losses is proved and the influence of main operating factors: height of the weir plate p_w , weir head H and their ration H/p_w on the relative head losses is disclosed. Obtained energy equation is the part of mathematical model for sharp-crested water flow that will improve weir calculation methods.

References

- [1] Herschy, R.W., Streamflow measurement. Elsevier: Amsterdam, London, New York, Third edition, 2009, p. 507.
- [2] Bruce R. Munson, Alric P. Rothmayer, Theodore H. Okiishi, Wade W. Huebsch. Fundamentals of Fluid Mechanics, 7th Edition / John Wiley & Sons, 2013, p. 796.
- [3] Kiselev P.G. Spravochnik po gidravlicheskim raschetam / P.G. Kiselev. – M.: Energiya, 1972, p. 316.
- [4] Khlapuk M.M. Udoskonalennya metodu hidravlichnoho rozrakhunku propusknoyi zdatnosti vodozlyviv z tonkoyu stinkoyu / M.M. Khlapuk, O.V. Bezusyak, V.I. Korniiichuk // Visnyk NUWMEE. – 2015. – V. 3(71), p. 118–126.

Przesłano do redakcji: 24.03.2017 r.

Przyjęto do druku: 25.09.2018 r.

Anna BOCHENEK¹
Katarzyna KLEMM²

EVALUATION OF THERMAL COMFORT OF THE CITY'S PUBLIC SPACES BY THE USE OF NUMERICAL SIMULATIONS

Decision making by those who play a key role in urban transformation can be supported by computer techniques. 3D-4D spatial simulations provide reliable information on the impact of spatial development changes on urban composition, microclimatic conditions and thermal comfort. Comprehensive approach to the subject of spatial changes during revitalization activities can contribute to guarantee high quality of life for people in urbanized areas, especially within public spaces. However, the current activities do not take into account microclimate issues, due to higher costs. As a result, an aim of this work was to evaluate microclimatic conditions and thermal sensation of people occupying two public spaces, i.e. Old Marketplace and Urban Square, which have been identified as priority areas in the process of city revitalization (Lodz). Results of studies may be presented to the local authorities to enrich analytical part of the urban development study, thus to enable appropriate decisions to be taken on land conversion.

Conducted studies have shown that microclimate of areas is strongly dependent on spatial planning method. Greater diversity of meteorological parameters, i.e. temperature and relative humidity of air is observed in the Old Marketplace. In both areas there are microclimatic conditions described as uncomfortable. In order to guarantee appropriate thermal conditions for users, it is necessary to implement changes in their structure. The authors proposed potential planning strategies aimed to alleviate the discomfort related to human presence in both public spaces.

Keywords: CFD simulator, urban environment, revitalization, comfort

1. Introduction

In recent decades, there have been a growing number of studies on the thermal comfort of man in the external environment. Rapid population growth causes the occurrence of negative phenomena, i.e. density and degradation of

¹ Corresponding author: Anna Bochenek, Politechnika Łódzka, Instytut Inżynierii Środowiska i Instalacji Budowlanych, al. Politechniki 6, 90-924 Łódź; tel. 607710889; an.bochenek@wp.pl

² Katarzyna Klemm, Politechnika Łódzka, Instytut Inżynierii Środowiska i Instalacji Budowlanych, al. Politechniki 6, 90-924 Łódź; tel. 601299913; katarzyna.klemm@p.lodz.pl

urban tissue, sealing of natural operative surfaces and thus modification of microclimate conditions [1]. In order to ensure the comfort and quality of life of the urban population, it becomes necessary to undertake comprehensive spatial planning activities. Therefore, it is necessary to provide stakeholders reliable and detailed information about the given area, i.e. population, economic development and changes in spatial planning. This data can be acquired from direct field studies, public digital databases (e.g. GIS system) and numerical simulations [2]. Currently, the most common methods are simulation analysis based on information from field measurements. This technique obtains in a relatively short period of time the data necessary to assess microclimate in urbanized areas. It enables comprehensive analysis of the impact of spatial development on the comfort in an external environment. It provides graphical presentation of the study results. As a result, the stakeholders are informed about required changes on the given area in an accessible way [3].

2. Thermal comfort

Thermal comfort is defined as “a state of mind that expresses satisfaction from thermal environment” (ASHRAE 55) [4]. According to Auliciems, thermal comfort is dependent on the physical and psychological feelings of man generated by a type of physical activity, exposure to environmental factors, expectations and previous experiences [5]. In addition, research shows that man adapts to changing conditions by acclimatization and clothing modification [6].

PMV (Predicted Mean Vote) is one of the most commonly used indicators to evaluate the thermal comfort of man. At first, it was used for testing indoor thermal comfort. By modifying the Fanger’s thermal balance equation by Jendritzky and Nübler, it has been adapted to the external environment [7]. PMV is dependent on the metabolism rate (M) and body thermal load (L), i.e. difference between the amount of heat produced by the body and its losses in the external environment. The parameter of body thermal loads takes into account metabolism rate, type of physical activity, water vapor pressure, air speed and temperature, average radiation temperature, clothing thermal insulation, as well as convection heat transfer coefficient [8].

According to ASHRAE-55 standard, PMV is defined as the average evaluation of the group of people determining their thermal impressions on a seven-stage scale. PMV values exceed much beyond this scale with regard to conducting study in the external environment. It results from the fact of calculating the index on the basis of initial data of atmospheric process simulation and average predicted thermal sensations of man. Divergence between data obtained in the questionnaire survey (seven-stage scale) and empirical results from lack of restrictions concerning minimum and maximum PMV values. In addition, this index depends on the local microclimate conditions, and therefore its values vary depending on the climate zone.

This fact is confirmed by the research conducted by Jihad and Tahiri. The authors showed that the value of PMV index depended on local microclimatic conditions, season of the year and spatial planning method, in particular on the ratio of buildings height forming the pedestrian area to the width of streets. The average value of index varied from [-4] to [11] per year, depending on the building geometry [9]. Thorsson et al. conducted research on the largest green area complex in Gothenburg, Sweden (moderate zone). In this case, the value of thermal comfort index ranged from [-11] to [11]. Thus, they have shown that there is a discrepancy between PMV values obtained during the questionnaire survey and those obtained from simulation (40% of cases) [10].

3. Characteristic of research area

Lodz is the third largest city in terms of population numbers (693 797 persons) and fourth in terms of area (29 325 ha) in Poland (51°46'36"N 19°27'17"E). Currently the most urbanized part of the city is undergoing major transformations. Twenty areas were selected in the downtown zone, which were included in "Revitalization of Lodz Centre Area". One of the project's objectives is to "create a friendly, lively and interesting living and working space for the residents". Refurbishment of buildings, transformation of areas in the immediate vicinity of facilities and change in the way of management of areas open to the general public, i.e. plazas and greenery areas, will be direct measures aimed to implementation of tasks.

Taking microclimate issues into account in the revitalization process can contribute to improvement of the quality of life of people in the city. Appropriate modification of the spatial planning can alleviate the thermal discomfort experienced by humans in the external environment. Therefore, the main objective of this study was to assess microclimatic conditions and thermal comfort within selected public spaces.

Two of the oldest spaces in the city were provided with analyses, which were selected as priority areas within the revitalization program. The first one – Old Marketplace – is located in the centre-north part of Lodz. Its shape is similar to a rectangle of 105 m x 85 m. The frontage of the square is formed by residential buildings with services on the ground floor with an average height of 3 storeys. From the southern side it is adjacent to a large complex of greenery. Concrete and asphalt are the dominant surface types. The second public space – Urban Square – is located by the city's main street – Piotrkowska. This square was created by withdrawal of one of the service buildings in the east direction. Its dimensions are about 43 m x 34 m. From all sides it is surrounded by residential and commercial buildings. The height of buildings varies from 3 to 5 storeys. In this case, concrete is the dominant type of surface.



Fig. 1. Priority area of revitalization in Lodz
(1 – Old Marketplace, 2 – Urban Square)



Fig. 2. Old Marketplace (view the South-East)



Fig. 3. Urban Square (view from the South)

4. Meteorological data

The model's input data was obtained from digital databases of Lodz-Lublinek meteorological station located in the south-western part of the city. Information stored as part of station activity concerned the values of meteorological parameters such as: temperature, air humidity, dew point temperature, atmospheric pressure, direction, speed and wind blast, precipitation and Wind Chill Index. The digital data format (.xls) enabled their adaption to the requirements of ENVI-met application, i.e. calculation of hourly meteorological parameters. The study concerned four cloudless days: 31/12/15, 02/04/16, 24/06/16 and 30/09/16. At first, spatial diversity of meteorological parameters was evaluated. In order to estimate the thermal comfort of man in the external environment, the PMV index was calculated for selected cloudless days within one year.

5. Simulations of atmospheric processes

Development of atmospheric process models requires specialized tools. Currently, one of the most popular is ENVI-met program, which enables to create three-dimensional, non-hydrostatic models taking into account the principles of fluid mechanics and heat flows [11]. It enables thermal simulations of surface – vegetation – air interaction in urbanized areas on a daily cycle (from 24 h to 48 h) [12]. The atmospheric processes were simulated for selected public spaces located in the centre of Lodz, within the area covered by revitalization program. At first, geographical location of each site was defined in order to determine the amount of solar radiation on the Earth's surface. Microclimate

conditions in the external environment were determined on the basis of data obtained from Lodz-Lublinek meteorological station in the hourly interval. Three-dimensional models of public spaces were then created by defining the geometry of buildings, building materials and surface types. For the Old Marketplace, the model size was 80 x 80 x 30 units with a resolution of 2 m x 2 m x 1 m. The basic materials used for modeling of buildings were concrete and glass. Concrete and biologically active surfaces were used as substrates. A significant area was covered with impermeable surfaces (86%). The size of the city square model was 90 x 80 x 30 units with a resolution of 1 m x 1 m x 1 m. The dominant types of building materials were concrete and glass. In this case, the substrate was entirely covered with impermeable materials.

6. Analysis of results

The first stage of study consisted in estimating spatial diversity of microclimatic conditions in the area of analyzed public spaces depending on the season of year. For this purpose, detailed analyses were carried out at four characteristic points located at the corners of buildings (point: 1, 4) and on the main square (point: 2, 3) (measuring stands are presented on Figures 6–9). The range of values of basic meteorological parameters, i.e. temperature and relative humidity of the air in an hourly interval, is presented on Figure 4–5.

The analysis of simulation results showed that greater diversity of microclimatic conditions prevails in the Old Marketplace. Extreme values of parameters, i.e. temperature and relative humidity of the air are observed in the first and fourth measuring point for each of analyzed periods. The highest average daily air temperature was recorded in the first point at the corner of the northern frontage building. This point also had the lowest average daily relative humidity value. This may result from the fact that concrete surface of substrate has been strongly heated; the space is closed from the west with a multi-family building block limiting the air flow and lack of greenery. The fourth measurement point was located at the corner of a building on the eastern frontage in immediate vicinity of a large greenery complex – Old Town Park. As a result, the minimum average daily temperature value was observed. Additionally, this area was characterized by the highest average daily relative humidity of air.

A similar outline of the spatial distribution of meteorological parameters is observed in the Urban Square. Maximum daily average air temperatures and minimum daily average relative humidity are noted in the first point. It results from the fact that the control point is protected from the west by a compact multi-family structure. Location of buildings in close proximity to each other contributes to weakening the air exchange in the northern part of square. The opposite situation is observed within the fourth point. It is located next to a communication line running from east to west, parallel to the dominant wind direction. Therefore, in the southern part of square a lower average daily air temperature value and higher average daily relative humidity are observed.

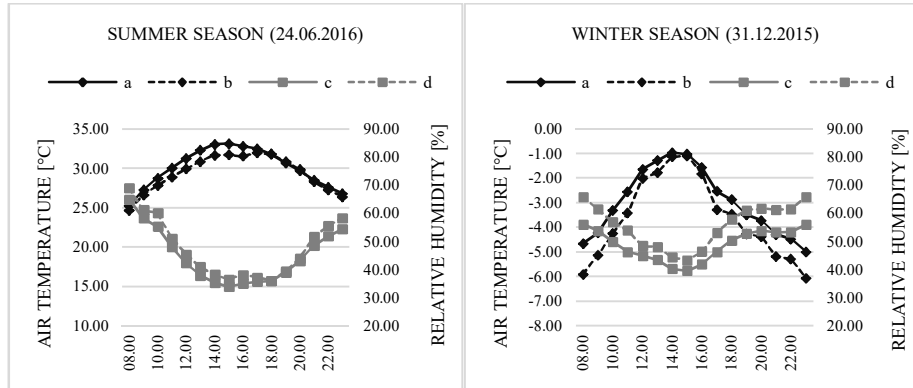


Fig. 4. Daily average values of meteorological parameters on the area of Old Marketplace (a – air temperature in point 1, b – air temperature in point 4, c – relative humidity in point 1, d – relative humidity in point 4)

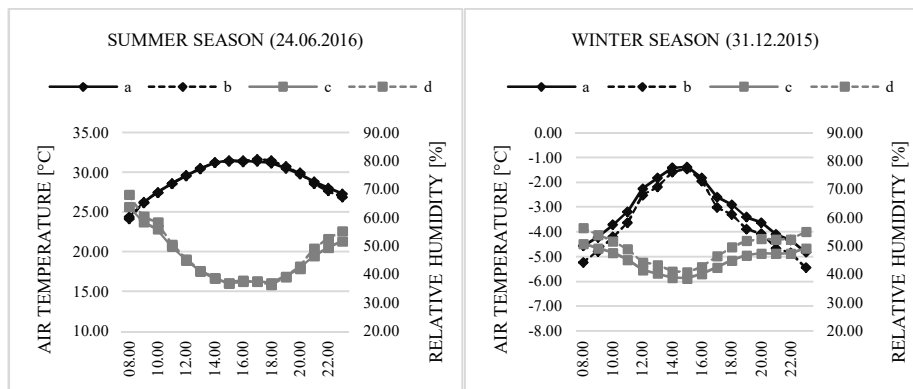


Fig. 5. Daily average values of meteorological parameters on the area of Urban Square (a – air temperature in point 1, b – air temperature in point 4, c – relative humidity in point 1, d – relative humidity in point 4)

The last stage of study consisted in estimating the thermal comfort in areas of selected public spaces. PMV index was calculated on the basis of obtained output data of atmospheric process simulation with an hourly interval. Additionally, it was necessary to determine the individual characteristics of humans, their clothes and type of physical activity. Thermal comfort was estimated for a 35-year-old man with a height of 1.75 m and weight of 75 kg, which moved at a speed of 1.21 m/s (average man's walking speed) [13]. Results of thermal sensations are presented on Figure 6-9.

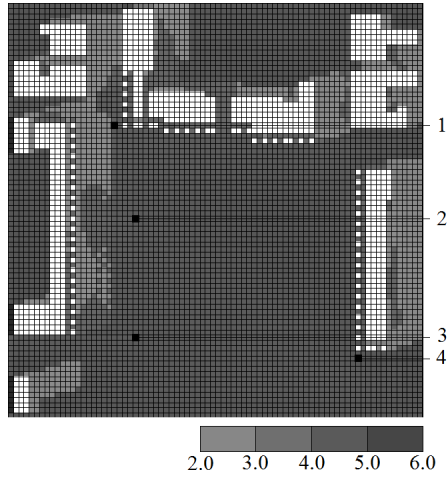


Fig. 6. PMV index – Old Marketplace (24/06/16)

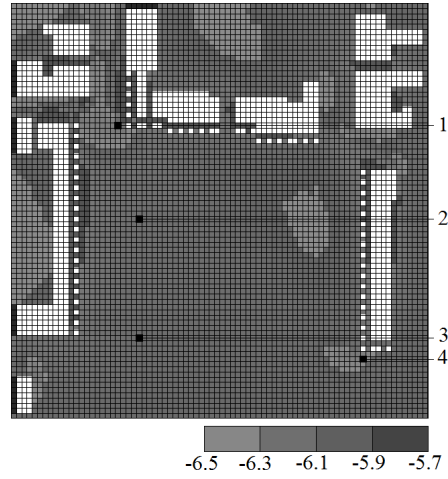


Fig. 7. PMV index – Old Marketplace (31/12/15)

Based on obtained research results, it can be concluded that similar values of the index were observed in both public spaces. During the summer period, the index significantly exceeded the theoretical scale between [3] and [+3]. According to ASHRAE-55 standard, this indicates the presence of microclimatic conditions known as “neutral”, “slightly warm” and “hot”. The most favorable thermal conditions were observed in the morning and late evening. During the day, the lowest PMV values were recorded on the leeward side of buildings and in the backyards surrounded by dense stone buildings (so-called manhole courtyard). It should be noted that this is an aerodynamic shadow zone. Conditions described as “discomfort” were found in strongly sunny areas.

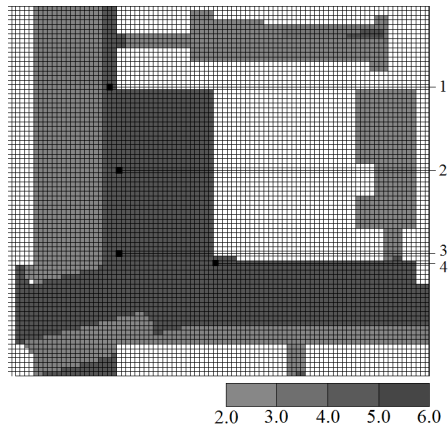


Fig. 8. PMV index – Urban Square (24/06/16)

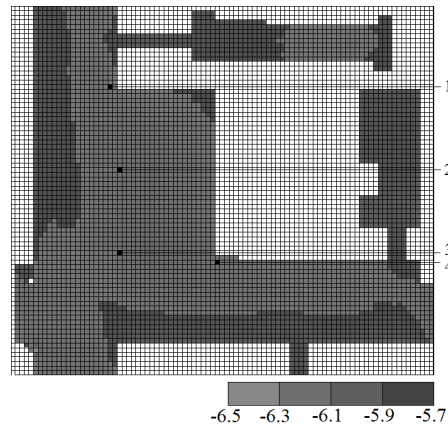


Fig. 9. PMV index – Urban Square (31/12/15)

In the winter period, the index values ranged from -7.21 to -5.21. In this case, the least favorable thermal conditions were observed around the corners of buildings, which were caused by an increase in the air flow in their vicinity. The most favorable conditions have been recorded on the leeward side of facilities.

7. Changes in spatial planning to ensure thermal comfort

Convenient conditions in the external environment can be ensured by modification of spatial planning on the given area. It is worth considering changing the location and geometry of facilities. Appropriate location of buildings in relation to each other ensures correct airflow. It is necessary to take into account the prevailing direction of wind flowing to the area. This ensures a cooling effect in high temperatures that reduces discomfort in the outdoor environment. The change of the height of objects can contribute to a decrease in the value of air temperature. Higher structures of buildings will reduce the amount of solar radiation reaching the ground atmospheric layers [14]. Studies conducted by Jihad et al. confirm that thermal comfort is dependent on the area morphology. The authors have shown that proportions of street canyons have an impact on microclimatic conditions in the given area. Comfort can be ensured by changing the installation parameters forming the street canyon or modifying its width [9].

Chatzidimitriou and Yannas have shown that the use of natural materials as a basic type of substrate can reduce the air temperature in the summer period – cooling effect, and cause its increase in winter period. The use of materials with a high albedo value can have a positive impact on the area's microclimate. Their application will reduce the amount of solar radiation absorbed by vertical and horizontal surfaces. A similar effect will be achieved by using materials with bright tinges [15].

According to Axarli and Chatzmidimitriou, high greenery contributes to reducing the amount of sunlight reaching the earth's surface. This reduces the temperature of horizontal surfaces, especially those made of materials with high thermal capacity. On the other hand, it increases relative humidity. Due to the appropriate location of green elements, it is possible to ensure thermal comfort in the external environment, especially in the summer period [16].

8. Conclusion

Simulation analyses conducted with programs of CFD type constitute the future alternative to traditional testing methods of microclimate and thermal comfort in urbanized areas. They enable obtaining information on meteorological parameters in a relatively short time and reduce financial outlays for research. Finally, there is an option to visually present the results of study.

In this way, information on the necessary changes in spatial planning method is provided in a way that is accessible to everyone – not only specialists.

Comparative analysis of research results showed that spatial diversity of microclimatic parameters occurs in the area of both public spaces. It results from the spatial planning method, i.e. geometry of building development, their location in relation to each other and existing vegetation. The research has shown that it is larger in the Old Marketplace.

PMV index enables the evaluation of the thermal comfort of humans in an external environment. Determination of the parameter supports taking a decision on the spatial planning method.

Transformation of downtown areas, in particular areas of historical meanings, requires additional arrangements with the historic conservationists. Interference with geometry of buildings is in many cases impossible due to their architectural qualities. The objects forming frontages of both squares have been entered into the municipal register of monuments. Therefore, consideration should be given to increasing the amount of greenery and permeable surfaces, which will not only improve thermal comfort, but also improve the microclimate. It will help to reduce the heat island, reduce concentration of pollutants and will also have a positive impact on the user's psyche. In tight urban interiors, green walls or green roofs can be a good solution. Improvement of conditions in the summer period can be achieved by placing water elements in the form of fountain or a water curtain.

References

- [1] Ragheb, A., El-Darwish, I., Ahmed, S.: Microclimate and human comfort considerations in planning a historic urban quarter, *International Journal of Sustainable Built Environment*, vol. 5, no. 1, 2016, pp. 156–167.
- [2] Ozkeresteci, I., Crewe, K., Brazel, A.J., Bruse, M.: Use and evaluation of the ENVI-met model for environmental design and planning: an experiment on linear parks, *Proc. ICC 2003*, pp. 402–409.
- [3] Oliveira, S., Andrade, H.: An initial assessment of the bioclimatic comfort in an outdoor public space in Lisbon, *International Journal of Biometeorology*, vol. 52, no.52, 2007, pp. 69–84.
- [4] ASHRAE: Thermal environment conditions for human occupancy, *ANSI/ASHRAE Standards*, 2010.
- [5] Auliciems, A.: Human Bioclimatology: an introduction. [in] A. Auliciems (ed.): *Human Bioclimatology: Advances In Bioclimatology*, 1998, pp. 1–6.
- [6] Nicol, J. F., Humphreys, M. A.: Adaptive thermal comfort and sustainable thermal standards for buildings, *Energy and Buildings*, vol. 34, no. 6, 2002, pp. 563–572.
- [7] Jendritzky, G., Nübler, W.: A model analyzing the urban thermal environment in physiologically significant terms, *Meteorology and Atmospheric Physics*, vol. 29, no. 4, 1981, pp. 313–326.

- [8] Ruiz, M. A., Correa, E. N.: Suitability of different comfort indices for the prediction of thermal conditions in tree-covered outdoor spaces in arid cities, *Theoretical and Applied Climatology*, vol. 122, no. 1–2, 2015, pp. 69–83.
- [9] Jihad, A., Tahiri, M.: Modeling the urban geometry influence on outdoor thermal comfort in the case of Moroccan microclimate, *Urban Climate*, vol. 16, 2016, pp. 25–42.
- [10] Thorsson, S., Lindqvist, M., Lindqvist, S.: Thermal bioclimatic conditions and patterns of behavior in an urban park in Göteborg, Sweden, *International Journal of Meteorology*, vol. 48, no. 3, 2004, pp. 149–156.
- [11] Hien, W. N., Ignatius, M., Eliza, A., Jusuf, S. K., Samsudin, R.: Comparison of STEVE and ENVI-met as temperature prediction models for Singapore context, *International Journal of Sustainable Building Technology and Urban Development*, vol. 3, no. 3, 2012, 197–209.
- [12] Huttner, S., Bruse, M., Dostal, P.: Using ENVI-met to simulate the impact of global warming on the microclimate in central European cities. [in:] H. Mayer, A. Matzarakis (eds.): *Berichte des Meteorologischen Instituts der Albert-Ludwigs-Universität*, 5th Japanese-German Meeting on Urban Climatology, 2008, pp. 307–312.
- [13] Gaspari, J., Fabbri, K.: A study of the use of outdoor microclimate map to address design solutions for urban regeneration, *Energy Procedia*, vol. 111, 2017, pp. 500–509.
- [14] Ghaffarianhoseini, A., Berardi, U., Ghaffarianhoseini, A.: Thermal performance characteristics of unshaded courtyards in hot and humid climates, *Building and Environment*, vol. 87, 2015, pp. 154–168.
- [15] Chatzidimitriou, A., Yannas, S.: Microclimatic Studies of Urban Open Spaces in Northern Greece, *Proc. PLEA 2004*.
- [16] Axarli, K., Chatzidimitriou, A.: Redesigning Urban Open Spaces Based on Bioclimatic Criteria: Two squares in Thessaloniki, Greece. *Proc. PLEA 2012*.

Przesłano do redakcji: 04.03.2018 r.

Przyjęto do druku: 31.03.2018 r.

Zuzana VRANAYOVA¹
Daniela KAPOSZTASOVA²
Zuzana POOROVA³

WATER MANAGEMENT OF “SMART” BUILDINGS AND CITIES

Now is the time to take our future more seriously and start providing solutions for tomorrow's world. The new notion or significant specification of the term “*BLUE to GREEN*” infrastructures in buildings in the modern information age is the expression of the sustainable development of a „smart city“ society and beyond. We introduce our experimental platforms representing different types of green roofs, green and water walls as possible solutions. These experimental sites in the University Campus were created on the basis of researches dealing with green roofs and their retention qualities, as well as green walls and their impact on the microclimate and the possibility of using rain and gray water that could be filtrated through the media of these structures. The paper describes the world-wide conditions on the basis of which this issue is up to date and addressed. The outputs from the individual measurements will be related to water cycle issues, green walls and roofs constructions.

Keywords: green roof, green wall, water cycle, water management

1. Introduction

Reports of water scarcity and many draughts due to climate changes are becoming increasingly common. The costs of water infrastructure have risen in every country. These and other aspects lead us to use alternative water sources as primary for building water supply. Massive use of reused water for non-potable purposes in buildings promotes the conservation of natural resources, water, and thus the overall sustainability in water management.

¹ Corresponding author: Zuzana Vranayova, Technical University of Košice, Faculty of Civil Engineering, Institute of Architectural Engineering, e-mail: zuzana.vranayova@tuke.sk

² Daniela Kaposztasova, Technical University of Košice; Faculty of Civil Engineering, Institute of Architectural Engineering; e-mail: daniela.kaposztasova@tuke.sk

³ Zuzana Poorova, Technical University of Košice, assistant professor, Faculty of Civil Engineering, Institute of Architectural Engineering; e-mail: zuzana.poorova@tuke.sk

The replacement of natural permeable green areas with concrete constructions and hard surfaces will be noticed in last decades. The densification of existing built-up areas is responsible for the decreasing vegetation, which results in the lack of evapotranspiration and cooling the air. Such decreasing vegetation causes so called urban heat islands.

Since roofs and pavements have a very low albedo, they absorb a lot of sunlight. Several studies have shown that natural and permeable surfaces, as in the case of green roofs or walls, can play crucial role in mitigating this negative climate phenomenon and providing higher efficiency for the building, leading to savings. Such as water saving, what is the main idea of our research.

The vision of our team – to introduce into reality the term “BLUE to GREEN” in the modern information age is the expression of the sustainable development of a smart cities society and beyond. The grey infrastructure is an urban engineering infrastructure (roads, drains, sewerage). The red one is a human community. The green parallels the grey. This is a network of natural area and open spaces. The last one is the blue (water) infrastructure. We expect that using our models and measurements can become a suitable tool to improve the life quality of residents and environmental awareness of the society.

Green building gives sustainability for the earth and it can protect it from the climate change, but it costs a lot of money to put the green wall or green roofs so we have to create something not so costly. Our idea is that we can build the building and build the green wall with it like two things in the sametime, so the plants can grow up when we finish the building. [4], [6]

2. Vision of sustainable green and smart buildings

The act of building green dividers and green rooftops ought to be advanced in urban regions in order to enhance the occupants' wellbeing and life quality. Its main aim is for aesthetic and energy saving in building. Green roof advantages concerning water management include the attenuation of flood peaks in extreme rain events due to stormwater runoff delay, acting like a meanders of the river through water storage in the layers of the green roof, and reduction into the public drainage system [1], [5], [7]. [9]. Water distress is an issue, which has brought an attention on the possibility using green roof/ walls structures to manage stormwater and allow their storage for later reuse.

In Portugal, ANQIP (Associação Nacional para a Qualidade nas Instalações Prediais) has developed a Technical Specification ETA 701 [2] for rainwater harvesting in buildings, being a valuable tool to couple with the green roof technology [3]. Green roofs/ walls have the potential to be the most common type of green structures in the city due to their characteristics, low maintenance and low weight to the buildings [3].

The green architecture and sustainable buildings is not a luxury academically and not a trend in theory or the aspirations and dreams have no place in reality,

but it represents a trend universally applied and exercise professional conscious began to make up her features and dimensions significantly among architects and engineers involved construction in the advanced industrial countries. These countries have come a long way in this area and there is a marked increase in the popularity of this trend by the public under the attention continued by the professionals themselves and engineers are as effective tools that can localize these techniques and establish it professional during the design of building projects and supervising its implementation. This all in turn requires the direction to education architectural and engineering in our university so that the laboratories of Architecture Engineering Institute went green architecture and sustainable buildings of professional perspective and to create environmental and economic solutions to the problems faced by the construction sector we urgently need to change traditional patterns followed in the design and implementation of our buildings more sustainable, and this change is needed to make them and must start from the main elements in it.

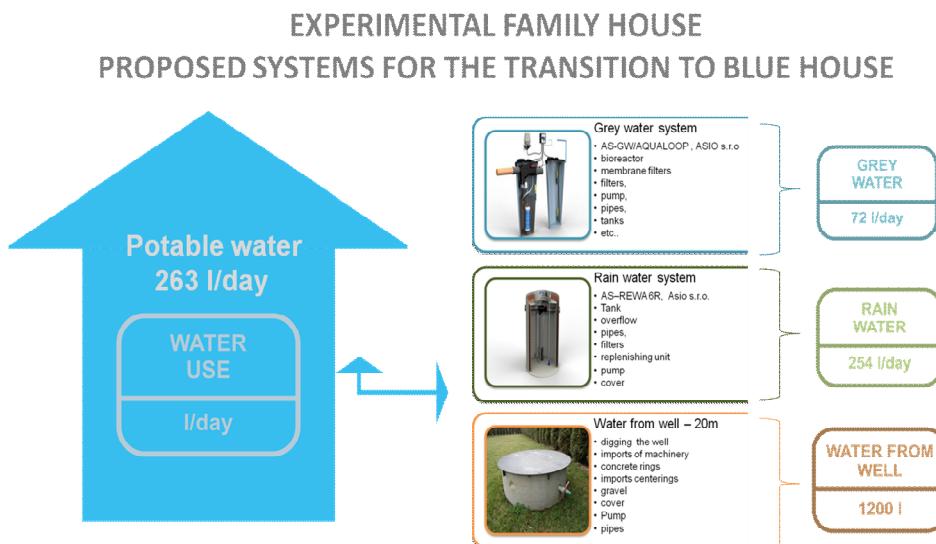


Fig. 1. Experimental house – proposed systems for transition from conventional to the blue one [4]

From the view point of grey water's recycle treatment re-use in green and smart house, the feasibility and rationality is validated when it apply to buildings as an effective program of domestic water use which can both expand resource and reduce consumption. Whilst undertaking a water audit, it may be identified that rainwater and grey water are insufficient on their own to meet a part of the water demand in building. It may be possible to combine rainwater, grey water, water from well and potable water to provide a viable water source to cover the whole water demand at the building level (Fig. 1). [4], [6], [8], [9], [10].

3. Experimental green and smart building

The main challenge of the 3rd millenium is to reduce water consumption and to introduce the water-saving culture in the context of climate change. There are no studies taken about the influence of buildings transformation to green living system.

For this reason our aim is to explore the green design that is blending of four co-operating infrastructure strands into a seamless system. In this paper we introduce our experimental platforms representing different types of green roofs and green/ water walls. These experimental sites in the University Campus were created on the basis of different research in the frame of doctoral thesis as well as grant project dealing with green roofs and their retention qualities, as well as green or water walls and their impact on the microclimate and the possibility of using rain and gray water that could be filtrated through the media of these structures. (see Fig. 2 and 3).



Fig. 2. Models of green roofs prepared for experimental study



Fig. 3. Models of green walls and water wall prepared for experimental study

3.1. Methods of study

This paragraph deals with our vision with proceeding on the topic future water management of the sustainable building in the smart cities. We would like to introduce our conception. This shows four most important parts of the work (past and mostly future). We called it MAMA conception because of the four main steps [7]:

- Monitoring,
- Analysing,
- Modelling,
- Assessment.

These main steps should divide our research work into four working blocks with each step having its own objectives and outputs.

Monitoring and analysing parts consist more or less of data collection and according to the topic (green roof/ green or water walls), on the base of studying background documents, developing own methodology and preparing experiments. The most important part of this step includes are on site measurements.

The next point of the MAMA conception is the analysis which provides all necessary documents and information about the place of interest. This step include not only studying all background documents but on site, questionnaires and own measurements. The objectives of analysis provide a complex overview and input data necessary for the modelling phase.

For modelling part is important to know what kind of data do we need for the model. One of our aims is reusing rain/ gray water. That means that modelling part in this specific case will be concerned to the rainwater harvesting as a part of source control measure in stormwater management. Our target is to observe what the necessary equipment will be and at the same time effectiveness of potable water saving. Reliable combination of source control measures require to know what the total runoff will be.

Final step is evaluation and environmental assessment. For green constructions the topic target is to observe water retention, discharge coefficient and water storage features of walls used in research. Last part of this step is an assessment of all obtained results from previous parts of research. Evaluation of retention, possible improving of the water and air parameters, etc. as well as design prototypes for future work. For the society is very useful to perform return of investment assessment and also environmental assessment with all advantages and disadvantages of designed system.

3.2. Experimental tools

For our study we will practically use following equipments (Fig. 2):

- 4 green exterior platforms / roofs,
 - 3 x 300 l tanks for rainwater accumulation,
 - 6 x 60 l small tanks for water samples.
- In the close future we start with monitoring of following parameters:
- ✓ Rainwater quality,
 - ✓ Quality of rainwater accumulated in the green roof,
 - ✓ Quality of rainwater filtered by exterior green walls,
 - ✓ Water amount caught by the green roof,
 - ✓ Water amount caught in the green walls,
- 2 interior green walls (Fig. 3):
 - ✓ Indoor environment quality improvement,
 - ✓ Treatment and recycle of grey waters,
 - Grey waster source – appliances in Laboratory of Institute,
 - Green wall layers – test of effect of different substrates/ greens for treatment process effectiveness.
- Monitoring:
- ✓ Grey water quality on the input to the green wall and following effect on its parameters,
 - ✓ Water quality after filtration by individual substrates,
 - ✓ Water amount caught by substrate and necessary for green development,
 - ✓ Filterd water amount suitable for next using,
 - ✓ Effect on the indoor environment quality–humidity, temperature, CO₂,
- 1 type of substrate,
 - 5 type of plants.

4. Conclusions

Potable water consumption of the Slovak households isn't above average at all but we use it in inappropriate ways. It is well known that around 60% of drinking water may be replaced by alternative water sources. This fact gives credit to reuse of potable water in building watercycle and better percentage weight in building environmental assessment.

In Slovakia, the results of questionnaire shows that most of our citizens are pro water saving oriented and open to new water ideas - as in building water cycle. There is a gap for water regulation and water supply of grey and rainwater systems. On the basis of the scientific, policy, economic and social impacts, our study pointed out challenges and recommendations to strengthen and enhance future of alternative water sources.

Our partial studies have shown that natural and permeable surfaces can play crucial role in mitigating this negative phenomenon and providing higher efficiency for the building.

Acknowledgements: *This work was supported by: VEGA 1/0202/15 Sustainable and Safe Water Management in Buildings of the 3rd. Millennium and Slovak Cultural and Education Grant Agency.*

References

- [1] Niachou, A., Papakonstantiou, K., Santamouris, M., Tsangrassoulis, A., Mihalakakou, G. (2001) *Energy and Buildings*, 33. Analysis of the green roof thermal properties and investigation of it energy performance, p. 719–729.
- [2] ANQIP (2012) Portuguese Association for Quality and Efficiency in Building Services. Technical Specification ETA 0701 – Rainwater harvesting systems in buildings.
- [3] Monteiro, C. M., Calheiros, C.S. C., Pimentel-Rodrigues, C., Silva-Afonso, A., Castro, M. L.P. (2016) Green roofs as a tool to promote water efficiency in buildings, IAHS World Congress on Housing. – Coimbra : Institute for Research and Technological Development in Construction Sciences, p. 1–8. – ISBN 978-989-98949-4-5.
- [4] Kaposztasova, D. (2015) Thesis Fulfillment of the Requirements for the Degree of associated professor, Technical university of Kosice. Let us talk about water Integrated water management at the building level, p. 117.
- [5] Pochwat, K., Slys, D., Kordana, S. (2017) *Journal of Hydrology* Vol. 549. The temporal variability of a rainfall synthetic hyetograph for the dimensioning of stormwater retention tanks in small urban catchments, p. 501–511. ISSN: 0022-1694.
- [6] Stec, A., Kordana, S. (2015) *Resources Conservation and Recycling* Vol. 105. Analysis of profitability of rainwater harvesting, gray water recycling and drain water heat recovery systems, p. 84–94. ISSN: 0921-3449.
- [7] Poórová, Z., Káposztásová, D., Vranayová, Z. (2015) *Bothalia*. Vol. 45, no. 2. Natural and artificial green design environment and its effect on people living and working in it, p. 23–32. ISSN 0006-8241 Spôsob prístupu: <http://www.bthla-journal.org/issue.php?v=45&i=2>.
- [8] Káposztásová, D., Rysulová, M., Purcz, P. (2015) *WSEAS Transactions on Environment and Development*. Vol. 11. Integrated building water management options p. 282–288. ISSN 2224-3496, <http://wseas.org>.

- [9] Markovič, G., Zeleňáková, M., Káposztásová, D., Hudáková, G. (2014) WIT Transactions on Ecology and the Environment, 181, Rainwater infiltration in the urban areas, pp. 313–320.
- [10] Jelenikova, I., Sikula, O., Perackova, J. (2011) In Proceedings of the International Conference Experimental Fluid Mechanics 2011. Liberec. Simulation of deposition the corrosion waste in a water distribution system, p. 698–705. ISBN: 978-80-7372-784-0.

Przesłano do redakcji: 24.03.2017 r.

Przyjęto do druku: 31.03.2018 r.

Maria MRÓWCZYŃSKA¹
Elżbieta GROCHOWSKA²
Sławomir GIBOWSKI³

MONITORING VERTICAL DISPLACEMENTS OF AN ENGINEERING OBJECT WITH MASONRY WALLS

The paper presents a method for conducting measurements and processing the results that makes it possible to determine the vertical displacements of measurement and control network points stabilized outside and inside a building in which changes in the form of scratches and cracks on the external and internal walls were noticed. These changes were so disturbing that a number of technical opinions were issued on the technical condition of the building, the ground and water conditions as well as the location of other buildings in relation to that object. The measurement methodology is generally known, but the problem of correctly defining a reference system and estimating the values of vertical displacements still remains to be solved. Moreover, the paper presents the characteristics of the object subjected to research, its technical condition in 2006 and in 2015 as well as an analysis of the impact of a heating duct on the behaviour of the building.

Keywords: vertical displacements, geodesic monitoring, engineering object

1. Characteristics of the object

The object has four storeys and a basement. The above-ground storeys are: the ground floor, the first and the second floors (Fig. 1). The object is used as an office and administration building. The main construction work was carried out in the years 1988–1998; however, in 2004 construction work was still in progress. Although the building was not built long ago, the construction documentation has not been preserved. At present, there are inspection documents (2008) and technical opinions.

The basement (the first storey) is used for technical purposes related to telephone installations. On the second (the ground floor), the third (the first floor)

¹ Corresponding author: Maria Mrówczyńska, Uniwersytet Zielonogórski, Wydział Budownictwa, Architektury i Inżynierii Środowiska, Instytut Budownictwa, ul. Z. Szafrana 1, 65-516 Zielona Góra, M.Mrowczynska@ib.uz.zgora.pl

² Elżbieta Grochowska, Uniwersytet Zielonogórski, Wydział Budownictwa, Architektury i Inżynierii Środowiska, Instytut Budownictwa, ul. Z. Szafrana 1, 65-516 Zielona Góra, E.Grochowska@ib.uz.zgora.pl

³ Sławomir Gibowski, Uniwersytet Zielonogórski, Wydział Budownictwa, Architektury i Inżynierii Środowiska, Instytut Budownictwa, ul. Z. Szafrana 1, 65-516 Zielona Góra, S.Gibowski@ib.uz.zgora.pl

and the fourth (the second floor) storeys there are offices. In the central section of the building there is a staircase, halls and toilets. The central section with the staircase, the hall and the other rooms is 2.40 m wider. The total length of the building is 47.14 m, its width is 12.60 m (without the protruding parts of the central section of the building), and its height is about 12.0 m.



Fig. 1. The building's elevation from of the main entrance, east side. The building's elevation from the north-east side

The building has masonry walls with interchangeably arranged prefabricated reinforced concrete ceilings of the "Żerań" type (hollow core slabs). The staircase has two flights of stairs with a 1.50 m wide well. No tie-beams were used in the building. The roof is flat and ventilated.

There is a heating duct running along the building, and its exact location is shown in Fig. 2.

Scratches and cracks have appeared on the inner and outer walls of the building. It is not known when it happened. The first scratches were described during an inspection carried out in 2004 when construction work was still in progress, but it was not exactly mentioned where they appeared.

1.1. Technical condition of the building in 2006

The technical condition of the building was first examined in 2004 and then in 2006. A particularly large number of scratches and cracks were observed on the walls in the hall on the second and first floors as well as on the top sections of the northern and southern walls and in their vicinity [10].

In the areas with particularly disturbing scratches and cracks, ten chalk control bands were installed. The bands were installed in June, 2006. After two weeks it was found that two of the bands were broken. At the beginning of August, 2006 another three bands broke. The old, broken bands were replaced with new ones.

Chalk seals are made of brittle material with a small tolerance for elastic and plastic deformations. Because of this feature a small change in the crack opening (below 0.1 mm) immediately causes the band or the plaster used to fasten it to break. The information that an expert obtains says only that "the

crack has changed its width". It is also often the case that gypsum breaks in the binding phase due to thermo-contractile deformations. Unfortunately, there is no information on the direction of the change (whether the gap becomes wider or narrower) and its value.

The width of the cracks on the intact bands (chalk control seals) ranged from 0.40 to 1.10 mm.

1.2. Technical Condition of the building in 2015

In December 2012 six crack width indicators WR-05 of stainless steel, manufactured by the company Neo-Strain were installed in the places where the chalk indicators had been installed (2006). The indicators were installed in rooms on the second floor (the fourth storey) [5, 6, 10, 11].

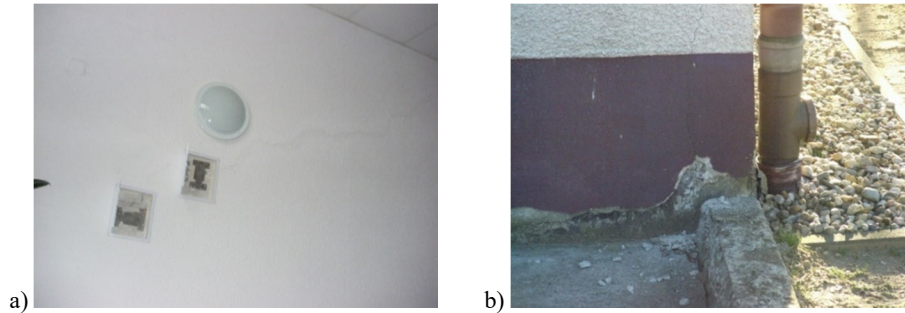


Fig. 2. a) The hall- landing (I-II), the width indicators installed; Fig. b) The corner of the north-west wall, the crack on the wall

The indicators made it possible to measure the width of the cracks in two perpendicular directions. The use of geometrical relations also made it possible to determine the rotation angle of the parts of the structure separated by the crack. The resolution of the readings from the indicator was 0.05 mm, and the measurement range was from -15 mm to +20 mm. There was no documentation (or a photograph) with a description of the indicators just after installation. It is not known whether the indicators were correctly installed. At present, the readings have to be regarded as 0.0.

Numerous scratches and cracks on the walls were found especially on the second floor of the building. They were the same cracks that had been described in the inspection report from 2006. No other, significant cracks were found inside the building (on lower storeys).

The scratches and cracks were plastered over or covered with nonwoven fabric wallpaper. They did not get wider and the wallpaper was intact, which indicates that the settlement of the building was stable.

Fig. 2 shows the inner corner of the north-west wall. At that place the wall is cracked. Point 4 of the external measurement network is located not far from that place. At that point the displacement is greatest (-2.93 mm).

1.3. Impact of the existing heating duct on the building

In order to determine and identify ground and water conditions, 11 holes were made with a depth of 4.0 to 6.0 m. A macroscopic description of the soils was prepared and observations of the groundwater were carried out.

The research showed that under a layer of humus or hardened surface, the ground in the area consisted of Holocene and Pleistocene sediments from the Quaternary Period. The Holocene is represented by building embankments with a thickness of up to 3.2 m, located on a series of Pleistocene sands. These are medium and coarse sands with an interbedding of fine-grained sands of fluvioglacial origin. No groundwater was found in the holes to a depth of 3.0 m. According to archival data, the first level of usable water is at a depth of 2.0–25.0 m below ground level.

The heating duct running in the vicinity of the building was built earlier than the building. Fig. 3 shows a sketch of the location of the structure in the ground vertically in the place closest to the heating duct.

The building was built on sandy made ground covering the area for many decades. After many years' deposition, sandy made ground can have the characteristics of medium compacted sand.

The heating duct, built earlier than the building, is located deeper. Fig. 3 shows that during the construction of the duct there was no need to prepare the ground for the future building.

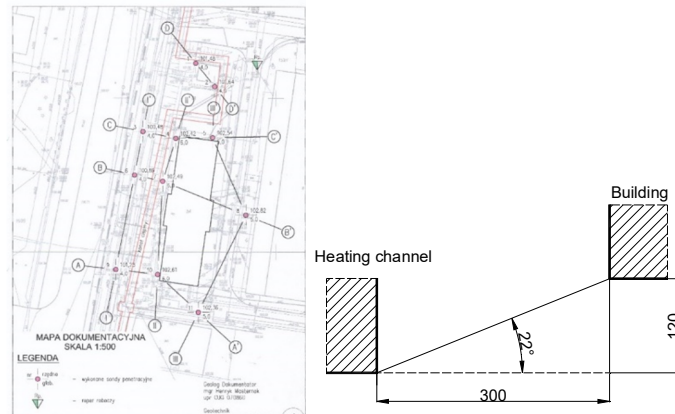


Fig. 3. A sketch of the location of the structure in relation to the heating duct

2. Course of the research

The central idea of the research presented in this paper was to estimate the value of uneven settlement of the building on the basis of known displacements of control points. The attempt to identify the dynamism of the phenomenon of

uneven settlement of the engineering object was carried out on the basis of the results of measurements carried out in a measurement and control network set up inside and outside the building on whose walls scratches and cracks had been noticed [7]. A sketch of the network set up on 10 control points is presented in Fig. 4, and the internal network consisting of 6 points is presented in Fig 5.

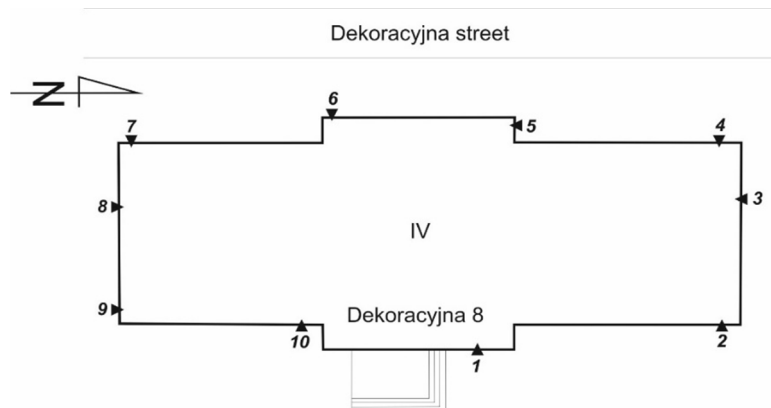


Fig. 4. A sketch of the measurement and control network set up outside the building

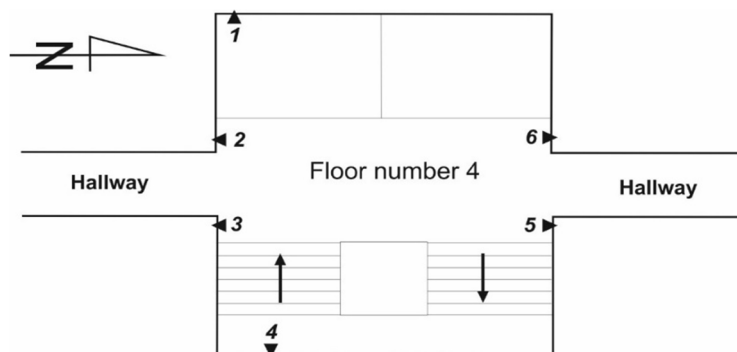


Fig. 5. A sketch of the measurement and control network set up inside the building on the fourth storey

The first measurement campaign, using the precision levelling method, consisted of five periodic measurements, which were carried out between June, 2006 and April, 2007. In the following years measurements were discontinued until 2014, when a periodic measurement was performed again. A reference point for all measurements and calculations was the zero measurement carried out in June 2006. The displacements of the measurement points that were determined are relative and provide sufficiently precise information about the stability of the building.

3. Algorithm for identifying a set of reference points

Determination of a geometrical displacement model for predicting the uneven settlement of engineering structures consists in identifying mutually fixed points on which the reference system is defined, and then determining the values of vertical displacements for all control points [4, 8, 9]. In the paper the reference points were identified on the basis of an algorithm consisting of two stages. The first stage, as a preliminary step in defining a reference system, consisted in minimizing the objective function in the form of a sum of absolute deviations, assuming that there were two n - element sets of points in the space R_1 : $\{S^1\}$ and $\{S^2\}$, which were sets of projections of physical points of the objects (O^1) and (O^2) under research onto the number line [3]. The points of both sets had definite heights $h_i^{(1)}$ and $h_i^{(2)}$ were obtained by adjusting the observations with minimum restrictions on the degrees of freedom [1]. If we denote the distances between the respective points of both sets by [2]

$$h_i = d(S^1, S^2) = |S^1 - S^2|, \quad i=1, 2, \dots, n \quad (1)$$

then we will search for a mutual location of the objects (O^1) and (O^2) which satisfies the condition

$$F(y) = \min_{x \in A} \sum_{i=1}^n |h_i - x| \quad (2)$$

In order to eliminate the points that are not mutually fixed, it is necessary to use the iterative method to check if the dependency is satisfied

$$w = |h' - h''| \leq m_0 1,4 \sqrt{n' + n''} \quad (3)$$

where: $w = |h' - h''|$, ($i=1, 2, \dots, n$) – the difference between the heights of a point in the initial and current measurement,

m_0 – the mean error of a single measurement, and n' and n'' denote the number of positions of the levelling instrument in the initial and current measurement.

The dependency (3) is tested in terms of the shortest path, and the points that satisfy this condition form a preliminarily identified reference system.

In the second stage, the reference system is finally defined. This is done by checking the reaction of the observation system consisting in an increase in the square of the norm of the correction vector. This is done by arranging changes of the absolute height differences w_i ($i=1, 2, \dots, n$) in order, and then by further adjusting the observations, assuming that the increasing number of fixed points is stable. An increase in the restrictions on the degrees of freedom will cause an increase in the sum of squares of corrections from the minimum value E_0 (adjustment with minimum restrictions on the degrees of freedom) to the value E_{\max} .

For any concentration of k fixed points, the critical value of the increment of the vector of the norm of corrections $\Delta E_k = E_k - E_0$ will be obtained from the formula [3].

$$\Delta E_k = -2 \left(m_0^2 + \frac{m_0^2}{2} \right) \ln \left(1 - 0,95^{\frac{1}{k}} \right) \quad (4)$$

where: m_0 – the mean error of a single observation from adjustment with minimum restrictions on the degrees of freedom,
 r – the number of extra observations.

The above course of makes it possible to define a reference system and to determine the values of vertical displacements (adjustment with conditions on the reference system) for all subsequent periodic measurements. For example, for the latest periodic measurement (August 2014) the reference system for the external network has been defined on points 1, 8, 9, and for the internal network on points 2, 3, 6. The values of relative displacements of points in the measurement and control networks for all periodical measurements are included in Tables 1 and 2, and presented in Figures 6 and 7.

Table 1. A compilation of the vertical displacements of points in the external measurement and control network

Nr pkt	Displacements of points				
	06.2006-07.2006 [mm]	06.2006-08.2006 [mm]	06.2006-12.2006 [mm]	06.2006-04.2007 [mm]	06.2006-08.2014 [mm]
1	-0,05	-0,02	-0,22	-0,09	-0,01
2	-0,24	-0,13	-0,50	-0,24	-1,36
3	-0,29	-0,42	-0,78	-0,67	-2,11
4	-0,39	-0,52	-0,96	-1,12	-2,93
5	-0,06	-0,05	-0,17	-0,20	-1,13
6	0,02	-0,03	-0,30	-0,33	-0,49
7	0,02	0,10	0,04	0,06	-0,46
8	-0,01	0,02	0,00	0,14	0,01
9	-0,01	-0,02	0,02	0,03	0,00
10	0,09	0,13	-0,09	-0,09	0,41

Table 2. A compilation of the vertical displacements of points in the internal measurement and control network

Nr pkt	Displacements of points				
	06.2006-07.2006 [mm]	06.2006-08.2006 [mm]	06.2006-12.2006 [mm]	06.2006-04.2007 [mm]	06.2006-08.2014 [mm]
1	-0,17	-0,36	-0,19	-0,17	0,45
2	0,10	-0,02	0,00	-0,03	0,07
3	0,03	-0,02	-0,10	-0,13	-0,08
4	-0,04	0,04	-0,05	0,03	1,18
5	-0,03	0,20	0,18	0,01	0,46
6	0,10	0,18	0,07	-0,20	0,01

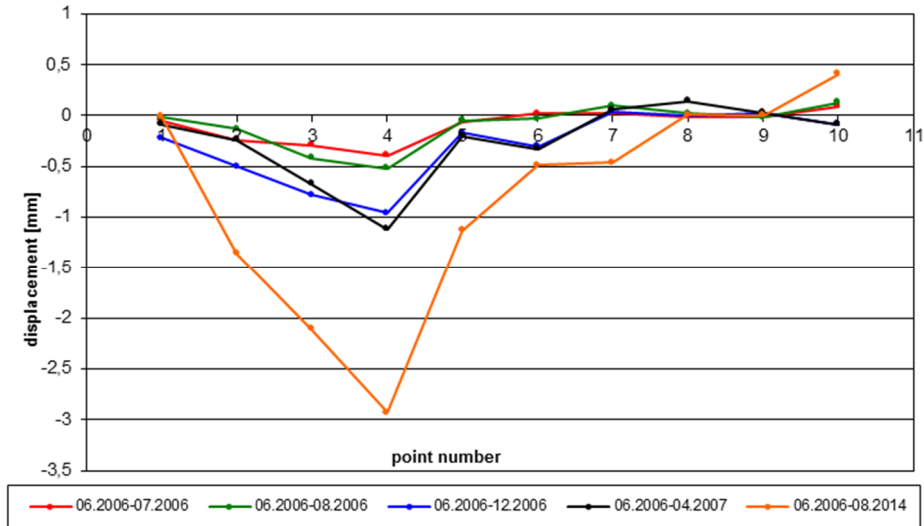


Fig. 6. A diagram of the displacements of points in the external measurement and control network between June 2006 and August 2014

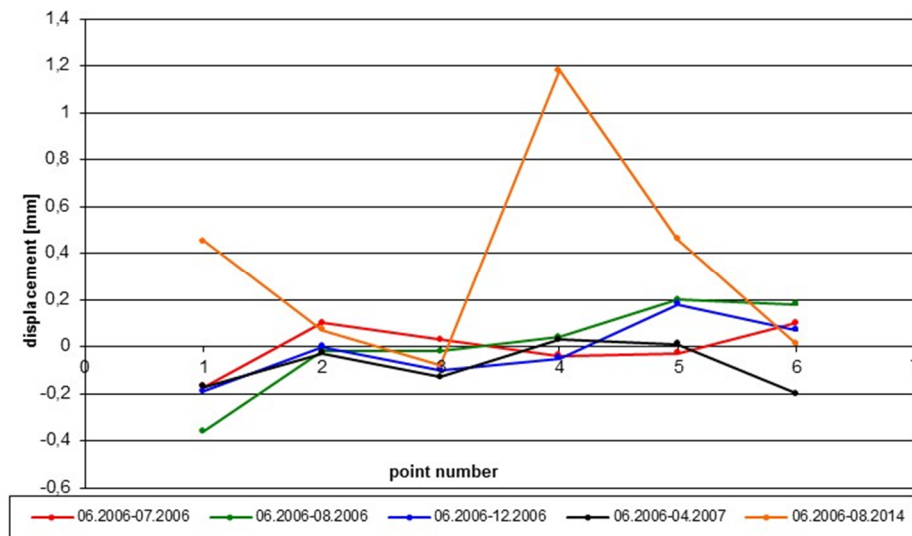


Fig. 7. A diagram of the displacements of points in the internal measurement and control network between June 2006 and August 2014

Knowing the displacement values for points in the external measurement and control network located at the foundations, it is possible to notice that these values range from 0.01 mm to -2.93 mm. The largest displacement (-2.93 mm) occurred for point 4 located in one of the corners of the building in the north-west. It should be emphasized that during the measurement campaign (June

2006–April 2007), the largest displacement values were also recorded for point 4. Significant displacements were also observed at points 2 and 3 located on the north wall of the building and at point 5 located on the west wall. The displacements at these points were -1.36 mm, -2.11 mm and -1.13 mm respectively. During the whole research period (June 2006–August 2014), the greatest displacements were observed for point 4. Counting from the beginning of the research, the total displacement of this point is 2.54 mm, which was recorded during the measurement carried out in August 2014.

The displacements of points in the geodesic network located inside the building have values from 0.01 mm to -1.18 mm. The greatest displacement was observed for point 4 located in the staircase on the east wall of the building and in comparison to the initial measurement (June 2006) there was an increase in displacements by 1.22 mm. At the other points of the internal network, displacement values are within the limits of the accuracy of the measurements carried out and do not change significantly in comparison to the initial measurement.

4. Conclusions

The analysis of the measurement data and the calculations carried out makes it possible to say that between 2006–2014 uneven settlements ranged from 0.01 to over -2.93 mm (the external network) and from 0.01 to -1.18 mm (the internal network). Because of the seven-year interval between the measurements, it cannot be determined whether the displacement values obtained during the latest measurement are maximum values and whether the changes observed are continuous or abrupt in character. It cannot be ruled out that there will be a further increase in uneven settlements caused by a number of random factors. In the case of objects susceptible to uneven settlement, it is important that settlement measurements should be continued and performed cyclically at regular intervals. The geodesic monitoring of engineering objects carried out in this way can be helpful in making decisions about the need to carry out protective work. It is worth emphasizing that the procedure for defining a reference system on the basis of minimization of absolute deviations is more efficient from the practical point of view, because a set of mutually fixed points is determined with the smallest value of the sum of the squares.

The results of geodetic measurements show that the building's settlement is not even, however, the displacements are very small. The highest value of internal displacement was recorded for point No. 4 and amounted to 1.2 mm. Compared with the previous measurements, this value refers to the rise of the building and not to its settlement.

There is sandy made ground under the street side of the building. The displacements measured under the building are small, and if the building had been properly built, with the use of tie-beams on the level of each storey,

the small differences in displacements that occurred would not be visible in the form of the existing open scratches.

The existing heating duct located next to the building and its possible disassembly will not affect the behaviour and safety of the building if the construction or demolition work is carried out properly and according to an appropriate plan.

The current state of the building should be regarded as stable.

References

- [1] Adamczewski Z., Nieliniowa analiza dokładności sieci geodezyjnej, Geodezja i Kartografia, t. XX, z. 3, Warszawa 1971.
- [2] Adamczewski Z., Algorytm numerycznej kontroli przylegania obiektów, Geodezja i Kartografia, t. XXVII, z.3, Warszawa 1979. Gil J., Wybrane elementy modyfikacji metody Cartesian Descent, Zeszyty Naukowe Akademii Rolniczej we Wrocławiu, nr 210, Wrocław 1991.
- [3] Gil J., Badanie nieliniowego geodezyjnego modelu kinematycznego przemieszczeń, seria: monografie nr 76, Wydawnictwo Wyższej Szkoły Inżynierskiej w Zielonej Górze, Zielona Góra 1995.
- [4] Kadaj R., Ein robuster Schätzer in der Deformationsanalyse, X. Internationaler Kurs für Ingenieurvermessung, München 12-17.09.1988.
- [5] Masternak H., Grzelak S., Opinia geotechniczna dla określenia warunków gruntowo-wodnych dla potrzeb zadania – Modernizacja i przebudowa systemu ciepłowniczego w Zielonej Górze – rozbiórka istniejącego kanału ciepłego na działce 153/8, ul. Dekoracyjna w Zielonej Górze, Sulechów 2013.
- [6] Matysiak A., Grochowska E., Hamudi K., Ocena stanu technicznego budynku na nieruchomości przy ul. Dekoracyjnej 8 w Zielonej Górze – ekspertyza techniczna nr 47/12/2015 r., Zielona Góra 2016.
- [7] Mrówczyńska M., Gibowski S., Opracowanie wyników pomiarów przemieszczeń pionowych punktów sieci geodezyjnej pomiarowo-kontrolnej na budynku przy ul. Dekoracyjnej 8 w Zielonej Górze, Zielona Góra 2006–2014.
- [8] Prószyński W., Kwaśniak B., Podstawy geodezyjnego wyznaczania przemieszczeń, Oficyna Wydawnicza Politechniki Warszawskiej 2006.
- [9] Skrzypczak I., Kogut J., Kokoszka W., Zientek D., Monitoring of landslide areas with the use of contemporary methods of measuring and mapping, Civil and Environmental Engineering Reports, Vol. 24 (1), p. 69–82.
- [10] Świtka R. „Ekspertyza stanu technicznego i możliwości sposobu naprawy budynku przy ul. Dekoracyjnej 8 w Zielonej Górze” Zielona Góra 2006.
- [11] Wujczyk K. „Protokół przeglądu stanu technicznego budynku położonego przy ul. Dekoracyjnej 8 w Zielonej Górze składającego się z lokali 1 i 2 – budynek administracyjno-biurowy” Zielona Góra 2014.

Przesłano do redakcji: 17.03.2018 r.

Przyjęto do druku: 31.03.2018 r.

Dominika KUŚNIERZ-KRUPA¹

MORET-SUR-LOING – CULTURAL HERITAGE, ITS VALUE AND PROTECTION

This article concerns the historic town of Moret-Sur-Loing in the context of preservation and revalorisation, which are connected to its sustainable development. It is one of many examples, besides e.g. Heppenheim, Lorsch, Weinheim and Provins, of small European historic towns which can suitably use their cultural potential for their multidirectional development. The town of Moret-Sur-Loing is located to the south of Paris, in the Île-de-France region, in the department of Seine and Marne. The cultural landscape of Moret comprises mainly historic buildings with the magnificent Notre Dame church and numerous small-town houses, defensive walls with gates and a donjon, as well as the urban layout. Bridges are also important elements of the cultural landscape, particularly Le pont et l'Église which, together with the medieval defensive ramparts, creates a unique panorama. Although the historic heritage of the town is related to its past, it also has a great impact on the urban development. Protecting their culture, tradition, historic architecture and urban design, the inhabitants and the authorities in Moret-Sur-Loing spare no effort to maintain the former climate of a medieval town. They are aware that for the sustainable development of the town to progress properly, they ought to preserve their heritage, revalorise it and allow it to survive for next generations. The article contains the characteristics of the cultural landscape of the town of Moret in the context of its protection and preservation for future generations, which constitutes an important factor of sustainable development. The town will certainly set a valuable example for other, also Polish, small historic towns.

Keywords: France, town, history, cultural heritage, architecture, urban design

1. Introduction

The town of Moret-Sur-Loing is located to the south of Paris, in the Île-de-France region, in the department of Seine and Marne. The town with the current population of less than 7,000 inhabitants is a very interesting example of a small historic French town with a rich cultural heritage. Protecting their culture, tradition and historic architecture and urban design, the inhabitants and the authorities in Moret-Sur-Loing spare no effort to maintain the former climate of

¹ Corresponding author: Dominika Kuśnierz-Krupa, Politechnika Krakowska, Wydział Architektury, ul. Podchorążych 1, 30-084 Kraków; tel. 126282419; dkusnierz-krupa@pk.edu.pl

a medieval town. The cultural landscape of Moret encompasses mainly historic buildings with the magnificent Notre Dame church and numerous small-town houses, defensive walls with gates and a donjon, as well as the urban layout. Bridges are also important elements of the cultural landscape, particularly Le pont et l'Eglise which, together with the medieval defensive ramparts, creates a unique panorama of Moret (fig. 1).

The aim of this article is characterising the most valuable elements of the cultural landscape of the historic town of Moret in the context of proper protection of its cultural heritage, so that it would survive for the next generations. Protecting cultural heritage is one of the pillars of the idea of sustainable development. Therefore, it can be claimed that the described town will set a valuable example for other small historic towns, particularly the ones located in Poland where both cultural heritage protection and the idea of sustainable development are not always satisfactorily realised.



Fig. 1. View of Moret-Sur-Loing from the north-east on an archive postcard from the 1st half of the 20th century. Postcard [in:] Author's Archive

2. Cultural heritage

Moret-sur-Loing was founded during the medieval period, although some scientists researching the origins of the town suggest a hypothesis about its Gaul-Roman roots. The early presence of man in the area has been confirmed by numerous archaeological finds in the form of prehistoric stone tools, pottery, objects and weaponry from bronze and iron.

The town was located on the River Loing, which is a tributary of the Seine (fig. 2, 3). The existing terrain conditions, primarily the vicinity of the aforementioned river, supported the defensive character of the place so important in the Middle Ages [1–3].

The early medieval urban layout constitutes a considerable value of the town. It is characterised by aiming at a regularity of the plan. However, that regularity is not complete here and does not allow for recognising the town as a defined, orthogonal layout. However, it can be regarded as a typical French town from the early medieval period [4].

The main street rue Grande runs through the centre of the layout, from the west to the east, and from one town gate to the other. In the centre of Moret it runs along the southern frontage of the market square. The remaining streets can be divided into those of primary (rue de la Pecherie, rue de l'Eglise, rue de la Tannerie, rue du Donjon, rue de Grez, rue du Pave Neuf, rue des Fosses and rue Ch. Geoffroy) and secondary importance (fig. 4, 5).

The market square is situated in the centre of the urban layout, and has the shape resembling a rectangle. It is rather small and surrounded by historic buildings representing various epochs (fig. 6a, b).



Fig. 4. Moret on an archive print from the 16th century. Author: Claude Chastillon.
Photo of the plan [in:] Author's Archive

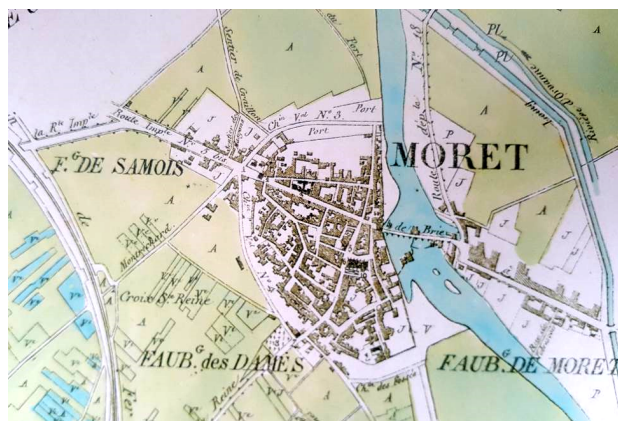


Fig. 5. Urban layout of Moret on the map from 1860. Copy of the map [in:] A. Didon: Moret-sur-Loing – Une cité au coeur de l'histoire..., Publ. Lys Editions Amatteis, 2008, p. 10



Fig. 6 a, b. The market square of Moret-sur-Loing, nowadays. Photo: D. Kuśnierz-Krupa, 2017

The medieval defensive perimeter is one of the most important cultural values of Moret. It was outlined in the 12th century and originally was 1,400 m long. It comprised the ramparts, the wall and 20 powerful towers some of which have survived till today. Three gates allowed access into the town. From the west it could be reached through the “Samois” gate (otherwise known as the “Paris” gate) where the road to Paris started. The gate was built soon after the walls had been erected, so still in the 12th century (fig. 7, 9). On the east side the “de Bourgogne” (Burgundy) gate was located, behind which there was the bridge on the River Loing and the road to Burgundy (fig. 8, 10). Both gates still exist today. It is worth noticing the fact that within the town both gates are



Fig. 7. “Samois” gate on an archive postcard from the 1st half of the 20th century. Copy of postcard [in:] Author’s Archive



Fig. 8. “De Bourgogne” gate on an archive postcard from the 1st half of the 20th century. Copy of postcard [in:] Author’s Archive



Fig. 9. “Samois” gate nowadays. View from the town. Photo: D. Kuśnierz-Krupa, 2017



Fig. 10. “De Bourgogne” gate nowadays. View from the river. Photo: D. Kuśnierz-Krupa, 2017

connected by one, straight communications route – rue Grande which runs as the main street through the entire town [3].

The third town gate in Moret was located on the south side of the town. It was called the “Grež” gate and it existed until the 19th century when it was demolished, possibly because of its poor state of preservation.

The Romanesque donjon, preserved till today, is an important element of the defensive layout of the town. Donjons were dwelling towers which were originally erected in the Romanesque style in France during the early medieval period (e.g. in Provins, Langeais, Fréteval, Loches, Bressuire and Beaugency [5].

The donjon in Moret was built in the south-east part of the town on the river, in the years 1128–1154 (during the same time as the Ganne tower in nearby Grez-Sur-Loing). Initially the donjon naturally fulfilled its residential function, serving as a royal seat. It was only during the reign of King Philip IV the Fair (1268–1314) that the tower was turned into a prison (fig. 11, 12).

During the following centuries the tower had various owners. It is worth mentioning, that towards the end of the 16th century it was renovated by Maximilien de Béthune de Sully (the Marshal of France and a minister to King Henry IV), who was its owner from 1594 to 1603, during the reign of Louis XIII. Then the donjon was restored to its former glory and once again became a residential object with an added garden complex.

Slightly later the building again began to serve as a jail. Nicolas Fouquet, the Superintendent of Finances in France during the reign of Louis XIV, accused of maladministration of the state funds in office, was kept in its dungeons.

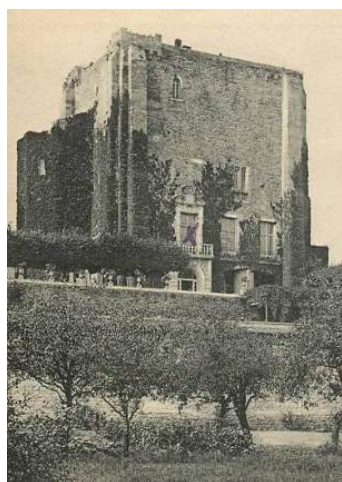


Fig. 11. Donjon from the south-east, on an archive postcard from the 1st half of the 20th century. Postcard [in:] Author's Archive



Fig. 12. Donjon from the north-west, nowadays. Photo: D. Kuśnierz-Krupa, 2017

The donjon was badly damaged during the French Revolution and remained in ruins until the 1870s. Then it was gradually revalorised by subsequent owners. However, a complete modernisation of that unique historic object was undertaken by Joanne Thirion who, with the help of an architect Pierre-Félix Julien and a team of artists and interior designers, converted a neglected donjon into a comfortable home [6]. Nowadays the overall ambience of the building is created by its Romanesque origins and the neo-Gothic elements introduced by the mentioned Pierre-Félix Julien.

An object of considerable cultural significance for the town is the Notre Dame church whose construction commenced around the year 1140. It might have been erected on the site of an earlier church. It is assumed that the church was consecrated by Thomas Becket, Archbishop of Canterbury. The church was built in stages and completed only as late as the 16th century, after the Hundred Years' War.

Notre Dame is a Gothic church. Its interior shaped throughout centuries makes an unforgettable impression. The apse is 46 m tall, while the nave reaches 21 metres. The harmony of interior decoration and lighting enhance the impression of spaciousness inside the church. The pilasters in the main nave dated back to the 14th century are decorated with small frescoes depicting the figures of saints: Matthew, Paul, Peter, John etc. (fig. 13, 14).

On the north side of the choir the bulk of the church is adjoined by a lavishly decorated bell tower. Nowadays it leans slightly sideways in relation to the vertical buttresses of the side aisles.

Most church furnishings were plundered or destroyed during the revolution. Some historic items e.g. a 13th-century baptismal font, a large wooden figure of Christ, a 17th-century clock and a 15th-century door to the chancel have survived until today [7].



Fig. 13. Notre Dame church from the south-east on an archive postcard from the 1st half of the 20th century. Postcard [in:] Author's Archive



Fig. 14. Notre Dame church from the south-east, nowadays. Photo: D. Kuśnierz-Krupa, 2017

The buildings in Moret date back to the various periods of the town's prosperity, though naturally their origins are rooted in the Middle Ages. It is worth paying attention to unique examples of Renaissance architecture with their valuable decorations in e.g. the town hall or the house of King Francis I. Other historic buildings are houses from the 18th and 19th century, partially renovated but still maintaining their historic value which allows them to still constitute an important element of the cultural landscape of Moret.

To sum up, it should be emphasised that most elements of the cultural landscape of the town have already been revalorised. That remark refers to the town walls and gates, and the most important public utility objects. The remaining ones, such as e.g. historic houses are systematically renovated in accordance with the conservation guidelines and taking care of the colour scheme, materials and details. The greatest value of Moret is its authenticity, both real and created owing to proper revalorisation, the conservation policy of the town authorities and the attitude of its inhabitants.

3. Conclusion – Protection, revalorisation and sustainable development

The historic heritage of the town, despite being related to its past, has also a huge impact on its development. Scientific publications addressing the issue of sustainable development never belittle the importance of cultural heritage in this process so crucial for the future of mankind. It is worth remembering here that sustainable development denotes changing the reality in such a way that the development would optimally satisfy the needs of modern man, while not violating the needs of future generations [8, 9]. Therefore, in order for the sustainable development of a given town to progress properly, its local authorities and inhabitants should protect their heritage, restore it and allow it to survive until the next generation. It is a lengthy process, an example of which is the town of Moret-sur-Loing that consistently tries to preserve its historic heritage and tradition, and build its future on those values. It ought to be emphasised that for many years French towns have effectively combined the policy of sustainable development with multi-plane cultural context that is one of the five contexts in the process of spatial planning [10].

The presented example of Moret-sur-Loing as a small French historic town in the context of the state and revalorisation of its historic heritage should be regarded as appropriate and valuable. The building development structure within the historic perimeter of defensive walls has not been modified. Houses have preserved their size, form, and most importantly the character of a small French historic town. Modern buildings develop outside the historic defensive perimeter. The need to protect that heritage is understood both by the local authorities and the town inhabitants. A similar situation occurs in the case of the historic urban layout which has preserved its original medieval character within the historic town. The consequences of protecting that spatial structure should also be emphasised.

The town of Moret-sur-Loing is one of many examples, besides e.g. Heppenheim, Lorsch, Weinheim or Provins, of small European historic towns which can effectively use their cultural potential for a multidirectional development of their towns [11, 12]. Thanks to initiatives concerning revalorisation of monuments, their accessibility to the public, promotion and documentation, not only do they protect their heritage for future generations, which is one of the directions of sustainable development, but also create new infrastructure relating to tourism, new workplaces and thus very comfortable living conditions.

References

- [1] Pougeois L. A.: L'Antique et royale cité de Moret-sur-Loing, Publ. Le Livre d'histoire, 2001, pp. 2–7.
- [2] Viatte J.: Moret-Sur-Loing, Publ. Le Livre d'histoire, 2004.
- [3] Didon A.: Moret-sur-Loing – Une cité au coeur de l'histoire..., Publ. Lys Editions Amatteis, 2008, pp. 8–13.
- [4] Gutkind E.A.: Urban development in western Europe: France and Belgium, vol. V, Nowy Jork – Londyn, 1970, pp.11–40.
- [5] Châtelain A.: Donjons romans des pays d'ouest. Étude comparative sur les donjons romans quadrangulaires de la France de l'Ouest. A. et J. Picard, Paris 1973.
- [6] Restauration du patrimoine – patrimoines en Seine-et-Marne, Publ. Conseil Général de Seine et Marne, 2011, s. 5–19.
- [7] Tribhout, A.: Moret-sur-Loing: son église, Moret-sur-Loing 1970.
- [8] Kuśnierz-Krupa D., Krupa M.: Messesstad Riem Messestadt Riem w Monachium jako modelowy przykład zrównoważonej dzielnicy miejskiej, „Czasopismo Techniczne”, no 3-A/2007, PK, p. 172.
- [9] Böhm A., Heczko-Hyłowa E.: Introduction, [in:] A sustainable development of Polish cities as a New challenge to spatial planning and management, E. Heczko-Hyłowa (edit.), Publ. PK, Kraków 2001, pp. 9–11.
- [10] Heczko-Hyłowa E.: Koncepcja zrównoważonego rozwoju miast we francuskim systemie planowania urbanistycznego, [in:] A sustainable development of Polish cities as a New challenge to spatial planning and management, E. Heczko-Hyłowa (edit.), Publ. PK, Kraków 2001, pp. 81–98.
- [11] Kuśnierz-Krupa D., Krupa M.: Heppenheim a model example of well – used cultural potential of a small town, „Czasopismo Inżynierii Lądowej, Środowiska i Architektury – Journal of Civil Engineering, Environment and Architecture – JCEEA”, vol. 34, iss. 64, no 3/2, 2017, pp. 161–180, DOI:10.7862/rb.2017.162.
- [12] Kuśnierz-Krupa D., Krupa M.: Lorsch – Carolingian heritage. Introduction to research on the cultural heritage of the town, „Wiadomości Konserwatorskie – Journal of Heritage Conservation, no 50/2017, pp. 20–29.

Przesłano do redakcji: 18.03.2018 r.

Przyjęto do druku: 31.03.2018 r.

Agata ZDYB¹
Piotr DRAGAN²
Arkadiusz JAREMEK³

THE ANALYSIS OF THE SOLAR POWER PLANT PERFORMANCE IN TEMPERATE CLIMATE

Due to gradual depletion of fossil fuels resources and emission of harmful chemicals accompanying the combustion process, the interest in alternative energy sources still increases. Among many kinds of alternative sources, solar radiation is very special because of its wide availability and large technical potential. Photovoltaic systems providing the electric energy are used in many countries. The most important part of photovoltaic system is a module, which parameters (e.g. efficiency, rated power, temperature coefficients of power and efficiency, short circuit current, open circuit voltage) are determined in laboratory tests under Standard Test Conditions (STC: 25°C, 1,000 W/m², air mass 1.5). However, in real outdoor conditions the modules exhibit lower efficiency since local climate influences their performance and different external factors generate energy losses in the whole system. The aim of this work is the performance analysis of a solar power plant connected to the grid, which total rated power is 2.985 MW and it works in temperate climate in eastern Poland. Insolation in the location was estimated according to Solargis data and the role of the modules tilt angle, of which the value is non-typical for the considered location was studied. The tilt angle smaller than optimal angle allows increasing the amount of the solar radiation collected in the summer period. The electric energy production based on the inverters data in 2016 and 2017 as well as yearly yield are presented. The results are compared to data coming from other solar power plants, also located at high latitude.

Keywords: photovoltaics, grid connected solar plant, photovoltaic performance, inclination angle, tilt angle

1. Introduction

The Polish National Renewable Action Plan required by the EU Renewable Energy Directive (2009/28/EC) predicts that electricity from all renewable energy

¹ Corresponding author: Agata Zdyb, Politechnika Lubelska, Wydział Inżynierii Środowiska, ul. Nadbystrzycka 40B, 20-618 Lublin, tel: 81538 4747, a.zdyb@pollub.pl

² Piotr Dragan, Politechnika Lubelska, Wydział Inżynierii Środowiska, ul. Nadbystrzycka 40B, 20-618 Lublin, tel: 81538 4747, piotr.dragan@wisznice.pl

³ Arkadiusz Jaremek, Politechnika Lubelska, Wydział Inżynierii Środowiska, ul. Nadbystrzycka 40B, 20-618 Lublin, tel: 81538 4747, arek.jaremek@gmail.com

sources (RES) should reach 19.13% of the final energy supply and their total share should achieve 15.5% in the gross final energy consumption by 2020. Since 2009, in Poland, some progress has been made in using of RES, especially wind, biomass and solar energy. Among many kinds of RES the Sun is the largest source, which can be considered as an infinite one from our perspective. The power of the solar radiation incoming to the Earth equals 120,000 TW annually and the solar radiation can be harnessed in all areas of the world [1]. Current energy demand equals to 15 TW and is supposed to grow up to 35 TW in 2050. Solar energy is a valuable alternative to fossil fuels combustion as it allows reduction of the release of harmful chemicals like oxides of carbon, sulfur and nitrogen as well as dust [2].

In 2017 in Poland cumulative installed photovoltaic (PV) capacity exceeded 200 MW (overall of 420 GW is installed in Europe) and nowadays it accounts for 2.3% of all renewable energy and 0.5% of the total capacity installed in the Polish energy system [3]. At present, according to the legal regulations introduced in 2016, net metering (up to 40 kW) and an auction mechanism for large-scale projects (over 40 kW) are two ways supporting photovoltaics, which replaced the green certificate mechanism in July 2016 (according to Renewable Energy Law introduced in Poland in 2015).

The most important parameter that has to be taken into account at the planning stage of photovoltaic system is solar irradiation. In Poland yearly irradiation is in the range of 950–1,250 kWh/m² at south azimuth and horizontal plane. Average value of irradiation is equal to 1,289 kWh/m² at 30° of inclination angle [4]. The important parameter that provides information about the access to solar energy in a given location is also sunshine duration expressed in hours, which is a general indicator of cloudiness and depends on the length of the day and kind of season. In Poland most of PV installations are situated in the SE part of the country due to good insolation and favorable values of the sunshine duration (1680 h) compared to other locations. In this region in 2017 over 80 MW were connected to the grid. The solar power plant where we perform our investigations is also located in this part of the country.

The role of the location of PV systems is widely analyzed. In the given place various climate elements influence the performance of PV installations [5–7]. The most important factors are: solar irradiation, ambient temperature, wind speed, however it is worth to notice that spectral changes, humidity and dust also have a significant impact on the PV performance. The particular location, especially the latitude value, determines also the inclination angle of the modules due to changes of Sun declination.

This paper is devoted to analysis of the performance of the solar plant situated in eastern Poland, under temperate climate conditions. The results of energy production are correlated with annual irradiation changes and the role of inclination angle of the modules, which differs from the optimum value, is also discussed.

2. Experimental facility

The entire capacity of the studied plant, situated in eastern Poland (longitude 22°54'E, latitude 51°10'N), is equal to 2.985 MW. There are two separate parts of the plant (0.995 MW and 1.99 MW), and both of them consist of typical pc-Si modules (Fig. 1), which are the most popular kind of modules in both residential PV systems and plants. Detailed specification of the modules is presented in Table 1. The values of crucial parameters such as efficiency, fill factor as well as temperature coefficient are determined in laboratory tests and provided by the manufacturer. The modules are oriented horizontally and inclined at an angle of 25°. The role of this non-typical inclination angle is discussed further. In addition to modules, other components such as 51 three-phase inverters Powador 30.0 TL3, transformer stations and steel construction elements were used.

Table 1. Technical data of modules (according to manufacturer datasheet)

Module type	Selfa SV60P.3
Dimensions	1.670 m × 0.983 m
Weight	19.4 kg
Maximum power	250 Wp
Fill factor	76.7%
Efficiency	15.3%
Temperature coefficient of power	- 0.42%/°C



Fig. 1. Photovoltaic power plant in eastern Poland

3. Results

The optimum inclination angle of PV array depends mainly on the latitude. The approximate values of optimum inclination angle can be determined according to the following formulas [8]:

$$\beta_{opt} = \varphi - \delta \quad (1)$$

in which δ – Sun declination, φ – latitude,

$$\beta_{opt} = \varphi \pm 10^\circ \quad (2)$$

where the positive and negative signs are used for winter and summer respectively [9],

$$\beta_{opt} = \varphi \pm 15^\circ \quad (3)$$

or it can be just equal to latitude [10].

Since the above simple calculation methods lead to different results, to improve the PV performance the year fixed accurate optimum tilt angle should be evaluated carefully in a particular region, not only on the basis of available solar radiation. At the latitude of about 51° , where the studied solar power plant is located optimal inclination angle changes from 15° in June to 64° in December. Because of the annual movement of the Sun there are significant differences of irradiance: from 218 W/m^2 at south azimuth in December to 570 W/m^2 at south azimuth and optimum inclination angle in July. At the described plant the modules are tilted 25° to the ground. The irradiation on the module plane at this untypical angle differs from the values obtained for the plane inclined at the optimal angle equal to 35° for the considered latitude. The estimates of long-term monthly irradiation averages in both cases are presented in Table 2.

According to Table 2, the average daily irradiation at the optimum angle is equal to $1.8 \text{ kWh/m}^2/\text{day}$ in winter and $5.065 \text{ kWh/m}^2/\text{day}$ in summer. At the angle of 25° the daily irradiation value in winter is smaller and equals to $1.75 \text{ kWh/m}^2/\text{day}$, in summer this value is higher, equal to $5.1 \text{ kWh/m}^2/\text{day}$. The tilt angle of 25° ensures thus better usage of available solar radiation in summer than the typical angle of 35° . Taking into account a correction factor of 1.12 [6], average yearly irradiation at the plane tilted by 25° is equal to $1,266 \text{ kWh/m}^2$. The amount of electric energy produced by the solar plant in year 2016 and 2017 is presented in Figs. 2, 3. In the warm half of the year (April to September) the generated electric energy is much higher than in cold part of the year (October to March) and achieves 78% of the total value.

Table 2. The irradiation on the plane tilted at 35° and 25° (south azimuth, latitude 51°), according to PVGIS data [11]

Month	Irradiation on optimally inclined plane [Wh/m ² /day]	Irradiation on plane at angle 25° [Wh/m ² /day]
January	1,020	938
February	1,680	1,590
March	3,680	3,530
April	4,890	4,830
May	5,450	5,540
June	5,530	5,690
July	5,410	5,530
August	5,160	5,150
September	3,950	3,830
October	2,700	2,530
November	1,240	1,150
December	844	771
YEAR average	3,470	3,430

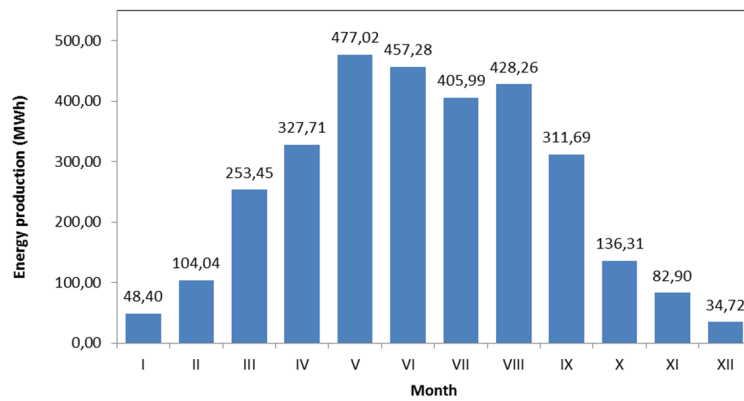


Fig. 2. Energy production in 2016

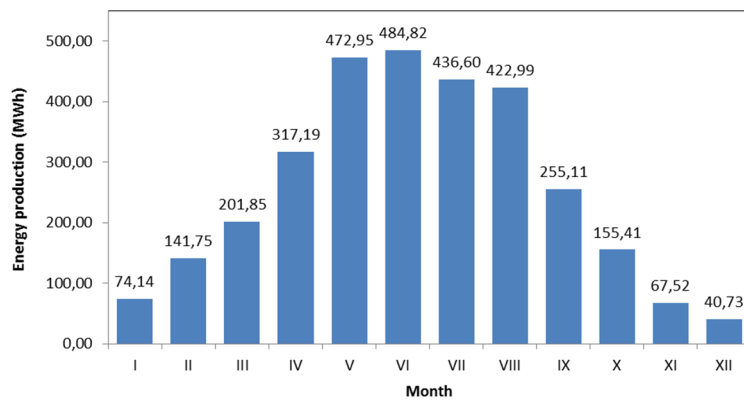


Fig. 3. Energy production in 2017

Basing on the energy production data, performance ratio, which is an important parameter characterizing the PV system, can be calculated according to the following equations:

$$PR = \frac{Y_f}{Y_r} \quad (4)$$

$$Y_f = \frac{E_o}{P_{DC}} \quad (5)$$

$$Y_r = \frac{Irr_p}{Irr_r} \quad (6)$$

in which: Y_f – final yield;

Y_r – reference yield;

E_o – final energy output [kWh];

P_{DC} – nominal DC power [kW];

Irr_p – total in-plane irradiation [kWh/m²];

Irr_r – PV reference irradiance [kW/m²].

PV reference irradiance is equal to 1,000 W/m². The performance ratio determined for the analyzed solar plant according to irradiation and energy output data of the PV system is equal to 81% which is a good value. The final yield of the photovoltaic power plant was compared with analogues values determined for other PV systems in Europe, including installations in countries located at higher latitudes such as Sweden, United Kingdom and Germany. The data in Table 3 show that the obtained final yield value is of the same order as in other places.

Table 3. The comparison of the data coming from different PV plants in Europe, according to data [12]

Plant location	Geographic coordinates	Nominal DC power [MWp]	Final energy output [MWh/year]	Yield, Y_f [kWh/Wp]
Kallinge Sweden	56°24'N 15°29'E	0.2	198	0.99
Liverpool United Kingdom	53°24'N 2°59'W	0.2	221	1.05
Trawniki Poland	51°10'N 22°54'E	3.0	3,068	1.03
Sława Poland	51°52'N 16°04'E	0.2	219	1.10
Bordziłówka Poland	51°51'N 23°10'E	1.4	1,530	1.09
Espenhain Germany	51°12'N 12°31'E	5.0	5,000	1.00
Cruas France	44°39'N 4°45'E	1.2	1,800	1.45
Pagliare de Tronto Italy	42°86'N 13°77'E	0.2	235	1.18

4. Conclusions

At high latitude where the photovoltaic power plant is situated the solar irradiation received in the warm half of the year is significantly higher than in the cold part of the year. In the considered location, the inclination of photovoltaic modules at a smaller angle (25°) than the yearly optimum angle (35°) enables the collection of more solar radiation in summer which is reflected in high electric energy production during this period. Because of the significant differences between insolation in summer and winter at higher latitudes it would be worth considering applying the inclination angle smaller than the optimum value and subsequently giving priority to the collection of radiation in summer over the collection in winter. In addition to the variation of insolation it is also important that in the cold part of the year snowfall often occurs and residual snow causes shading and losses in energy production during this period. Therefore the horizontal orientation of modules, as in the case of the analyzed plant, is also a good solution that reduces negative consequences of residual snow.

References

- [1] Wolden C.A., Kurtin J., Baxter J.B., Repins I., Shaheen S.E., Torvik J.T., Rockett A.A., Fthenakis V.M., Aydil E.S.: Photovoltaic manufacturing: Present status, future prospects, and research needs, *Journal of Vacuum Science and Technology A*, vol. 29, 2011, pp. 030801-1 – 030801-16.
- [2] Dragan P., Zdyb A.: Reduction of Pollution Emission by Using Solar Energy in Eastern Poland, *Journal of Ecological Engineering*, vol. 18, 2017, pp. 231–235.
- [3] Report “Photovoltaic Market in Poland 2017”, Institute for Renewable Energy 2017.
- [4] Šuri M., Cebecauer T., Skoczek A.: Solar Data and Online Applications for PV Planning and Performance Assessment, *Proceedings of 26th European Photovoltaics Solar Energy Conference*, September 2011, Hamburg, Germany, pp. 4648–4651.
- [5] Faiman, D.: Assessing the Outdoor Operating Temperature of Photovoltaic Modules, *Progress of Photovoltaics: Research and Applications*, vol. 16, 2008, pp. 307–315.
- [6] Gökmen N., Hu W., Hou P., Chen Z., Sera D., Spataru S.: Investigation of wind speed cooling effect on PV panels in windy locations, *Renewable Energy*, vol. 90, 2016, pp. 283–290.
- [7] Zdyb A., Krawczak E.: The influence of external conditions on the photovoltaic modules performance, *Environmental Engineering V*, eds.: M. Pawłowska, L. Pawłowski, CRC Press Taylor&Francis Group 2017, pp. 261–266.
- [8] Pluta Z.: *Podstawy teoretyczne fototermicznej konwersji energii słonecznej*, Oficyna Wydawnicza Politechniki Warszawskiej, Warszawa 2000.
- [9] Lunde P.J.: *Solar thermal engineering*, Wiley, New York 1980.
- [10] Jain D., Lalwani M.: A Review on Optimal Inclination Angles for Solar Arrays, *International Journal of Renewable Energy Research D.*, vol. 7, 2017, pp. 1053–1061.
- [11] <http://photovoltaic-software.com/pvgis.php> {dostęp 10.04.2018}.
- [12] <https://www.sunnyportal.com/> {dostęp 10.04.2018}.

Przesłano do redakcji: 18.03.2018 r.

Przyjęto do druku: 31.03.2018 r.

Jakub JURA¹
Małgorzata ULEWICZ²

IMPACT OF GLASS AND CERAMIC WASTE ON SELECTED PROPERTIES OF MATERIALS WITH A CEMENT

The article presents the impact of selected waste materials (usable ceramics, sanitary ceramics, CRT glass cullet) on the physical and mechanical properties of cement-based materials (cement mortars). The samples of cement mortars made were 10, 20 and 30% addition of waste material. Physical and mechanical properties of modified cement mortars were compared with standard mortar. The highest compressive strength obtained mortar with the addition of usable and sanitary ceramics in the amount of 30%. The mortar was also characterized by the lowest decreases in compressive strength after frost resistance tests. The use of 30% sanitary ceramics resulted a compressive strength drop of 3.5% compared to 18% for the standard mortar. The absorbability of all samples differed slightly.

Keywords: cement mortars, mechanical properties, utilitarian ceramics, sanitary ceramics, CRT glass

1. Introduction

The development of industry and economy causes an increase in post-production and post-use waste. Many of the generated waste creates difficulties during processing, while others do not apply and are completely deposited in landfills. This results in a threat to the natural environment and obliges the public to look for new pro-ecological technologies for their management.

One of the sectors that produces large amounts of waste materials is construction. This sector, and especially the construction materials sector, also offers opportunities for managing different types of post-use and post-production waste emerging in other sectors of the economy (dust and slag from the steel industry, waste from the glass industry, waste from polymer processing). On the laboratory scale, attempts are made to use construction waste materials such as demolition materials [1, 2], ceramic hollow bricks [3, 4], sanitary ceramics [5–8],

¹ Corresponding author: Jakub Jura, Politechnika Częstochowska, Wydział Budownictwa, ul. Akademicka 3, 42-201 Częstochowa; jura@bud.pcz.czyst.pl

² Małgorzata Ulewicz, Politechnika Częstochowska, Wydział Budownictwa, ul. Akademicka 3, 42-201 Częstochowa; ulewicz@bud.pcz.czyst.pl

fibers and glass waste [9–11], rubber waste [12], polymeric materials [13], cork [14], rice husks [15, 16], or ashes from the co-firing of biomass [17, 18]. The use of waste requires each time to determine their physicochemical properties and physical and mechanical properties of the newly created building materials. This paper attempts to determine the impact of selected ceramic and glass waste on the strength of cement mortars.

2. Research procedure

The research used utility ceramics (post-production waste of pots and covers), sanitary ceramics (used sinks and toilet seats) and cracked glass CRT (glass from the screen and a cone of used monitors), and crushed to a fraction of 0.0–2.0 mm using a jaw crusher and disintegrator (Fig. 1). Fragmentation the waste after crushing had sharp edges, characteristic for broken aggregate. The chemical composition of the tested materials determined using X-ray fluorescence presented Table 1.



Fig. 1. Shredded: a) utilitarian ceramics waste, b) sanitary ceramics waste, c) CRT glass

Cement mortar samples were made using Portland cement CEM I 42.5 R (Cemex), standard sand (Kwarcmix) and tap water with pH 7.7 and $Cl^- = 31 \text{ mg/dm}^3$ and $NO_3^- = 37 \text{ mg/dm}^3$ from the intake Czestochowa. The composition of the tested cement mortars is shown in Table 2. Standard mortar (PK) and mortar samples were made, in which 10, 20 and 30% of the cement mass was replaced with functional ceramics (CU1–CU3), sanitary ceramics (CS1–CS3) or glass cullet (SS1–SS3). The waste was used as a substitute for standard sand.

Table 1. Chemical composition of the investigated waste

Compound	Chemical composition, %		
	Usable ceramics	Sanitary ceramics	CRT cullet
SiO ₂	58.2	69.8	60.4
CaO	6.9	0.5	0.8
K ₂ O	2.0	2.7	4.0
Al ₂ O ₃	19.3	22.4	1.5
Na ₂ O	1.3	1.6	5.6
MnO	1.0	0.6	0.6
PbO	-	-	11.6
SrO	-	-	5.2
Inne	11.3	2.4	10.3

Table 2. Composition of cement mortars – mixing ratios

Composition	Series									
	PK	CU1	CU2	CU3	CS1	CS2	CS3	SS1	SS2	SS3
Cement, g	450	450	450	450	450	450	450	450	450	450
Water, cm ³	225	225	225	225	225	225	225	225	225	225
Standard sand, g	1,350	1,305	1,260	1,215	1,305	1,260	1,215	1,305	1,260	1,215
Usable ceramics, g	-	45	90	135	-	-	-	-	-	-
Sanitary ceramics, g	-	-	-	-	45	90	135	-	-	-
CRT cullet, g	-	-	-	-	-	-	-	45	90	135
Waste, %	0	10	20	30	10	20	30	10	20	30

The beams with dimensions 40×40×160 mm were made in accordance with PN EN 196-1. The products were arranged in forms after making the mixture, compacted and covered with a glass plate and left for 24 hours. After this time they were demoulded and put into water at 20°C. After 28 days, compressive strength, frost resistance and water absorption tests were performed on the bars. The compressive strength test (average of 6 samples) was carried out on the tails halves with an accuracy of 0.1 MPa on a Tonitechnic hydraulic press and the compressive strength was determined with such accuracy. Measurements of compressive strength after frost resistance tests (average of 6 samples) were performed after 25 cycles of freezing and thawing in the Toropol machine.

3. Methodology and test results

Samples of cement mortars were subjected to compressive strength tests after 28 days. The control sample (PK) obtained a compressive strength of

47.4 MPa (Fig. 2). With the increase in the addition of utilitarian ceramics, an increase in the strength value of the beams was observed by 1–4% in comparison with the control beams. The highest compressive strength obtained samples containing 30% of utilitarian ceramics. The use of sanitary ceramics resulted in greater disparities between the three series of mortars. Compressive strength increased as the amount of additive grew (0.5% to 8.5%), relative to the standard mortar. An addition to the cement mortar CRT cullet increased the average compressive strength only for the series with the addition of 10% waste.

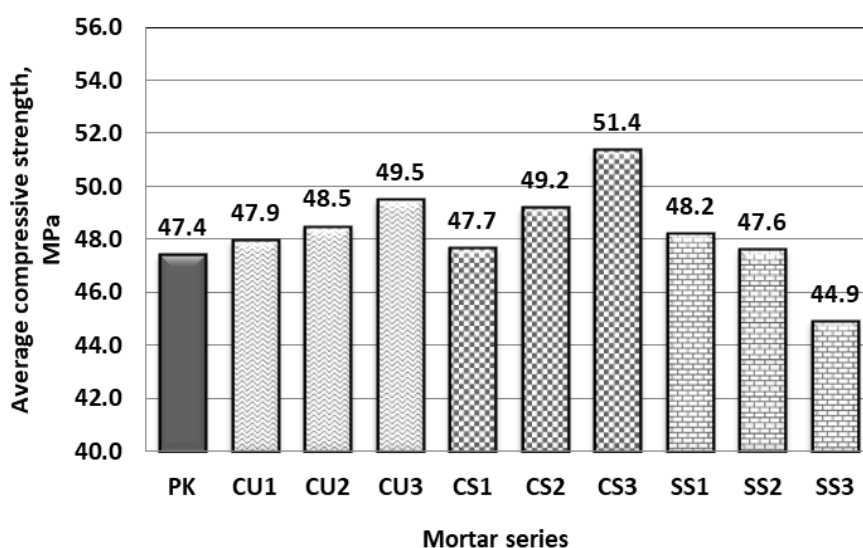


Fig. 2. Average compressive strength of investigated cement mortars

In the next stage of the tests, the frost resistance of the beams was determined in accordance with the PN-88/B-06250 standard. Samples of 28 days in water were weighed and subjected to 25 freezing cycles at $-18^{\circ}\text{C} \pm 2^{\circ}\text{C}$ for 4 hours and thawing in water at $+18^{\circ}\text{C} \pm 2^{\circ}\text{C}$ for 4 hours. Then they were weighed again and subjected to compressive strength tests. The obtained results were presented as a percentage decrease in compressive strength after frost resistance tests compared to witness samples that were not frozen. The decrease in compressive strength after freezing tests of standard mortar amounted to 18.2% (Fig. 3). Samples with sanitary ceramics obtained the smallest drop in resistance to dripping in abrasion with samples of waste household ceramics or CRT glass. Samples with sanitary ceramics had the smallest drop in compressive strength in comparison to samples of consumer ceramic waste or CRT glass. The lowest decrease in compressive strength after frost resistance tests was observed in bars with the addition of 30% of utilitarian and sanitary ceramics, which amounted to 5.5% and 3.5%. The mortar beams contain the glass cullet and have slightly less dips in the resistance to dripping than the standard mortar.

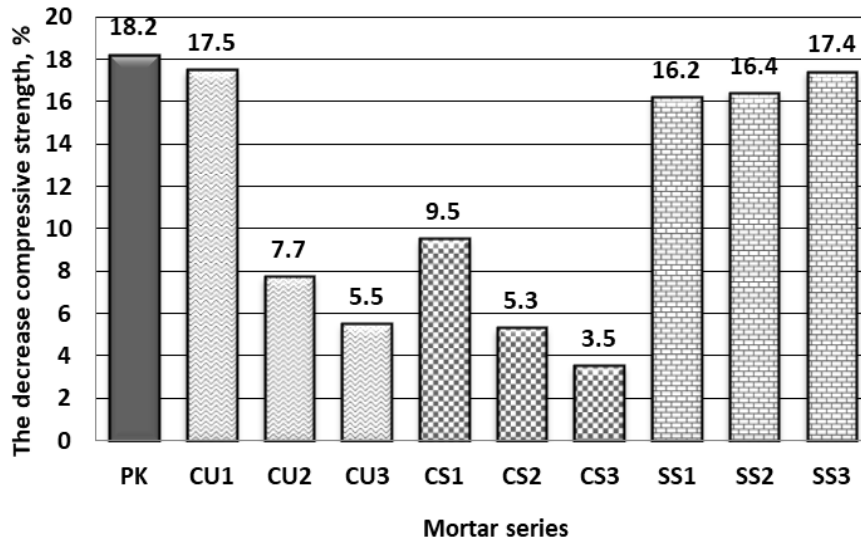


Fig. 3. Decrease compressive strength of the cement mortars after frost resistance tests

Another test carried out was absorbability of cement mortars. Samples after 28 days of being in water to obtain a constant weight, were dried at 105°C to obtain differences between weighings not exceeding 0.1%. The standard mortar has achieved an absorption of 8.5% (Fig. 4). The absorbability of the other cement mortars made was only slightly different. It can be noticed that the increasing amount of each of the additives increased the absorbability of cement mortar beams.

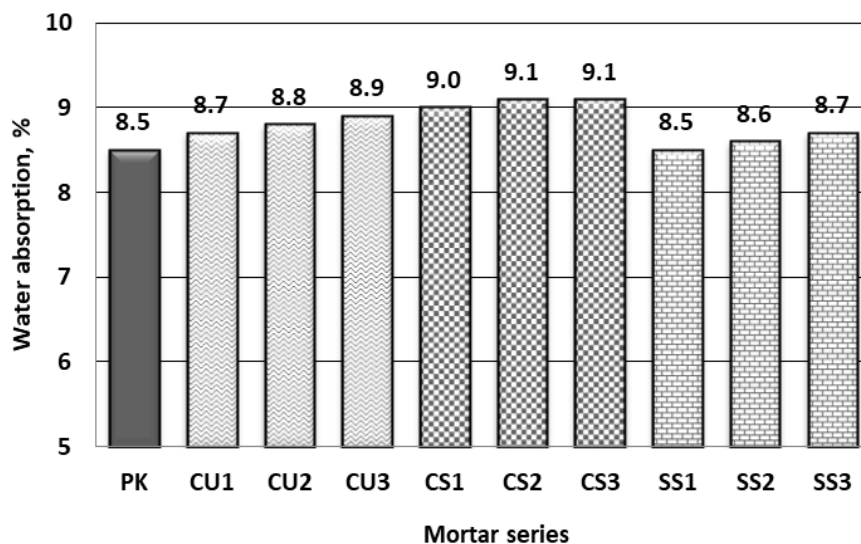


Fig. 4. Water absorption of cement mortars

4. Conclusions

The research results showed that waste materials can be used as a substitute for sand in cement mortars. The use of usable and sanitary ceramics in the amount of 10, 20 and 30% causes an increase in the average compressive strength with the increase of the additive amount. However, in the case of CRT cullet, an increase in compressive strength was observed only for a series of mortars containing 10% of waste material. The use of utilitarian ceramics and sanitary ceramics reduces the decrease of compressive strength of cement mortars after 25 freezing cycles. The lowest drop of compressive strength (3.5%) was found in cement mortar samples containing 30% sanitary ceramics. The addition of CRT glass cullet did not have much impact on this mortar property. The use of waste materials had little effect on water absorption of mortars. The difference between the results obtained by the standard mortar and mortar with waste materials was a maximum of 0.6%.

References

- [1] Chen H., Yen T., Chen K., Use of building rubbles as recycled aggregates, *Cement and Concrete Research*, 33, 2003, 125–132.
- [2] Yuan F., Shen L., Li Q., Energy analysis of the recycling options for construction and demolition waste, *Waste Management*, 31, 2011, 2503–2511.
- [3] Binici H., Effect of crushed ceramic and basaltic pumice as fine aggregates on concrete mortars properties, *Construction and Building Materials*, 21, 2007, 1191–1197.
- [4] Malaiskiene J., Vaiciene M., Zurauskiene R., Effectiveness of technogenic waste usage in products of building ceramics and expanded clay concrete, *Construction and Building Materials*, 25, 2011, 3869–3877.
- [5] Halicka A., Ogrodnik P., Zegardło B., Using ceramic sanitary ware waste as concrete aggregate, *Construction and Building Materials*, 48, 2013, 295–305.
- [6] Halicka A., Zegardło B., Odpady ceramiki sanitarnej jako kruszywo do betonu, *Przegląd budowlany*, 7–8, 2011, 50–55.
- [7] Medina C., Frías M., Sánchez de Rojas M.I., Thomas C., Polanco J.A., Gas permeability in concrete containing recycled ceramic sanitary ware aggregate, *Construction and Building Materials*, 37, 2012, 597–605.
- [8] Medina C., Frías M., Sánchez de Rojas M.I., Microstructure and properties of recycled concretes using ceramic sanitary ware industry waste as coarse aggregate, *Construction and Building Materials*, 31, 2012, 112–118.
- [9] Ismail Z., Hashmi E., Recycling of waste glass as a partial replacement for fine aggregate in concrete, *Waste Management*, 29, 2009, 655–659.
- [10] Langier, B., Pietrzak A., Innovative cement used in concrete technology, *Construction of optimized energy potential*, 1(17), 2016, 41–46.
- [11] Park S., Lee B., Studies on expansion properties in mortar containing waste glass and fibers, *Cement and Concrete Research*, 34, 2004, 1145–1152.

- [12] Lia G., Garricka G., Eggersb J., Abadie C., Stubblefield M., Pang S., Waste tire fiber modified concrete, *Composites: Part B*, 35, 2004, 305–312.
- [13] Asokan P., Osmani M., Price A., Assessing the recycling potential of glass fibre reinforced plastic waste in concrete and cement composites, *Journal of Cleaner Production*, 17, 2009, 821–829.
- [14] Panesar D.K., Shindman B., The mechanical, transport and thermal properties of mortar and concrete containing waste cork, *Cement & Concrete Composites*, 34, 2012, 982–992.
- [15] Chao-Lung H., Anh-Tuan B. L., Chun-Tsun Ch., Effect of rice husk ash on the strength and durability characteristics of concrete, *Construction and Building Materials*, 25, 2011, 3768–3772.
- [16] Van Tuan N., van Breugel G. Ye, K., Fraaij A. L.A., Dai B. D., The study of using rice husk ash to produce ultra-high performance concrete, *Construction and Building Materials*, 25, 2011, 2030–2035.
- [17] Kosior-Kazberuk M., Odporność betonów zawierających popiół lotny ze współpalania węgla kamiennego i biomasy na wnikanie jonów chlorkowych, *Budownictwo i Inżynieria Środowiska*, 1, 2010, 131–136.
- [18] Wang S., Miller A., Llamazos E., Fonseca F., Baxter L., Biomass fly ash in concrete: mixture proportioning and mechanical properties, *Fuel*, 87, 2008, 365–371.

Przesłano do redakcji: 26.03.2018 r.

Przyjęto do druku: 31.03.2018 r.

Wojciech RADWAŃSKI¹
Tomasz PYTLOWANY²
Izabela SKRZPCZAK³

THE ANALYSIS OF ROAD BUILDING TECHNOLOGY WITH A DATA NORMALIZATION METHOD

The paper presents a data normalization method for processing the data that makes it possible to choose the road building technology. There are two technologies for road construction, a flexible one and a rigid one, and both of them have their advantages and disadvantages. The main advantage of rigid pavement lays on the fact that it doesn't require higher financial expenditures within 30 years of exploitation (provided that necessary pavement maintenance treatments are carried out). In the case of flexible pavement it is necessary to mill the wear off layer of the road already after 9 years. It leads to the question: which of these technologies should be chosen, which one is better? The problem of the choice of technology for road building still remains to be unresolved.

The work hereby carries on the analysis concerning a comparison of the technologies for road building; the flexible pavement and the rigid pavement. Based on the analysis carried out using the data normalization method it was found that the achieved values of synthetic coefficient for flexible and rigid pavements are close to each other which may indicate that both technologies are comparable within the sectors taken for analyses in relation to accepted technological-technical and usability features.

Keywords: road, pavement, choice, data normalization method

1. Road - categories and classes

In Poland the road category is connected with its function in a road network. The Bill of Public Roads [2] distinguishes the following road categories: state roads, provincial roads, district roads and community roads. A road included in one of these categories, in the understanding of Bill [2] of Public Roads, must meet the technical and usability requirements determined for the following classes:

¹ Corresponding author: Wojciech Radwański, Państwowa Wyższa Szkoła Zawodowa w Krośnie, Instytut Politechniczny, Zakład Budownictwa, ul. Rynek 1, 38-400 Krosno, r74@o2.pl

² Tomasz Pytlowany, Państwowa Wyższa Szkoła Zawodowa w Krośnie, Instytut Politechniczny, Zakład Budownictwa, ul. Rynek 1, 38-400 Krosno, tompyt@pwsz.krosno.pl

³ Izabela Skrzypczak, Politechnika Rzeszowska, Wydział Budownictwa, Inżynierii Środowiska i Architektury, ul. Poznańska 2, 35-959 Rzeszów, izas@prz.edu.pl

- State road – A (motorway), S (express road) or GP (main road for accelerated traffic),
- Provincial road – GP (main road for accelerated traffic) or G (main),
- District road – GP (main road for accelerated traffic), G 9 (main) or Z (collect),
- Community road – GP (main for accelerated traffic), G (main), Z (toll), l (local) or D (access roads).

The road class determines technical and usability requirements. The decree of the Minister of Infrastructure of March 2, 1999 concerning technical conditions to be met by public roads and their location (Dz. U. No 43, pos. 430, with later amendments)[3] introduces the division of roads into the following classes: motorways, express roads, main roads for accelerated traffic, main roads, toll roads, local roads and access roads.

Assignments concerning road building, re-building, repair, maintenance, protection and administration and financed by:

- Minister responsible for road transport via General Director for National Roads and Motorways in relation to state roads,
- Provincial self-government administrator in relation to province roads,
- District administrator in relation to district roads,
- Community administrator in relation to community roads.

Within the borders of bigger towns, assignments connected with financing road building, re-building, repair, maintenance, protection and the administration of public roads are paid out of the budgets of these towns. The financing of building, re-building, repair, administration and the protection of private roads is done from the money of their administrators [3,4].

The General Director for National Roads and Motorways plans to build about 860 km of roads with rigid pavement until the year 2020. In 7 years the share of rigid pavement in fast road networks will increase from 18% to almost 27% [4].

2. Road building technologies

In the road infrastructure market two road building technologies exist: a flexible one and a rigid one and each of them has its advantages and disadvantages [4–34]. Flexible pavements are the most commonly used. For flexible pavements it is very important to properly characterize the behaviour of subgrade soils and unbound aggregate layers as the foundations of the layered pavement structure [4]. Flexible pavements will transmit wheel load stresses to the lower layers through grain-to-grain transfer through the points of contact in the granular structure. The wheel load acting on the pavement will be distributed to a wider area and the stress decreases with the depth. Taking advantage of this stress distribution characteristic of flexible pavements normally has many layers. Hence, the design of flexible pavement uses the concept of a layered system [3]. Flexible pavements generally suffer from rutting which results from heavy traffic

and severe environmental condition [5]. Flexible pavements are those having negligible flexural strength and are flexible in structural actions under loads [14].

The major flexible pavement failures are fatigue cracking, rutting, and thermal cracking. The fatigue cracking of flexible pavement is due to the horizontal tensile strain at the bottom of the asphaltic concrete. The failure criterion relates the allowable number of load repetitions to tensile strain and this relation can be determined in a laboratory fatigue test on asphaltic concrete specimens. Rutting occurs only on flexible pavements as indicated by a permanent deformation or rut depth along the wheel load path. Rutting in flexible pavements is a major distress mode and relatively difficult to simulate in computational analyses, mainly for the following reasons:

- The constitutive relations of the materials are nonlinear and complex. Most pavement materials are very difficult to characterize under repeated and moving loads.
- The asphalt concrete material is viscoelastic and viscoplastic, i.e., strong loading time and temperature dependent. The other unbound materials base, sub base, and subgrade are only slightly time dependent.
- The temperature and moisture of the materials vary with every load repetition.

Rigid pavements have sufficient flexural strength to transmit the wheel load stresses to a wider area below. Compared to flexible pavement rigid pavements are placed either directly on the prepared subgrade or on a single layer of granular or stabilized material. Since there is only one layer of material between the concrete and the subgrade this layer can be called base or sub-base course [3]. In rigid pavement the load is distributed by the slab action and the pavement behaves like an elastic plate resting on a viscous medium. Rigid pavements are constructed with Portland cement concrete (PCC) and should be analysed using the plate theory instead of layer theory, assuming an elastic plate resting on a viscous foundation. The plate theory is a simplified version of the layer theory that assumes the concrete slab as a medium thick plate which is plane before loading and is to remain plane after loading. The bending of the slab due to wheel load and temperature variation results in tensile and flexural stress. The stress condition of rigid pavement was analysed using finite element analysis [12]. The cement concrete pavement slab can serve well as a wearing surface and as an effective base course. Therefore, usually the rigid pavement structure consists of a cement concrete slab below which a granular base or sub base course may be provided [14]. Concrete pavements, often called rigid pavements, are made up of Portland cement concrete and may or may not have a base course between the pavement and subgrade. As a general rule, the concrete, exclusive of the base, is referred to as the pavement. The concrete pavement, because of its rigidity and high modulus of elasticity, tends to distribute the applied load over a relatively wide area of soil; thus, the major portion of the structural capacity is supplied by the slab itself [18].

The advantage of a rigid pavement lies in the fact that within 30 years of exploitation it will not require large financial expenditures (providing that necessary surface maintenance is carried out). In flexible pavement, milling of the wear off layer is already necessary after 9 years [5–15]. This leads to the question: which technology to choose, which one is better?

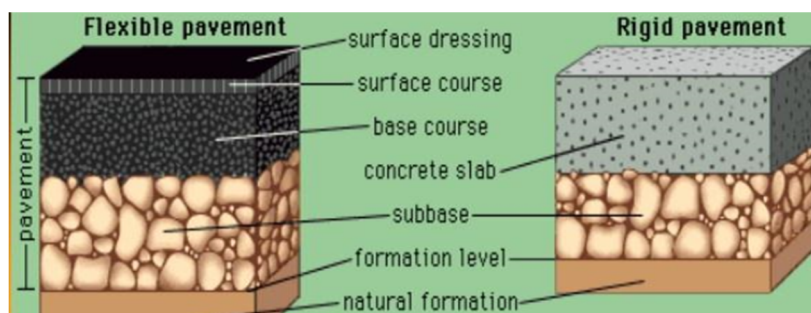


Fig. 1. Road building technologies: a flexible pavement and a rigid pavement according with [35]

3. The analysis concerning with road building technologies

The comparative analysis of two road building technologies: a flexible one and a rigid one are presented. It is assumed that all variables: technological-technical – usable ones, statistically are of the same importance and can positively or negatively influence the choice of road pavement technology. For the calculations, the normalization method and synthetic coefficient of development was used [36–38]. In accordance with Table 1 and Table 2, the divisions and features important for the choice of road building technology were determined for features in divisions were calculated as well as meters for individual divisions and synthetic meters for both technologies. Five groups – thematic divisions were determined (Table 1).

Table 1. Thematic divisions for road building technologies

No.	Feature
1	Building costs per 1 m ²
2	Maintenance cost per 1 m ²
3	Usability features
4	Environmental protection
5	Investment process

For the purpose of analysing the values of weights for individual divisions, as well as the weights for individual features in divisions were defined subjectively. The sum of weights is always 1.0.

Table 2. Defined features for individual divisions [1,4–34]

No.	Feature	Unit	Flexible pavement	Rigid pavement	Weight
Building costs per 1 m²					
1	KR1	PLN/m ²	169.17	177.39	0.167
2	KR2	PLN/m ²	204.54	189.79	0.167
3	KR3	PLN/m ²	249.14	266.84	0.167
4	KR4	PLN/m ²	288.92	278.69	0.167
5	KR5	PLN/m ²	319.27	302.39	0.167
6	KR6	PLN/m ²	346.62	316.96	0.167
Maintenance costs per 1 m²					
1	KR1	PLN/m ²	533.28	370.00	0.167
2	KR2	PLN/m ²	653.10	396.91	0.167
3	KR3	PLN/m ²	707.70	481.41	0.167
4	KR4	PLN/m ²	764.12	516.31	0.167
5	KR5	PLN/m ²	810.88	570.55	0.167
6	KR6	PLN/m ²	854.54	605.46	0.167
Usable features					
1	Longitudinal evenness		1	0.6	0.2
2	Furrowing		0.1	1	0.2
3	Anti-slip properties				
3.1	Motorways	Conclusive factor of friction	0.39	0.51	0.10
3.2	State roads	Conclusive factor of friction	0.44	0.47	0.10
4	Noise [21]	Average (4.1 to 4.6)	10.20	10.23	0.06
Motorways					
4.1	50 km/h	Index CPX	92.8	90.1	
4.2	80 km/h	Index CPX	100.1	97.4	
4.3	110 km/h	Index CPX	104.6	102.4	
State roads					
4.4	50 km/h	Index CPX	90.4	92.1	
4.5	80 km/h	Index CPX	97.8	100	
4.6	110 km/h	Index CPX	102.5	104.6	
5	Colour of pavement				
5.1	Visibility		0.7	1	0.025
6	Surface heating	Degrees C	46.97	36.08	
Calculation value as 1//Degrees*100			2,13	2,77	0.025
6	Resistance to permanent deformation		0.7	1	0.19
7	Breaking distance at 100 km/h	Average [m] (7.1 to 7.2)	1.20	1.38	0.10
7.1	Wet surface	m	109	96	
7.2	Dry surface	m	58	49	
Environmental protection					
1	Emission of CO ₂	Average (1.1 to 1.4)	11.3	2.56	0.34
1.1.	Emission of CO ₂ From asphalt and concrete production (kg of CO ₂ /ton) [17]	kg CO ₂ /t	27.4	694	
1.2	Emission of CO ₂ from production of 1 t of mineral-asphalt mixture and 1 t of concrete (kg of CO ₂ /t) [18]	kg CO ₂ /t	10.3	107.3	

Table 2 (cont). Defined features for individual divisions [1,4–34]

No.	Feature	Unit	Flexible pavement	Rigid pavement	Weight
1.3	Emission of CO ₂ from building 1 km of asphalt and concrete motorway (kg of CO ₂ / km)[20]	kg CO ₂ /km	347	1497	
1.4	Emission of CO ₂ from maintenance of 1 km of asphalt and concrete motorway (kg of CO ₂ /km) [20]	kg CO ₂ /km	500	1610	
2	Index of influence of building 1 km of motorway on the environment	Aaverage (2.1 to 2.4)	5.81	3.61	0.33
2.1	Greenhouse effect potential (GWP) [19]	[kg of CO ₂ equivalent]	1712501.5	2765765	
2.2	Stratospheric ozone layer deterioration potential (ODP) [19]	[kg of CFC-11 equivalent]	0.395	0.13	
2.3	Photo oxidant synthesis potential (POCP) [19]	[kg of C ₂ H ₄ equivalent]	422	384.5	
2.4	Acidification – potential (AP) [19]	[kg of SO ₂ equivalent]	8353.5	6426	
2.4	Eutrophication – potential (EP) [19]	[kg PO3-4]	1248	1092	
3	Index of influence on the repair and exploitation of 1km of motorway on the environment		5.81	3.61	0.33
3.1	Greenhouse effect potential (GWP) [19]	[kg of CO ₂ equivalent]	996135	62245.5	
3.2	Stratospheric ozone layer deterioration potential (ODP) [19]	[kg of CFC-11 equivalent]	0.225	0.01	
3.3	Photo oxidant synthesis potential (POCP)	[kg of C ₂ H ₄ equivalent]	294	46	
3.4	Acidification – potential (AP) [19]	[kg of SO ₂ equivalent]	5638.5	267.5	
3.5	Eutrophication – potential (EP) [19]	[kg PO3-4]	743.5	36.5	
Investment process					
1	Stage of design				
1.1	Knowledge of the design engineers		1	0.8	0.15
1.2	Experience of the design engineers		1	0.1	0.15
2	Stage of building				
2.1	Number of offers – big contracts	number of offers	28	26	0.35
2.2	Number of offers – local market small contracts	number of offers	5	2	0.35

Calculations were performed based on the following algorithm [36–38]:

- Based on the matrix of standardized in-coming data for all analyzed features, in each division a model object was appointed having coordinates (standardized changeable values) in accordance with (1):

$$\mathbf{O}_0 = [z_{oj}], \quad j=1,2,\dots,m. \quad (1)$$

- Coordinates of the model object for each feature in each division was determined based on the following formulation (2):

$$z_{oj} = \begin{cases} \max_i \{z_{ij}\} \text{ dla } z_j^S \\ \min_i \{z_{ij}\} \text{ dla } z_j^D \end{cases}, \quad j=1,2,\dots,m. \quad (2)$$

- For each division its distance to model object was calculated based on Euclidean metric as follows (3):

$$d_{i0} = \left[\sum_{j=1}^m (z_{ij} - z_{0j})^2 \right]^{\frac{1}{2}}, \quad i=1,2,\dots,m. \tag{3}$$

- Standardized features for individual divisions were calculated according to formulations (4) to (7):

$$s_i = 1 - \frac{d_{i0}}{d_0}, \quad i=1,2,\dots,m. \tag{4}$$

where:

$$d_0 = \bar{d}_0 + 2R(d_0) \tag{5}$$

$$\bar{d}_0 = \frac{1}{n} \sum_{i=1}^n d_{i0} \tag{6}$$

$$R(d_0) = d_{\max} - d_{\min} \tag{7}$$

The standardization of features (Table 3) was the introductory phase which enables obtaining total multi-criteria assessment of each considered division.

Table 3. Standardized features

No.	Feature	Flexible pavement	Rigid pavement	Weight
1	Building costs per 1 m ²	0.43	0.71	0.24
2	Maintenance costs per 1 m ²	0.60	1.00	0.24
3	Usable features	0.16	0.27	0.24
4	Environmental protection	0.60	1.00	0.18
5	Investment process	1.00	0.60	0.10

- Synthetic coefficient for both technologies were obtained by the aggregation of measures within each division for the analyzed technology. The value of the synthetic coefficient is a value of the weight average of individual synthetic measures calculated for all analyzed divisions (formulation 8, Table 4):

$$M_k = \sum_{k=1}^5 (S_j w_k) \quad (i = 1, \dots, 34 \text{ and } i = 1, \dots,) \tag{8}$$

Synthetic coefficient takes a value from the interval [0;1]. The nearer a given object is to the model, the higher these values are.

Table 4. Synthetic coefficients for individual types of pavement

No.	Pavement	Synthetic coefficient
1	Flexible pavement	0.96
2	Rigid pavement	0.98

Based on the analyses made with the use of the data normalization method, it can be said that the obtained values of synthetic coefficients for flexible and rigid pavements are quite close which indicates that the technologies within the divisions taken for analyses in relation to the features technological- technical-usable ones are comparable.

4. Conclusions

When choosing a road building technology the choice cannot be limited only to building costs but it is necessary to consider the costs of maintenance and exploitation some 30–40 years later as well. When choosing the road building technology the main purpose is to build the roads of such quality that their long time exploitation and usage would be fulfilled. Based on the analyses made with the use of the normalization method it is possible to state that both technologies the asphalt one and the concrete one can be competitive since it leads to their progress and development. Considering the growth of traffic on the roads concrete can be perceived as a technical and economic alternative to asphalt structures which is confirmed by presented analyses.

References

- [1] Główny Urząd Statystyczny, <https://stat.gov.pl/>.
- [2] Ustawa z dnia 21 marca 1985 r. o drogach publicznych.
- [3] Rozporządzenie Ministra Transportu i Gospodarki Morskiej z dnia 2 marca 1999 r. w sprawie warunków technicznych, jakim powinny odpowiadać drogi publiczne i ich usytuowanie, Dz.U. 1999 nr 43 poz. 430.
- [4] Szydło A., Mackiewicz P., Ed. Polski Cement (2005).
- [5] Deja J., Techniczno-ekonomiczne aspekty budowy betonowych nawierzchni drogowych w Polsce; Polski drogi, Przegląd Techniki Drogowej i Mostowej, 2003.
- [6] Szydło A., Nawierzchnie drogowe z betonu cementowego –teoria, wymiarowanie, realizacja, Wyd. Polski Cement, 2004.
- [7] Szydło A., Mackiewicz P., Nawierzchnie betonowe na drogach gminnych. Wyd. Polski Cement, 2005.
- [8] Deja J., Nawierzchnie betonowe coraz bardziej popularne w Polsce, Drogi: Lądowe, Powietrzne, Wodne, 2009.
- [9] Deja J, Kijowski P., Drogi betonowe – doświadczenia z budowy i eksploatacji cz. II, <https://edroga.pl/drogi-i-mosty/drogi-betonowe-doswiadczenia-z-budowy-i-eksploatacji-cz-ii-22062301/all-pages>.

- [10] Gruszczyński M., Beton wałowany – szansą na tanie i trwałe drogi, *Przegląd Budowlany* 1/2016.
- [11] Woyciechowski P., Harat K., Nawierzchnia drogowa z betonu wałowanego, *Budownictwo Technologia Architektura*, 2012.
- [12] Senderski M., Beton wałowany– idea i zastosowanie, *Inżynier Budownictwa*, 4/2015.
- [13] Frost Durability of Roller Compacted Pavements, Canada, Portland Cement Association, 2004.
- [14] Roller Compacted Concrete Pavements Design and Construction, US Army Corps of Engineers, Washington DC, 2000.
- [15] Production of Roller Compacted Concrete, Portland Cement Association, 2008.
- [16] Compaction of Roller-Compacted Concrete, Miller R., 2000.
- [17] Guide Specification for Construction of Roller-Compacted Concrete Pavements, American Concrete Institute, Farmington Hills, 2004.
- [18] Plantmix Asphalt Industry of Kentucky (PAIKY).
- [19] Milachowski Ch., Stengel T., Gehlen Ch., EUPAVE, 2011, https://www.eupave.eu/wp-content/uploads/eupave_life_cycle_assessment.pdf.
- [20] *Production of Roller Compacted Concrete*, Portland Cement Association, 2008.
- [21] Miller R., *Compaction of Roller-Compacted Concrete*, ACI 309.5R-00 became effective February 23, American Concrete Institute, 2000.
- [22] American Concrete Institute, Farmington Hills, 2004.
- [23] *General Technical Specifications*, GDDKiA, 2013.
- [24] Czarnecki L., Woyciechowski P., Adamczewski G., Risk of concrete carbonation with mineral industrial by-products, *KSCE Journal of Civil Engineering*, 22(2), 2018, pp. 755–764.
- [25] Czarnecki L., Woyciechowski P., Modelling of concrete carbonation; is it a process unlimited in time and restricted in space?, *ACI Materials Journal*, 109(3), 2012, pp. 275–282.
- [26] M. Dobiszewska, Waste materials used in making mortar and concrete, *Journal of Materials Education*, 39 (5–6), 2017, pp. 133–156.
- [27] Beycioglu A., Gultekin A., Aruntas H., Huseyin Y. et al., Mechanical properties of blended cements at elevated temperatures predicted using a fuzzy logic model, *Computers and concrete*, 20(2), 2017, pp. 247–255.
- [28] Konkol J., Prokopski G., The use of fractal geometry for the assessment of the diversification of macro-pores in concrete, *IMAGE Analysis & Stereology*, 30(2), 2011, pp. 89–100.
- [29] Manko Z., Jakiel P., Assessment of aggressive environment effect on changes in properties of weathering resistant steel 12HNNb in railroad bridges, *Nordic Steel Construction Conference '95, Proceedings, Vol. 1 and 2*, 1995, pp. 445–452.
- [30] Ślęczka L., Component-based modelling of beam-to-column joints subjected to variable actions, *Recent progress in steel and composite structures*, pp. 457–462 (2016).
- [31] Sztubecka M., Bujarkiewicz A., Sztubecki J., Optimization of measurement points choice in preparation of green areas acoustic map, *Civil and Environmental Engineering Reports*, 23(4), pp. 137–144 (2016).

- [32] Optimum Flexible Pavement Life-Cycle Analysis Model. Available from: https://www.researchgate.net/publication/245306205_Optimum_Flexible_Pavement_Life-Cycle_Analysis_Model (accessed May 25 2018).
- [33] <http://www.fdot.gov/design/training/designexpo/2012/Presentations/UwaibiEmmanuel-PavementTypeSelectionProcess%20.pdf>(accessed May 25 2018).
- [34] Skrzypczak I., Radwański W., Pytlowany T., Durability vs technical – the usage properties of road pavements, materiały po recenzji w druku, Inrafeko 2018.
- [35] https://www.researchgate.net/figure/Pavement-courses-both-flexible-and-rigid-pavement_fig1_319620565.
- [36] Skrzypczak I., Radwański W., Pytlowany T., Choice of road building technology – statistic analyses with the use of the Hellwig method, materiały po recenzji w druku, Inrafeko 2018.
- [37] Pluta W., Wielowymiarowa analiza porównawcza w modelowaniu ekonometrycznym, PWN, (1986).
- [38] Len P., Oleniacz G., Skrzypczak I. et al., The Hellwig's and zero notarization methods in creating a ranking of the urgency of land consolidation and land exchange work SGEM 2016, Vol. II *Book Series: International Multidisciplinary Scientific*, GeoConference-SGEM, pp. 617–624 (2016).

Przesłano do redakcji: 17.02.2018 r.

Przyjęto do druku: 31.03.2018 r.

Tadeusz NOCH¹

THE USE OF A HEAT PUMP AND SOLAR ENERGY IN THE HEAT DEMAND

The article presents the energy performance of a heat pump. The coefficient of performance was taken into account, which is the ratio of the heating energy obtained to the supplied electrical energy necessary for the compressor operation. The focus was on the issue of operating costs of using heat pumps. These costs are mainly influenced by two factors. Firstly, energy performance and the purchase price of electricity. The second factor is investment costs. Heat gains from solar energy were characterized. The value of the solar radiation transmission coefficient for the double glazing was assumed ($TR = 0.7$). Solar gains were shown in January for windows on the eastern and western facades. The analysis covered the seasonal heat demand for heating. The studies and calculations took into account the occurring heat losses and heat gains from the sun and internal sources with their utilization rate. Particular attention was paid to the fact that the peak power of heating appliances can be calculated by knowing the value of the annual energy demand for heating a building that takes into account the most severe external conditions prevailing in a given climate zone, i.e. the minimum outside temperature.

Keywords: heat pump, solar energy, Coefficient of Performance COP, energy performance, heat losses and gains, heat power, heat source, heating, heating appliances, temperature, investment costs, heat demand

1. Introduction

Heat pumps pump heat in the opposite direction to natural running [1]. It can be said that the pumps are not a source of heat, they only move it to the place where it is effectively used [2].

Heat pumps are widely used as heating or air conditioning appliances for single-family houses and small rooms. During the heating season, they are used as a heat pump. In the summer season, they are air conditioners operating in the reverse cycle. The thermal power of these devices usually ranges from a few to several dozen kilowatts. The compressors are mainly used and these are: air-air, air-water or water-water, water-air (surface, i.e. floor, ceiling and wall). Research shows that heating individual buildings is less efficient than the system

¹ Corresponding author: Tadeusz Noch, Gdańska Szkoła Wyższa, Wydział Nauk Inżynierskich, ul. Biskupia 24B, 80-875 Gdańsk; tadeusz.noch@gsw.gda.pl; tel. 602 130 709

of more consumers with the use of associated heating systems. According to statistical research, the air-air heat pump meets the consumer's needs for heat for space heating and hot water during the year in the case of [3, 4]:

- multi-family buildings – 70÷80%,
 - a complex of single-family houses – 60÷70%,
 - single-family detached houses – 50%
- of annual power demand.

It is stated that a device with a capacity of several kilowatts is sufficient for preparing hot usable water for consumers.

In various types of technical installations there is a flow of fluids in channels with a wide range of diameters, from very small (in mini- or microscale) to large (in macro scale). Technological progress in recent decades has led to the miniaturization of a number of technical devices in all branches of industry. This also applies to heat exchangers used in industry. Boiling heat transfer coefficients α are an order of magnitude higher than in single-phase, forced fluid motion and reach values of about $10^5 \text{ W/m}^2 \text{ K}$ for conventional devices [5]. Direct formulas obtained for conventional channels cannot be directly used to calculate heat exchange and flow resistance for mini- and microchannels. The phenomenon of generating vapour bubbles in a limited space and a significant predominance of capillary forces over gravitational forces are more important than viscous energy dissipation and axial conduction in single-phase flows [6, 7].

2. Use of a heat pump

When using a heat pump, its energy performance is particularly important. It was found that the performance of the heat pump (compressor, condenser, expansion valve and evaporator) is determined by the ratio of the amount of heat obtained in the condenser, i.e. the heat source with a higher temperature to the amount of energy used to drive the compressor. It is called the coefficient of performance COP. The coefficient of performance is the ratio of the heating energy obtained to the supplied electrical energy necessary for the compressor operation. The higher, the heat pump works more efficiently [8, 9].

$$COP = \frac{Q_g}{P_e} \quad (1)$$

where: Q_g – upper heat source power [kW];
 P_e – mechanical power of the drive motor [kW].

The size of the coefficient depends on the design of the heat pump and on the temperature of the lower and upper heat sources. Energy performance depends primarily on the temperature difference between the lower and upper heat sources. The influence of these factors on COP is described by equation [8, 9]:

$$COP = 4,77 + 0,081T_D - 0,041T_G \quad (2)$$

where: T_D – lower heat source temperature [°C];
 T_G – upper heat source temperature [°C].

According to the presented dependence (2), the temperature of the lower heat source has a different impact on the coefficient of performance than the temperature of the upper source. As the temperature of the lower source increases, the COP increases – a change of temperature by 10°C causes a change of this coefficient by 0.81. On the other hand, an increase in the temperature of the upper source by 10°C causes a reduction of this coefficient by 0.44. Significantly weaker effect of the upper heat source temperature compared to the lower heat source temperature is particularly beneficial from the point of view of the heat pump's operation for preparing hot usable water or heating residential premises.

The size of the COP coefficient says simply about the expected costs of heating. If the annual heat demand in the building is known, then after dividing it by the coefficient of performance, one will get the payable amount of energy. Operating cost is limited to the cost of purchasing electricity.

The lower heat source is one of the basic conditions for the effective operation of a heating system with a heat pump. In Poland, groundwater or soil is most often used as the lower heat source, much less air due to the fact that it is characterized by high temperature variability both in the 24-hour period and the whole heating season.

The soil is a good heat accumulator, because it maintains relatively uniform temperatures throughout the year (in the order of 7 to 13°C at depth 2 m). Soil energy can be taken through the horizontal collector or through the vertical collector – ground probes. The length of the collectors is determined on the basis of the heat pump's set heating power. Through the collector or ground probes flows brine, which is a mixture of water and glycol (does not freeze at subzero temperatures). This medium absorbs heat from the ground and transports it to the heat pump's evaporator. However, the horizontal collector requires a large plot area. If there is not enough space for putting a horizontal collector in the ground, then ground probes placed vertically in the ground can be used.

In order to take heat from groundwater, one needs to drill two wells. From one of them, water is pumped into the heat pump. The second well (discharge) drains the chilled water back to the ground. The advantage of groundwater as a lower heat source is that they have a high temperature of 8 to 12°C, constant throughout the year. The problem is the mutual location of the recharge and discharge well due to the direction of groundwater flow. It cannot be that the chilled water from the discharge well returns to the well that supplies the heat pump. The unchanging efficiency of the recharge well must also be ensured.

3. Operating efficiency

The study did not deal with the calculation of heating costs; it was limited to operating costs, in which only the costs of fuel and energy were included. The operating costs of using heat pumps are mainly influenced by two factors. On the one hand, energy performance and the purchase price of electricity. On the other hand, investment costs. Operating costs vary within wide limits. For example, for the upper heat source temperature 55°C and the lower heat source temperature -7°C energy performance is 1.75; respectively, for temperatures 30°C – underfloor heating and 5°C – ground, performance will be 3.55. This means that in this particular case the cost of obtaining a heat unit may vary from 0.113 PLN / kWh (with the electricity price 0.46 PLN / kWh and performance 4.06) to 0.25 PLN / kWh (at the price of 0.46 PLN / kWh and performance 1.75). Therefore, the guideline for low operating costs is to find a heat source that will have the highest possible temperature. The annual energy cost for heating the building and water, depending on the COP, is presented in Table 1 [10].

Table 1. Annual energy cost for building heating and hot water depending on the COP [10]

Lower heat source temperature [°C]	Upper heat source temperature [°C]	Energy performance COP	Energy performance COP	The cost of electricity for generating one kWh of heat [PLN/kWh]	The cost of energy for heating the building and hot water [PLN/a]
12	30	4.50	4.06	0.113	1 279
10	30	4.35	3.91	0.118	1 332
5	30	3.94	3.55	0.130	1 467
0	40	3.13	2.81	0.164	1 853
-5	45	2.52	2.26	0.204	2 304
-7	55	1.94	1.75	0.263	2 976
5	50	3.12	2.81	0.164	1 853

Decreasing the temperature difference between the receiver (upper source) and the lower source causes the efficiency of the heat pump to increase significantly. The greatest benefits from using a heat pump are obtained in low-temperature underfloor heating, where the water temperature is around 28–30°C and by using groundwater as the lower heat source assuming that it has a temperature of around 10°C. In this configuration, the COP coefficient reaches the highest values. One should definitely be discouraged from using heating with a heat pump in a system with radiators or with a radiator-floor system, because the minimum temperature of the upper source is then 50°C, which causes the COP to drop considerably below the value of 4. The basic advantage of the heat pump is lost, which is the low heating costs. Therefore, when designing the installation, it is necessary to take very close attention to the temperature, because only then one can expect low operating costs. It all depends on the conditions in which the heat pump works.

4. The use of solar energy

This article focuses on heat obtained from solar energy. The analysis carried out refers to the heating of a passive house. Heat gains from solar energy are calculated from the formula:

$$Q_{SL} = 0.6A_S \cdot TR \cdot S \cdot Z \text{ [kWh/month]} \quad (3)$$

where: A_S – total area of windows on a given facade [m^2];

TR – coefficient of solar energy transmittance of windows;

S – monthly sum of total solar radiation per unit of area in a given month [kWh];

Z – shading coefficient;

0.6 – frame share in the window area.

Monthly sums of total solar radiation in watt-hours per one square meter [Wh/m^2] for differently oriented surfaces are shown in Table 2 [11].

Table 2. Solar radiation [Wh/m^2] for variously oriented surfaces [11]

Solar energy		
Month	Orientation	
	West	East
January	14 880	13 392
February	29 568	26 208
March	49 848	49 104
April	66 960	71 280
May	81 840	95 976
June	81 360	87 840
July	92 256	89 280
August	75 144	78 864
September	46 800	49 680
October	29 760	34 224
November	12 240	13 680
December	8 184	9 672

The windows in the building are located on the east and west facade. The shading coefficient is equal to one for both facades, because in the vicinity of the building there are no obstacles that would hinder the inflow of solar radiation to a given facade [12, 13]. The values of the solar radiation transmission coefficient, depending on the type of glazing, are presented in Table 3 [11].

Table 3. The values of the solar radiation transmission coefficient depending on the type of glazing [11]

Type of glazing	Solar radiation transmission coefficient TR
Single	0.82
Double	0.7
Single or triple glazing pane with one low-E coating	0.64
As above, but the space between the panes filled with argon	0.64
Double glazing pane with a low-E coating	0.55
Special glass	0.5

The value of the solar radiation transmission coefficient for the double glazing was assumed ($TR = 0.7$). Solar gains in the month of January for windows on the east facade, based on (3): $Q_E = 0.6 \cdot 9.66 \cdot 0.7 \cdot 13.392 \cdot 1 = 54.3$ kWh; for the west facade: $Q_W = 0.6 \cdot 13.63 \cdot 0.7 \cdot 14.88 \cdot 1 = 85.1$ kWh. In the remaining months, the calculations were made identically and the results are summarized in Table 4.

Table 4. Total solar gains [kWh / month]

Solar gains			
Month	East facade Q_E	West facade Q_W	Total gains
January	54.3	85.1	139.5
February	106.3	169.2	275.5
March	199.2	285.3	484.5
April	289.2	383.3	672.5
May	129.8	156.1	286.9
September	33.5	44.6	78.2
October	138.8	170.3	309.2
November	55.5	70.0	125.5
December	39.2	46.8	86.0
Total [kWh/a]			2 457.3

5. Heat demand for heating

Seasonal heat demand for heating Q_h is calculated as the difference between heat losses and heat gains from the sun and internal sources, taking into account the use of heat gains. Thanks to the use of mechanical ventilation with heat recovery, it is possible to minimize losses to the heating of ventilation air, as well as to use internal and solar gains in their entirety. The following efficiency of heat recovery was adopted $\eta = 85\%$. The calculations of the annual heat demand for heating include the following data:

- annual heat loss by penetration calculated as the sum of losses from all months of the heating season: $Q_{ASEZ} = 8\,938$ [kWh/a];
- annual ventilation heat loss calculated as the sum of losses from all months of the heating season: $Q_{vent\ SEZ} = 1\,8984.7$ [kWh/a];

- internal heat gains calculated as the sum of gains from individual months in the heating season: $Q_{zysk\ wew} = 3\,459.4$ [kWh/a];
 - solar heat gains calculated as the sum of gains from individual months in the heating season: $Q_{zysk\ S} = 2\,457.3$ [kWh/a];
- Annual heat demand for heating:

$$\begin{aligned}
 Q_H &= Q_{ASEZ} + Q_{went\ SEZ} - Q_{zysk\ S} - \eta(Q_{went\ SEZ}) \quad [\text{kWh/a}] \\
 Q_H &= 8938,24 + 18984,72 - 3459,4 - 2457,3 - 0,85 \cdot 18984,72 = \quad (4) \\
 &= 5869,2 \quad [\text{kWh/a}]
 \end{aligned}$$

Annual heat demand indicator with respect to the area of 211 m²:

$$E_0 = \frac{Q_H}{A_f} = 27,8 \quad [\text{kWh}/(\text{m}^2 \cdot \text{a})] \quad (5)$$

where: A_f – the area $A_f = 211$ m².

The calculations show that the demand for energy for building heating has dropped almost eightfold. As a result of the use of insulation ensuring the heat transfer coefficient of 0.15 W/m² K for walls and roof, windows and doors with 0.8 W/m²·K insulating power, losses have been drastically reduced by external partitions. Despite the high insulating power of partitions in the building balance, ventilation losses are a significant part of the losses. Only high-efficiency heat recovery from the exhaust air gives the opportunity to significantly reduce the energy consumption of the building.

The selection of thermal power of heat sources in a building is of crucial importance. The peak power of heating appliances can be calculated by knowing the value of the annual energy demand for heating a building that takes into account the most severe external conditions prevailing in a given climate zone, i.e. the minimum outside temperature [14]:

$$q_{moc} = \frac{Q_H (T_i - T_e)}{24Sd} \quad [\text{kW}] \quad (6)$$

where: Q_H – annual heat demand $Q_H = 5\,869.2$ kWh;

T_i – internal calculation temperature, $T_i = 20^\circ\text{C}$ as the average temperature of all heated rooms in the building;

T_e – the lowest external calculation temperature in the given climate zone, for the first climatic zone $T_e = -18^\circ\text{C}$ [15];

Sd – number of degree days for the building location according to meteorological data from PN-B-02025 calculated for internal temperature;

$T_i = 20^\circ\text{C}$, $Sd = 3924$.

The demand for thermal power at the peak load is:

$$q_{moc} = \frac{Q_H (T_i - T_e)}{24Sd} = \frac{5869,2(20 - (-18))}{24 \cdot 3924} = 2,36 \text{ [kW]}$$

The demand for thermal power at the peak load in the building before modernization is:

$$q_{moc} = \frac{Q_H (T_i - T_e)}{24Sd} = \frac{40559,1(20 - (-18))}{24 \cdot 3924} = 16,36 \text{ [kW]}$$

The demand for thermal power of the source dropped almost sevenfold. With such a small heat demand, when the building is well insulated, the computational power of the heat source can be increased due to the heating hot water by 0.25 kW for each user [8]. Therefore, the power that a heating system should have at a time when the building is used by four consumers should be 3.36 kW.

An important element of the building is to minimize the energy demand during operation. The effectiveness in limiting this demand is so great that, in theory, the building itself may no longer require any other active heating sources. In practice, reheating is needed, often with the use of a heat pump or solar plant. Such buildings can most definitely be used in Polish climatic conditions. It is connected with an increased investment cost by 10÷20% [16]. The problem is also the design and construction of the building, as this type of construction (passive) is very dependent on many factors (orientation of the building in the area, the presence of trees or other objects that can obscure the sun, shape of the building, etc.). In the event of even the smallest executive errors, the payback time can be extended up to three times.

Passive houses are among the so-called “smart homes”. A smart home is where electrical installations and devices, such as lighting, audio/video devices, ventilation, an alarm system, automatic garden spraying, have been integrated and operating according to the user’s wishes [17]. They require accurate ventilation control and additional heat sources. The goal is to achieve high technical quality of the building and the comfort of its users with the least possible environmental burden and minimal energy consumption. In passive construction, ecological premises are combined with economy and quality. Smart air conditioning control enables constant maintenance of comfortable temperature. An intelligent lighting concept is key in the pursuit of minimizing electricity consumption.

6. Summary

Increasing prices of energy carriers from year to year mean that rational energy management is being increasingly discussed. Heating costs are rising, therefore a group of building users and investors is expanding, and they understand the need to save energy. Many buildings undergo thermo-modernization, newly constructed buildings are being built to meet European energy consumption standards.

In building designs, more and more often there is a carefully designed thermal insulation of good materials with insulation parameters far exceeding the standard recommendations. Good windows or ventilation with heat recovery (recuperation) are slowly becoming the standard [14, 18].

The application of the heat balance equation to the building's room arrangement requires the assumption that it is one zone (all rooms have the same internal temperature). The air exchange rate calculated with this assumption determines the average ventilation intensity in all rooms of the building, so that heat is lost to the external environment, and the heat gains are limited to house-related, from solar radiation through transparent partitions and from electrical devices in the building.

Solar gains are the result of the greenhouse effect and occur in every room where there are windows. The solar radiation penetrating through the glass turns into heat inside. To determine the amount of heat obtained, the orientation, shading and radiation transmittance are determined for all windows. Based on the location of the facility, the long-term average solar radiation intensities are determined.

The modern installation is responsible for overseeing and regulating the other devices that support the building. The temperature and air quality can be measured and optimized by adjusting the parameters of the fan supplying the air. Sensors installed in rooms can automatically turn off the light if the room is left for a long time. Proper control and management of the building requires a good recognition of its structural solution, the whole and individual elements, including the implementation technology and the construction materials used. Obtaining full optimization of energy consumption and minimizing heating costs as well as low failure rate of heat pumps will affect energy efficiency.

References

- [1] Brodowicz K., Dyakowski T.: *Pompy ciepła*, Wyd. PWN, Warszawa 1990.
- [2] Klugmann E., Klugmann-Radzimska E.: *Ogniwa i moduły fotowoltaiczne oraz inne niekonwencjonalne źródła energii*, Wyd. Ekonomia i Środowisko, Białystok 2005.
- [3] Chwieduk D.: *Odnawialne źródła energii źródłem ciepła dla pomp ciepła*, Materiały Ogólnopolskiego Forum „Mała energetyka”, Chańcza, maj 1996.
- [4] Zalewski W.: *Pompy ciepła sprężarkowe, sorpcyjne i termoelektryczne*, Wyd. IPPU MASTA, Gdańsk 2001.

- [5] Trela M., Kwidziński R.: Analiza wrzenia i spadku ciśnienia przy przepływach dwufazowych w makrokanałach, *Zeszyty Naukowe Gdańskiej Szkoły Wyższej*, Vol. 16, 2016, pp. 333–360.
- [6] Saraceno L., Celata G.P., Furrer A., Zummo G., Flow boiling heat transfer of refrigerant FC-72 in microchannels, *Int. Journal of Thermal Sciences* 53 (2012).
- [7] Del Col D., Bisetto A., Bartolato M., Torresin D., Rosetto L., Experiments and updated model for two-phase frictional pressure drop inside minichannels, *Int. Journal of Heat and Mass Transfer* 67 (2013).
- [8] Gnyra K.: Pompa ciepła w budynkach jednorodzinnych. *Technika Chłodnicza i Klimatyzacyjna*, No. 9, 2007.
- [9] Knaga J., Trojanowska M., Kempkiewicz K.: Efektywność pompy ciepła ze sprężarką spiralną, *Wyd. Zakład Energetyki Rolniczej AR, Kraków*.
- [10] Obliczanie kosztów energii na potrzeby ogrzewania budynku i ciepłej wody pompą ciepła, *Gdańsk 2008*.
- [11] PN-B-02025:1999 Obliczanie sezonowego zapotrzebowania na ciepło do ogrzewania budynków mieszkalnych i użyteczności publicznej.
- [12] Feist W., Munzenberg U., Thumulla J., Schulze Darup B.: *Podstawy budownictwa pasywnego*, *Wyd. Polski Instytut Budownictwa Pasywnego, Gdańsk*.
- [13] Rylewski E.: *Energia własna*, *Warszawa 2000*.
- [14] Norwisz J.: *Termomodernizacja budynków dla poprawy jakości środowiska*, *Wyd. Biblioteka Fundacji Poszanowania Energii, Gliwice 2004*.
- [15] PN-82/B-02403 *Ogrzewnictwo – Temperatury obliczeniowe zewnętrzne*.
- [16] *Drewno zamiast benzyny.pl*, <http://www.drewnozamiastbenzyny.pl> {access 20.02.2017}.
- [17] *Murator dom.pl*, <http://www.murator.com.pl> {02.06.2017}.
- [18] *Kompleksowa termomodernizacja budynków – opłacalna inwestycja. Świat Ociepleń. Magazyn firm budowlanych*, *Wyd. Rockwool, No. 2, 2006*.

Przesłano do redakcji: 12.03.2018 r.

Przyjęto do druku: 31.03.2018 r.

Piotr KONCA¹

THE EFFECT OF POZZOLANS ADDITION ON CEMENT MORTARS

The addition of microsilica was widely used in concretes and mortars since the second half of the 20th century (in high and very high strength concretes). Silica fume consists of very fine spherical particles. This additive, thanks to its properties, fills the space between cement particles and aggregates which affects: porosity, watertightness, shrinkage reduction and increased strength. The microsilica has pozzolanic properties and reacts with calcium hydroxide and gradually forms a uniform and continuous contact phase C-S-H (calcium-silicat hydrate). The interfacial zone between cement paste and aggregate has been considered as a zone of weakness. Zeolite is a material lesser known in civil engineering which can be used as an alternative to microsilica. The article presents the investigation of the physical properties of mortars containing these two types of pozzolan. In mixes pozzolan additives at 0 to 20 percent by mass of portland cement are used. Testing of such properties of fresh mortar as workability and air content was carried out. The properties of hardened mortar such as strength, water absorption, frost resistance and capillary suction were also determined.

Keywords: cement mortars, microsilica, zeolite, physical properties, freeze-thaw resistance, capillary suction

1. Introduction

In humid, saline or other outdoor environments the classic concrete formula (aggregate, cement, water) has ceased to be sufficient nowadays. Research on improving the composition of mortars and concretes is carried out all the time. The materials currently used must endure the external environment conditions. The following admixtures and additives are widely used nowadays: the ones improving the properties of the finished product, increasing durability, enhancing resistance to aggressive environment and counteracting significant capillary suction. The frost destruction of the material (mortar, concrete) consists in the direct physical action of water freezing inside the pores. Water increases the volume by about 9% during freezing. [1].

¹ Corresponding author: Piotr Konca, Lodz University of Technology, Faculty of Civil Engineering, Architecture and Environmental Engineering, Department of Building Physics and Building Materials, al. Politechniki 6, 90-924 Łódź, Poland; tel. +48 42 631 35 63; Piotr.Konca@p.lodz.pl

Cement composites have begun to be modified in the first half of the 20th century. Plasticizers in the form of unmodified lignosulfonates have been used at that time [2]. Plasticizers are used to enhance the fluidity of the concrete without adding water. This allows to reduce the cement content in the concrete composition and also influences its properties positively. This article presents the results of research on the influence of pozzolan additives on the physical properties of mortars. Two types of materials are used: silica dust and zeolite. Microsilica is a commonly used addition improving the properties of mortars and concretes. This is a by-product of the production process of metallic silicon and ferrosilicon alloys [3]. This dust consists of particles much smaller than the dimensions of cement grains (about 100 times smaller). The second type of additive used in the research is zeolite. It is an aluminosilicate mineral that has not yet gained popularity and is not widely used as an addition to mortars in construction.

The purpose of the work is to show the effect of adding various amounts of microsilica and zeolite on fresh mortar properties as workability and air content was carried out. The properties of hardened mortar such as strength, water absorption, frost resistance and capillary suction are also determined. Pozzolan additives during the tests are treated as an additional mass, not a replacement for cement. The article assumes that the use of microsilica and zeolite has a similar effect on the properties of the mortar. The additives are supposed to improve the mechanical parameters, reduce capillary suction and increase the frost resistance.

2. Composition of cement mortar

The mortar composition has a constant w/c ratio and different contents of two types of additives. The mortar consistencies are obtained using the same amounts of super-plasticizer at appropriate pozzolan contents. Reference material (marked as Z1) – is a mortar without additives. In mixes is used as a pozzolan at 10 to 20 percent by mass of portland cement. Mortar compositions are shown in Table 1.

Table 1. The content of mortar ingredients

	Z1 [g]	Z2 [g]	Z3 [g]	Z4 [g]	Z5 [g]
Portland cement	1 500	1 500	1 500	1 500	1 500
Water	600	600	600	600	600
Sand	3 000	3 000	3 000	3 000	3 000
Plasticizers	15	16.5	27	16.5	27
Zeolite	0	150	300	0	0
Microsilica	0	0	0	150	300

The mortar is prepared by mixing the ingredients in a laboratory mixer according to EN 196-1 [4]. After pre-mixing the material is left for 5 minutes and after this time it is mixed again. To compare the influence of a plasticizer on the consistency of mortars the same amounts of this admixture are used in matching mixtures.

2.1. Characteristics of the main ingredients

Research carried out on microsilica from the Laziska steelworks shows that this additive does not have a radiological hazard. Amorphous silica is a basic component of silica fumes and the chemical composition is very constant. With its proper application, it enables a significant improvement in the strength properties of mortars and concretes. Based on the tests described by Cz. Wolska-Kotanska [1], the addition of silica dust, as a cement replacement in the amount of 10–30% of the cement mass, the water demand increases by 20–40%. The author of the research shows that the influence of microsilica on the strength of mortar is not as explicit as in the case of concrete. Silica fumes affect the transition zone at the interface of the cement matrix and aggregate. Similar studies have been carried out by I. Przerada M. Lubas [5]. The authors has confirmed the above conclusions indicating also the increase in strength along with the lengthening of the hardening process of the mortar and concrete.

The second pozzolan additive is zeolite - a natural volcanic mineral with unique properties. The chemical composition of the zeolite is similar to the composition of fly ash. It is the material with a density of 2.4 g/cm^3 and has a surface area about 50 times greater than cement. Many studies have been conducted on the effects of using zeolite as an additive and as a substitute for cement. Studies conducted by Bundyra-Oracz G., Siemaszko-Lotkowska D. [6] indicate that the presence of zeolite does not significantly affect the setting time. However, it increases the water consumption of the cement paste, which requires the use of an effective plasticizer. Among the carried out tests there are also studies of the addition of zeolite to renovation plasters [7] as a material allowing to reduce costs.

Pozzolan additives thanks to a large fine degree accelerate the increase of strength and durability of the final product. They improve the properties of concrete or cement paste due to the pozzolanic reaction and their role as a micro-filler. This also affects the mortar tightness, because pozzolans react with calcium hydroxide which is released in the hydration process of silicates found in Portland cement. A large fine degree makes the reaction proceeding rapid. The very small pozzolan particles fill the spaces in the cement paste more tightly, which results in a thickening of the fresh mix.

The other ingredients of the mixes are Portland cement CEM I 42.5 R and a superplasticizer based on polycarboxylates.

3. Methodology and test results

The research is carried out in two groups: fresh mortar tests and investigations of hardened mortars. In the first group the following tests are performed: consistency, bulk density and air content. For hardened samples tests are carried out: density, absorbability, linear changes, strength, frost resistance (frost resistance after 50 cycles) and capillary suction.

Constant temperature of $23\pm 2^{\circ}\text{C}$ and relative humidity RH of $50\pm 5^{\circ}\text{C}$ are maintained during samples testing and conditioning. The consistency test is performed using the cone penetration procedure in accordance with PN-B-04500 [8].

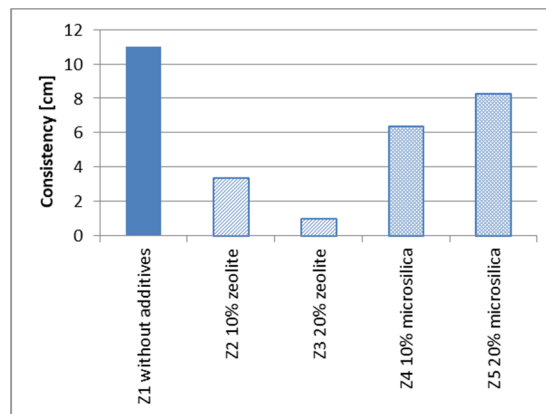


Fig. 1. Consistency test of Mortar

For comparative purposes, identical proportions of plasticizer are used for additives of 10% and 20% pozzolan, respectively. Zeolite thickened the mixture much more than the addition of microsilica. A density test does not show significant changes in individual types of fresh mortar and this parameter is maintained between 2.14 and 2.17 g/cm^3 .

The test specifying the air content (Air Meter Method) is made using a special testing device with a metal sample container and a cover assembly [9]. The idea of the test is to compare the known value of air volume (located in a sealed chamber) at a specified pressure to an unknown value of air volume in the sample mortar. The meter is pressurized to the appropriate level and then the pressure is released into the main chamber. The results are recorded as the air content of the mortar.

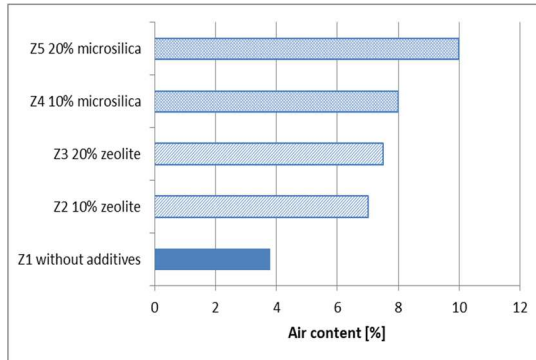


Fig. 2. Air content in fresh mortar



Fig. 3. A measuring device to determine the air content

Increasing the zeolite content in the mortar composition does not cause a significant growth in the air content. It is different considering microsilica. Increasing the addition of silica fume from 10 to 20% results in an increase in the air content by 2%. Higher air content in the paste may improve the frost resistance of the settled mortar. Water absorption tests on absorbability are made for hardened mortars [8].

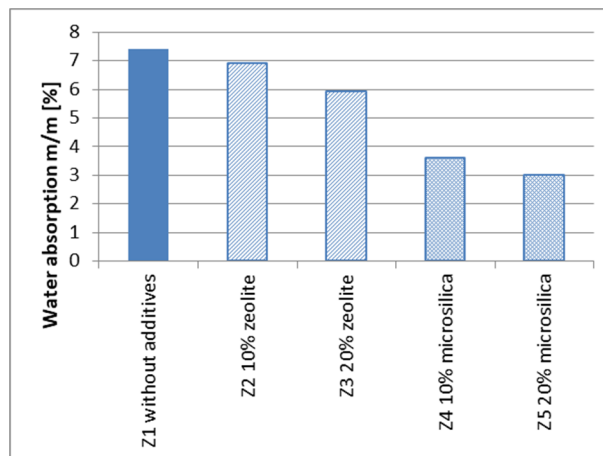


Fig. 4. Water absorption tests

The test allows determining what how much water the sample is able to absorb at normal atmospheric pressure. The greatest water mass (7.4% of the mass) is absorbed by the mortar without additives. Increasing the zeolite content to 20% allows to reduce the absorbability to the level of approx. 5.9%. Relatively better parameters are obtained for microsilica. Its addition allowed to lower the absorbability to 3.6% for Z4 mortar and 3.0% for Z5 mortar.

Compressive strength tests are made according to EN 196-1 [4]. Samples are stored in water after demoulding. The tests are performed after 14, 28 and 90 days from demoulding. The results are shown in Fig. 5 and 6.

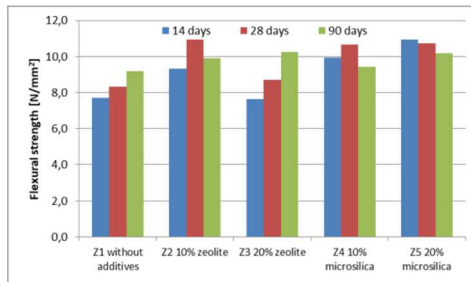


Fig. 5. Flexural strength after time

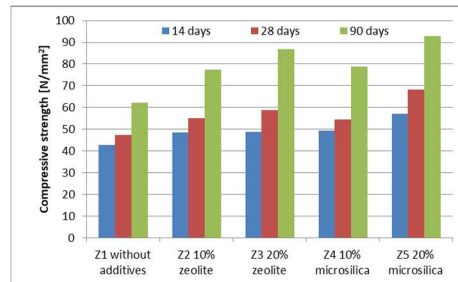


Fig. 6. Compressive strength after time

The results of bending strength tests after application of pozzolan additive oscillate around 10 N/mm^2 which is a very good result in the case of cement mortars. In compressive strength tests, the effect of the mortar maturing over specific time is evident. The use of zeolite has a similar effect as the corresponding microsilica additive.

The frost resistance test is aimed at determining the decrease in strength and weight loss caused by cyclic freezing and thawing of samples. After a 28 day curing time, the samples are dried to a constant weight. The samples are subsequently placed in water until full saturation. Samples are stored in a freezer equipped with automatic temperature control. Freezing lasted 4 hours at $-20 \pm 2^\circ\text{C}$, then the samples are placed in water at $20 \pm 2^\circ\text{C}$ for 4 hours. The freezing and thawing process is repeated cyclically. The results of compressive strength tests after 50 cycles are shown in Fig. 7, and the reduction in strength compared to the control samples in Fig. 8.

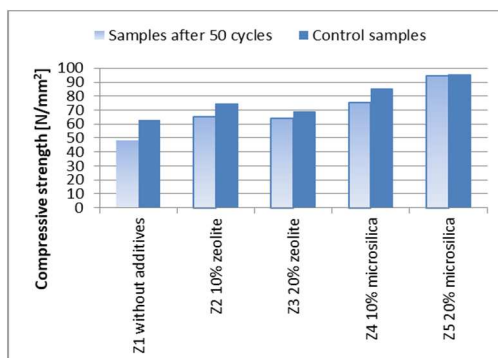


Fig. 7. Compressive strength of control samples and after 50 cycles of freezing – thawing

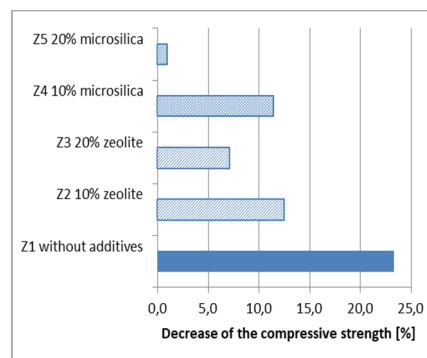


Fig. 8. Decrease of the compressive strength after 50 cycles of freezing - thawing

The greatest decrease in strength after 50 cycles of freezing and thawing is recorded for samples without pozzolan. It is assumed that a reduction of up to 25% is acceptable under frost resistance. Samples without additives are close to this limit. The best results are obtained with a 20% microsilica additive, but the use of zeolite is also an effective method of obtaining frost resistance.

The purpose of the capillary rising test is to determine the level of moisture of the sample stored in the container with water and to determine the increase in its mass. The test is carried out according to EN 1015-18 [10] using beams. The samples are immersed in water in a vertical position. The container is topped up with water at a temperature of $20 \pm 2^\circ\text{C}$, so that the water reached up to about 1 cm height of beams. During the test, the mass gain was measured after 1, 3, 6 and 24 hours.

The capillary water absorption coefficient is the gradient of the straight line obtained by plotting the cumulative mass of water absorbed per unit area against the square root of time t obtained from this first stage according to the following equation:

$$A_w = \frac{\Delta B}{A \cdot \sqrt{t}} \quad [\text{kg}/(\text{m}^2 \cdot \text{min}^{0.5})] \quad (1)$$

where: ΔB – the mass of the absorbed water [kg],

A – the surface area of the cross section of the specimen [m^2],

t – time [min].

This estimation way is known as the one tangent method. The test is carried out on samples after 50 cycles of frost resistance and control samples.

Table 2. The capillary water absorption coefficient [$\text{kg}/(\text{m}^2 \cdot \text{min}^{0.5})$] of comparison mortars and after 50 cycles of freezing – thawing

	Z1	Z2 10%	Z3 20%	Z4 10%	Z5 20%
	-	Zeolite		Microsilica	
Control samples	0.23	0.16	0.09	0.06	0.02
Samples after 50 cycles	0.30	0.19	0.13	0.09	0.02

The capillary water absorption coefficient depends on the progressive frost destruction. The mortar containing 20% microsilica does not show changes in this parameter and at the same time the lowest reduction in strength is observed for this material. The addition of pozzolan to the material resulted in its sealing. Samples containing fine aggregate of this additive have lower water absorption coefficient and better frost resistance of the mortar.

4. Conclusions

The article presents the investigation of the physical properties of mortars containing two types of pozzolan. In mixes pozzolan additives at 0 to 20 percent by mass of portland cement are used. Increasing the amount of pozzolan additive two times, causes a small increase in the air content in the fresh mortar, but at the same time reduce the absorbability. The compressive strength test shows that the addition of pozzolan improves this property after 14 days and this tendency remains after 90 days. The use of both zeolite and microsilica in the amount of 20% by weight results in an increase in strength by about 30% after 90 days of hardening, compared to samples without this additive.

The use of pozzolan as an additive while testing frost resistance is an effective method to improve this parameter. Reduction in strength after 50 cycles of freezing - thawing at 10% of the addition of microsilica and zeolite is at a similar level. The most preferred solution is the one with microsilica in the amount of 20% of cement mass. The addition of zeolite on this level is also preferred. After the frost resistance test capillary suction analysis is performed. The addition of microsilica greatly improves mortar properties by sealing it and preventing from the absorption of larger amounts of water.

The addition of pozzolan to the mortar composition has a positive effect on their physical properties. Zeolite can be used as an alternative to microsilica.

References

- [1] Wolska-Kotańska C.: Stosowanie pyłów krzemionkowych do wykonywania betonów narażonych na działanie wybranych warunków środowiskowych. Instrukcja ITB nr 362/99. ITB, Warszawa 1999.
- [2] Domieszki do betonów. Izolacje 11/12/2012.
- [3] https://pl.wikipedia.org/wiki/Dodatki_do_betonu {access 20.04.2018 r.}.
- [4] EN 196-1:2016-07: Methods of testing cement. Determination of strength.
- [5] Przerada I., Lubas M.: Wpływ dodatku popiołu lotnego i mikrokrzemionki na właściwości zapraw cementowych i betonów Materiały Budowlane 1/2004.
- [6] Bundyra-Oracz, G. Siemaszko-Lotkowska, D.: Zeolit – dodatek pucolanowy do betonu Budownictwo, Technologie, Architektura X-XII/2010.
- [7] Wpływ dodatku zeolitu na właściwości fizykomechaniczne tynków renowacyjnych Izolacje 9/2014.
- [8] PN-B-04500:1985: Mortars. Physical and mechanical tests.
- [9] EN 1015-7:2000 Methods of test for mortar for masonry. Determination of air content of fresh mortar.
- [10] EN 1015-18:2003 - Methods of test for mortar for masonry. Determination of water absorption coefficient due to capillary action of hardened mortar.

Przesłano do redakcji: 18.03.2018 r.

Przyjęto do druku: 31.03.2018 r.

Marek JABŁOŃSKI¹

Iwona SZER²

Jacek SZER³

RISK ANALYSIS ON SCAFFOLDINGS EXPOSED TO NOISE

The article presents the results of environmental tests performed on scaffolding that were focused mainly on the sound level. The parameters on which we base our analysis are the value of daily noise exposure level and peak sound levels on scaffolding. The noise that affects construction workers on scaffolding, may increase the risk of accidents. We present the results of measurements for twenty two scaffolds in five cities. The analyses carried out confirmed the qualitatively expected dependencies but they allowed us to quantify the impact of the noise on which construction workers on the scaffolding are exposed. The noise occurs continuously throughout the day and can cause faster fatigue, thereby it can increase the risk of accidents in noisy work environment.

Keywords: environmental studies, noise, scaffolding, sound level

1. Introduction

The main use of construction scaffolding is to support construction work at elevated locations or those that are more difficult to reach. In addition, the scaffolding is also used in other areas, such as the renovation of technological lines, in shipyards, as support structures for advertising, as a cover for mass events, as estrangements, as temporary structures, as decorative elements, etc. The often complex design of scaffolding causes the multiplicity of opportunities for occurrence and development of dangerous situations, understood as all unforeseen events which are a threat to people in or around the scaffolding. Employee behavior and their psychophysical state largely depend on structural stability and environmental factors. Environmental factors, i.e. physical stimuli of the external environment, affect both the people at work, and the construction.

¹ Corresponding author: Marek Jabłoński, Politechnika Łódzka, Katedra Fizyki Budowli i Materiałów Budowlanych, al. Politechniki 6, 90-924 Łódź; tel. 42 631 35 56; marek.jablonski@p.lodz.pl

² Iwona Szer, Politechnika Łódzka, Katedra Fizyki Budowli i Materiałów Budowlanych, al. Politechniki 6, 90-924 Łódź; tel. 42 631 35 56; iwona.szer@p.lodz.pl

³ Jacek Szer, Politechnika Łódzka, Katedra Fizyki Budowli i Materiałów Budowlanych, al. Politechniki 6, 90-924 Łódź; tel. 42 631 35 56; jacek.szer@p.lodz.pl

These include impacts such as noise, temperature, humidity, pressure, wind, light, vibration, dust, rainfall, icing, electromagnetic fields, radiation.

The subject literature deals primarily with accidents that occurred on scaffolding, e.g. [1–3], aspects of strength testing of scaffold components, FEM modelling [4] or wind behavior [5]. There is little information on the impact of noise, which is one of the important environmental factors.

The paper presents an analysis of noise impact on people working on scaffolding. All scaffolds tested were located in large cities (Łódź, Warszawa, Poznań, Wrocław, Lublin), while several of them in smaller cities near large agglomerations.

Work carried out on a scaffold by a construction worker is counted among particularly dangerous occupations of increased risk. The division of factors affecting occupational safety has been presented in [6–8]. One of the harmful factors is the noise that occurs on the scaffolding and its surroundings.

Noise can be severe, disruptive and can adversely affect human health. The negative effects of noise on the human body are varied, and their size and subsequent consequences depend on many factors. The effects of noise on the human body can be auditory and non-auditory.

Prolonged exposure to noise, with an equivalent sound level A above 80 dB, usually results in permanent loss of hearing. Permanent hearing loss may also occur in the case of single exposure to noise, if the peak sound pressure level exceeds 135 dB [9].

Non-auditory effects of noise on the human body are a stress factor leading to disorders of the respiratory system, circulatory system, and other organs. The noise also has a negative effect on the nervous system. In addition, noise reduces speech intelligibility and the perception of warning audio signals. The masking of speech and warning signals not only makes communication difficult, but above all increases the risk of accidents in a noisy environment. Noise is also a problem when we perform activities related to controlling and signaling. To a large extent, it limits the ability to observe and analyze information. It slows down the reaction time and has a negative impact on the decisions made.

2. Subject of study

The measurements and their results described in this paper were a part of the bigger research on façade frame scaffoldings [10]. This research was conducted by five teams consisting of employees from: Faculty of Civil Engineering and Architecture (Lublin University of Technology), Faculty of Management (Lublin University of Technology), Faculty of Civil Engineering, Architecture and Environmental Engineering (Lodz University of Technology) and Faculty of Civil Engineering (Wrocław University of Science and Technology).

As part of the research activities, the following studies were planned: collecting general information about scaffolding, scaffolding inventory, damage inventory, load inventory, surveying measurements, scaffolding force measurements, anchoring measurements, research of the bearing capacity, dynamic measurements of the scaffolding, atypical event recording [11], employee life parameters measurements, surveys with employees, measurements of environmental parameters, lighting intensity, atmospheric pressure, air temperature, relative humidity, wind speed [12–13], sound level, air pollution.

Sound level tests were conducted in the middle of the span. The measurements were carried out in six, nine or twelve places on the scaffolding (the number depends on the size of the scaffolding).

Measurements were taken in the extreme fields and fields evenly spaced on the scaffold using the following scheme:

- 3 or 4 measurements at the first full level (work platform),
- 3 or 4 measurements at half height (work platform),
- 3 or 4 measurements at the highest level (work platform).

An exemplary scaffolding with the arrangement of measuring points is shown in Figure 1.

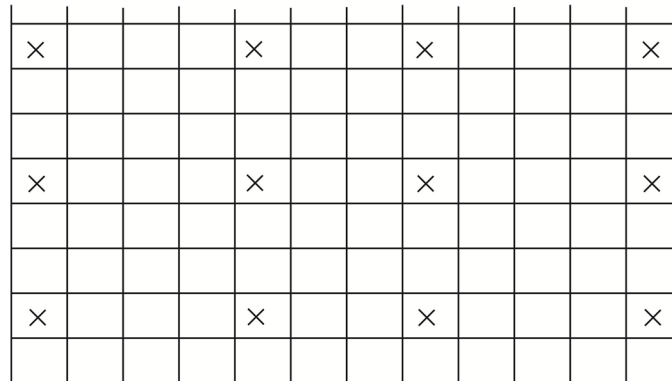


Fig. 1. Scaffolding view and exemplary arrangement of measurement points

Measurements were made at 3-hour intervals, i.e. the first round of tests from 8.00, second round of research from 11.00, third round of research from 2.00 PM. The aim of recording data at various times of the day was to obtain information on how the level of noise during the day changes. Measurements were carried out for five consecutive days of the week. As a result, a fairly complete view of the noise impact on workers' performance on the scaffolding was obtained.

The DB200 sound level meter was used to measure the sound level. Two parameters were recorded simultaneously at each measuring point for approximately six minutes: A-weighted equivalent sound level – L_{Aeq} and C-Weighted peak sound level – L_{Cpeak} .

Noise sources, typical for construction works that occur on scaffolding or in their vicinity most often that have an impact on noise affecting employees are grinders, drills, winches, table saws, hammers, concrete mixers, excavators, pneumatic hammers, blowers. The power level of these sources is usually quite large and the impact depends on the source distance from the specific employee.

The basic groups of noise sources are:

- machines that are energy sources, e.g. combustion engines (maximum sound levels A up to 125 dB), compressors (up to 113 dB),
- pneumatic tools and motors, e.g. manual pneumatic tools: hammers, cutters, grinders (up to 134 dB),
- cutting machines, circular saw blades for metal (up to 115 dB),
- machining machines, e.g. mechanical hammers (up to 122 dB),
- metal cutting machine tools, e.g. grinders, drills (up to 104 dB).

There are also other noise sources, not related to construction works that have impact on the resultant sound level that affects employees. These are communication noises coming from streets adjacent to the construction site [14].

Because of construction noise is generally fluctuating, it is reasonable to use the continuous steady-state indicator $L_{Aeq,T}$, which is calculated by taking an average of the fluctuant noise level during a period of time (1). Noise exposure level $L_{EX,8h}$ is calculated by normalizing $L_{Aeq,T}$ to the length of a typical working day, according to the calculation procedures proposed in PN-EN ISO 9612:2011 (2, 3).

$$L_{Aeq,Tm} = 10 \log \left[\frac{1}{N} \sum_{i=1}^N 10^{0,1L_{Aeq,Tmi}} \right] \quad (1)$$

$$L_{EX,8h,m} = L_{Aeq,Tm} + 10 \log \left(\frac{T_m}{T_0} \right) \quad (2)$$

$$L_{EX,8h} = 10 \log \left[\sum_{m=1}^M 10^{0,1L_{EX,8h,m}} \right] \quad (3)$$

where:

m – the divided task m ,

N – the total number of task samples,

T_m – the duration of task m ,

T_0 – the reference duration, $T_0 = 8$ h,

$L_{Aeq,Tm}$ – the A-weighted equivalent continuous sound pressure level for task m ,

$L_{EX,8h,m}$ – the noise contribution from task m to daily noise exposure level.

The basic type of noise that is assessed at workplaces is the noise in an audible range. The risk assessment resulting from exposure to noise can be made on the basis of recorded parameters. If A-Weighted maximum sound level

L_{Amax} is lower than 109 dB or C-Weighted peak sound level L_{Cpeak} is lower than 129 dB, it is considered that the risk of exposure to noise is low (negligible). If A-Weighted maximum sound level L_{Amax} is higher than 109 dB but lower than 115 dB or C-Weighted peak sound level L_{Cpeak} is higher than 129 dB but lower than 135 dB the risk of noise exposure is medium (acceptable). Where A-Weighted maximum sound level L_{Amax} is higher than 115 dB or C-Weighted peak sound level L_{Cpeak} is higher than 135 dB, noise exposure is considered to be massive (unacceptable) [9].

3. Results of research

The results of the recorded acoustic parameters from all noise sources for the selected day, selected hour and selected one measuring point are shown in Figure 2. For each measurement point, in each hour from the recorded data A-Weighted equivalent sound level $L_{Aeq,T}$ were calculated and C-Weighted peak sound level L_{Cpeak} and A-Weighted maximum sound level L_{Amax} was determined.

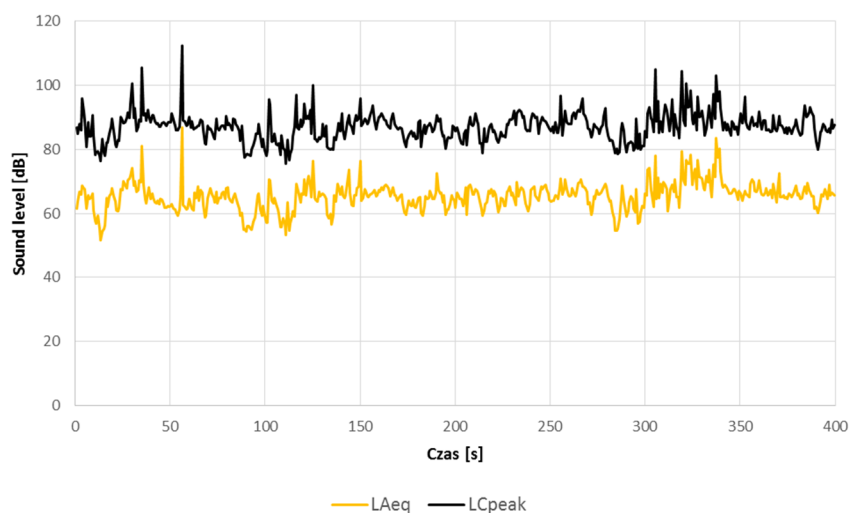


Fig. 2. C-Weighted peak sound level (upper graph) and A-weighted equivalent sound level (lower graph) registered at one measuring point

In this analysis, for each measurement point, in each round from the recorded data C-Weighted peak sound level L_{Cpeak} was determined and A-weighted equivalent sound level $L_{Aeq,T}$ were calculated from which $L_{EX,8h}$ was calculated.

The analysis of noise was not conducted strictly according to the PN-EN ISO 9612 standard. The specifically customized research program, which took the unusual characteristics of work on scaffoldings into consideration, was developed. The proposed program deviated from analysis standards commonly applied for workplaces.

The basic element of all statistical analyzes of a finite cardinality is the determination of the variable distribution observed in this cardinality, i.e. the assignment of values assumed by a given variable of their respective frequency occurrence. The distribution of the analyzed variable can be represented by a histogram. The histogram is used to visually assess the nature of the variable distribution. In the frequency distribution graph, for example, you can see which value occurs most frequently, whether most of the observed values are close to the average, etc. Such charts were created for 22 tested scaffolds in individual cities.

Since the change in the sound level by 1 dB is imperceptible, and only the change by 3 dB is palpable, the measurement range of sound levels is divided into 3 dB subranges, in which the occurrence frequency of a given sound level was calculated.

The diagrams (Fig. 3) show the distribution of the equivalent sound level, maximum sound level and peak sound level for one selected area.

Table 1. The probability of a dangerous situation occurrence having impact on an employee's health

Location	The number of exceeded L_{Cpeak} values = 129 dB	The number of all measurements	The probability of exposure to excessive noise
Łódź	5	2 827	0.0017
Lublin	29	2 280	0.0127
Poznań	8	2 258	0.0035
Warszawa	29	2 335	0.0124
Wrocław	32	2 532	0.0126

The occurrence frequency of excessive sound level values on scaffolds was also analyzed. Table 1 illustrates the probability of a dangerous situation occurrence having impact on an employee's health due to exposure to noise. The values were defined as the ratio of the number of measurements for which peak sound level exceeding 129 dB was observed to the number of all measurements on analyzed scaffoldings.

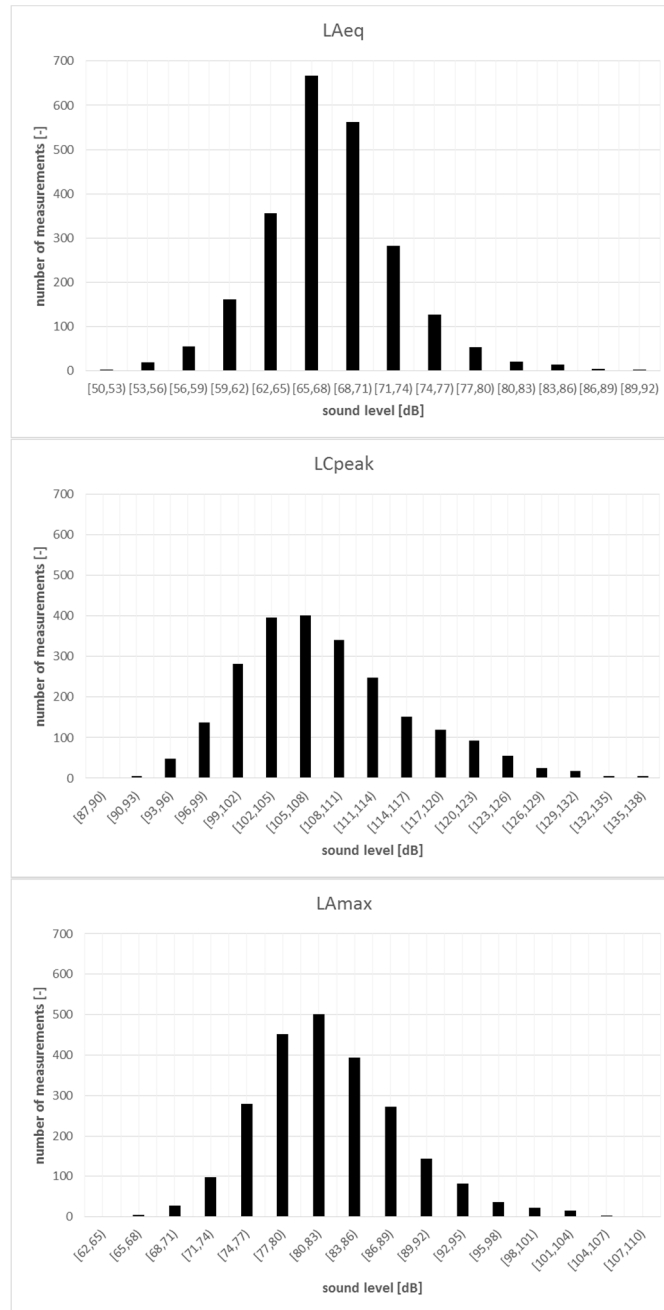


Fig. 3. A-weighted equivalent sound level, C-weighted peak sound level and A-weighted maximum sound level LAmx registered on scaffoldings in Warszawa

4. Conclusion

Exposure to noise on scaffolding is primarily associated with the performance of specific activities, machinery usage or technological processes. Noise is the most common detrimental factor in this work environment. A construction worker working on a scaffolding is frequently exposed to the noise that exceeds acceptable levels.

Based on the presented graphs, it can be concluded that the A-weighted equivalent sound level most often reached values between 65–68 dB and the A-weighted maximum sound level between 80–83 dB. The A-weighted equivalent sound level registered on the analyzed scaffolds varied from 50 dB to 90 dB and the A-weighted maximum sound level from 62 dB to 110 dB.

C-Weighted peak sound level usually reached values between 105 dB and 108 dB, but it exceeded 129 dB many times, which can be considered dangerous. This situation took place on 38 scaffoldings from 110 tested.

Values above 135 dB, which are unacceptable values, also occurred during taking measurements on 7 scaffoldings. Such situations should be considered harmful to health, and a high-risk, due to the protection of hearing.

The level of exposure to noise can be more effectively reduced by incorporating preventive measures into the design of work stations and places of work and by selecting work equipment, procedures and methods so as to reducing the risks at source.

Employers should make adjustments in the light of technical progress and scientific knowledge regarding risks related to exposure to noise, with a view to improving the health and safety protection of workers.

***Acknowledgement:** The paper has been prepared as a part of the project supported by the National Centre for Research and Development within Applied Research Programme (agreement No. PBS3/A2/19/2015 “Modelling of Risk Assessment of Construction Disasters, Accidents and Dangerous Incidents at Workplaces Using Scaffoldings”).*

References

- [1] Błazik-Borowa E., Szer J.: The analysis of the stages of scaffolding “life” with regard to the decrease in the hazard at building works. *Archives of Civil and Mechanical Engineering* 15 (2015), 516–524.
- [2] Whitaker S.M., Graves R.J., James M., McCann P., Safety with access scaffolds: development of a prototype decision aid based on accident analysis. *Journal of Safety Research* 34 (2003), 249–261.
- [3] Bellamy L.J., Exploring the relationship between major hazard, fatal and non-fatal accidents through outcomes and causes. *Safety Science* 71 (2015), 93–103.
- [4] Pieńko M., Błazik-Borowa E.: Numerical analysis of load-bearing capacity of modular scaffolding nodes. *Engineering Structures* 48 (2013), 1–9.

- [5] Wang F., Tamura Y., Yoshida A. Interference effects of a neighboring building on wind loads on scaffolding. *Journal of Wind Engineering and Industrial Aerodynamics* 125 (2014), 1–12.
- [6] Błazik-Borowa E. i inni, *Bezpieczeństwo pracy w budownictwie*. Wydawnictwo Politechniki Lubelskiej, Lublin 2015.
- [7] Szer J., Błazik-Borowa E.: *Bezpieczeństwo użytkowników w trakcie budowy i użytkowania rusztowań*. *Materiały Budowlane*, 10/2014, 2014, 190–192.
- [8] Hoła B.: *Bezpieczeństwo pracy w procesach budowlanych*, Oficyna Wydawnicza Politechniki Wrocławskiej, Wrocław 2016.
- [9] Rozporządzenie Ministra Gospodarki i Pracy z dnia 5 sierpnia 2005 r. w sprawie bezpieczeństwa i higieny pracy przy pracach związanych z narażeniem na hałas lub drgania mechaniczne. (Dz.U. z 2005 r., Nr 157, poz. 1318).
- [10] Błazik-Borowa E, Szer J.: Basic elements of the risk assessment model for the occurrence of dangerous events on scaffoldings, *Przegląd budowlany*, vol. 10, 2016, 24–29.
- [11] Błazik-Borowa, E., Bęc J., Robak A., Szulej J., Wielgos P., Szer I.: Technical factors affecting safety on a scaffolding, in *Towards better Safety, Health, Wellbeing, and Life in Construction*, Emuze Fidelis, Behm Mike Ed. Bloemfontein: Department of Built Environment Central University of Technology, 2017, 154–163.
- [12] Szer I., Błazik-Borowa E., Szer J.: The influence of environmental factors on employee comfort based on an example of location temperature, *Archives of Civil Engineering*, vol. LXIII, 2017, 193–174.
- [13] Szer I., Szer J., Cyniak P., Błazik-Borowa E.: Influence of temperature and surroundings humidity on scaffolding work comfort, *Prevention of Accidents at Work*, Bernatik A., Kocurkova L., Jørgensen K., Taylor & Francis Group, 2017, 19–23.
- [14] Jabłoński M., Szer I., Szer J., Błazik-Borowa E.: *Klimat akustyczny na rusztowaniach*. *Materiały Budowlane*, 8/2017, 2017, 32–34.

Przesłano do redakcji: 24.02.2018 r.

Przyjęto do druku: 31.03.2018 r.

Alicja TAMA¹
Katarzyna ADAMEK²
Karolina PARGIEŁA³
Agnieszka OCHAŁEK⁴
Artur KRAWCZYK⁵
Michał LUPA⁶

MONITORING OF HISTORICAL LAND USE CHANGES CAUSED BY UNDERGROUND MINING IN MIEDZIANKA TOWN, BASED ON A WEBGIS TOOL AND INSAR OBSERVATIONS

The article presents land surface changes caused by historical mining of metal ores on in the country town of Miedzianka in Lower Silesia, Poland. From the 19th until the middle of 20th century, mining in Miedzianka was in depression. Due to long-term and widespread mining activity, the town almost completely disappeared. The scale of the devastating effects of the mining appeared on the surface of the land, which led to the decision to abandon Miedzianka. Despite the damage the local authority made efforts to renew regional tourism. Unfortunately, it is impossible to carry out revitalization without recognizing the current threat of post-mining excavations. Therefore, the authors focused on analyzing collected archival documentation to understand the mining processes that have occurred and may still be occurring under the surface. The archival maps presented in the article have been indicated land use changes from 1886 to 1951. The current situation display WMS layer from Geoportall website. The collected materials allowed the spatiotemporal changes that occurred in Miedzianka to be presented. Additionally, the information

¹ Corresponding author: Alicja Tama, AGH University of Science and Technology, Faculty of Mining Surveying and Environmental Engineering, Aleja Adama Mickiewicza 30, 30-059 Cracow; alicja.tama@gmail.com

² Katarzyna Adamek, AGH University of Science and Technology, Aleja Adama Mickiewicza 30, 30-059 Cracow; adamek.kasia@gmail.com

³ Karolina Pargieła, AGH University of Science and Technology, Aleja Adama Mickiewicza 30, 30-059 Cracow; pargielakarolina@gmail.com

⁴ Agnieszka Ochalek, AGH University of Science and Technology, Aleja Adama Mickiewicza 30, 30-059 Cracow; aga.ochalek@gmail.com

⁵ Artur Krawczyk, AGH University of Science and Technology, Aleja Adama Mickiewicza 30, 30-059 Cracow; tel. 12 617 22 76, artkraw@agh.edu.pl

⁶ Michał Lupa, AGH University of Science and Technology, Aleja Adama Mickiewicza 30, 30-059 Cracow; tel. 12 617 33 76, mlupa@agh.edu.pl

base has been enriched with InSAR results for monitoring terrain deformation. The observations demonstrate that the biggest changes have taken place before 1936. In addition, current urban development constitute less than 25% of historical buildings. Analysis of InSAR method indicate that the research area require more accurate technique, because of the occurrence of large number of agricultural and forest areas.

Keywords: revitalization, historical mining impact, urban development, WebGIS tool, InSAR technique

1. State of the art

Miedzianka and its surroundings become famous thanks to the rich deposits of valuable minerals extracted there since at least the 19th century [1]. Due to this, over the years this area attracted the interest of many people, institutions, entrepreneurs and others. Centuries of extraction were an incentive for the creation of various data sets that allowed the mining history and city itself to be tracked. It should be noted that over time the methods of data storage changed, which makes analyzing and extracting information and relationships between data a challenging task. An integrated approach to the problem of creating an information system that allows for basic interoperability between these storage formats seems to be the right direction in which to proceed. In general, the term ‘interoperability’ refers to the ability of different applications to communicate between each other [2], but with GIS solutions it can also be applied to different kinds of spatial data. Using websites as a space for sharing spatial data has gained increasing attention since the end of last century [3]. Referring to [3], a geoportal is defined as “a web site where geographic content can be discovered”, with emphasis on the fact that a primary focus of the website is this geographic content. In a broader scope it also fits solutions like web-based applications, one of which is presented in this paper.

As described by [2], infrastructures for spatial data, no matter the form, can be implemented on four levels. The highest level is the international one, for which there are many great examples, like the services provided by Copernicus [4]. Many international and national geoportals and services in Europe are the result of the European INSPIRE directive, whose main goal is to improve the flow of spatial information between countries [5].

On the national level, spatial data infrastructures provide data access for various units like private entrepreneurs, local governments [2] and many others. The third level distinguished by [2] is the regional level, which is represented by e.g. geoportals of voivodeships. Over recent years, a significant increase in the number of regional geoportals has been observed. Moreover, the spectrum of shared data has widened [6].

The last level, which is also a concern of this paper, is the local level, at which data about a particular city or small area are presented. For this purpose, geoportals or smaller web-based applications can be used. These are suitable for

projects dedicated to a particular case or local area. This paper presents a simple application created for Miedzianka as an example of a local-level spatial data infrastructure. The usefulness and usability of this type of solution is described with the use of various examples of applications across a vast number of categories. Sharing spatial data on a local level is also used in tools that provide access to project data to project members. A solution like this allows diverse team members to share and organize results and knowledge, as for example described by [7]. The multitude of applications that are created worldwide are as varied as the needs of those who create and use them. The popularity of this type of solution rests on the ease of use of web-based GIS solutions, the low cost, and the possibility of providing data access to large groups of people [8]. Many ready-to-use solutions are offered, such as www.giscloud.com, or those provided by Esri. ArcGIS Online, also known as AGOL, allows user-friendly platforms to be created [9]. One of the objectives of this paper is to present a cloud-based WebGIS application to track changes in Miedzianka as a use case. The authors believe that creating an application for sharing and visualizing data about Miedzianka will be an important step in integrating the data organizing processes that have been created and collected over centuries.

2. The research area

Miedzianka is a small town located in the Western Sudetes, at an altitude of over 500 m above sea level, between the Bóbr River and the Copper Stream Valley (Fig. 1). In the years of its glory, it was considered one of the most beautiful towns in Lower Silesia. Due to mining damage, Miedzianka is currently mostly ruined [10].

The urban infrastructure in Miedzianka was inseparably related to the mining industry. The first confirmed reports of the existence of the historical mine and its surroundings appeared in the 14th century. More recently, in the 16th century the

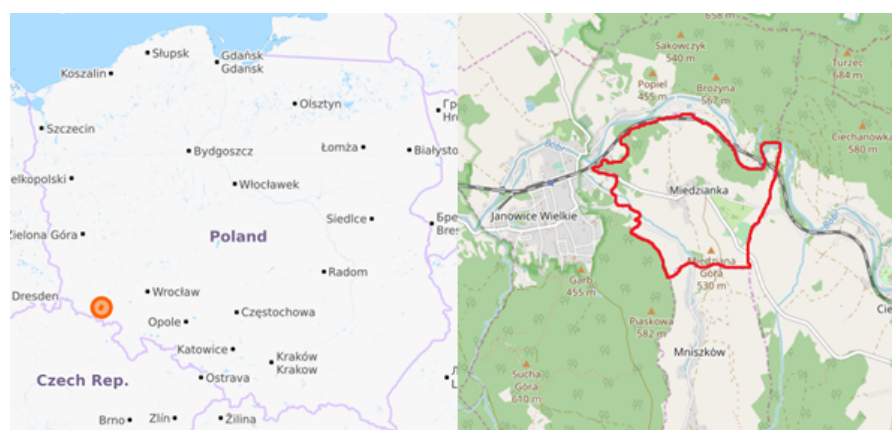


Fig. 1. Location of Miedzianka (Lower Silesia). Source: www.openstreetmap.org

mining activity intensified for several decades, with a focus on shallow deposits. Another boom of underground works occurred in the 18th century with the extraction of bornite and chalcocite, with the deepest shafts reaching 110 m. Pyrite and copper also started to be extracted but the deposits turned out to be significantly poorer than expected and mining ceased after several years. Some low-level activity was recorded until 1925 [11]. In Miedzianka, the copper ore deposits are the biggest. Analysis carried out by German researchers show that the copper ore extracted at Miedzianka until 1925 contained 18.7% Cu, 22.82% Fe, 2.42% Zn 1.32% Pb, 1.18% Ag, 1.25%, 0.22% Ag and 0.09% Sn. In the past, silver and iron were also extracted in this region [12].

Before World War II, copper was mined in Miedzianka, with four fields of exploitation. In the 1930s, uranium was also extracted [13]. One of the last episodes of mining at Miedzianka happened after World War II in 1948–1952, with much more intensive works at “Miedzianka” mine site [11]. Exploratory works were carried out again for uranium ores. Old shafts were partly renovated; more than 15 km of historical mining drafts, shafts and adits in total were reported. This is a clear indication of the scale of historical exploitation [12]. Apart from reusing old tunnels, about 40 km of new drifts and one adit were routed next to new shafts [11]. The depth of roadways reached about 250 meters [14].

In the early 1950s the “Sudeckie Zakłady Górnicze” company (translated as Sudety Mining Plants) was created, with “Miedzianka” mine being part of it [15]. The Miedzianka deposits were carefully mapped again to document the ore resources. Work was completed in 1955 and the mine was finally closed by decision of Polish government due to the lack of prospects for profitable mining of any ore or minerals [16]. In the 1990s some gold deposits were documented in the Miedzianka area [17].

Due to the extensive exploitation in Miedzianka, many sinkholes often formed both in the main part of the city and in agricultural areas [18]. The rapid extraction was also accompanied by landslides. For this reason, surface structures were and are still the most threatened, including well-known architectural monuments such as The Church of St. Cross, The Church of St. John The Baptist, the “Schwarzer Adler” house and the old brewery. Nowadays, only the last three of these structures survive.

3. Project assumptions

In 2002, the non-profit Kaczawski Association was founded. Since then, with the aim of revitalizing abandoned cities and restoring tourist infrastructure, it has been running social campaigns for the development of the Kaczawski Foothills, of which the Miedzianka area is an important part. One of the successes of this association is the creation and running of the Sudeten Educational Farm (SZE). One of the statutory aims of SZE is also to preserve the history of regional mining, of which Miedzianka is a natural part. Therefore, there is a need to undertake

research on the history of mining in the area of Miedzianka and to verify local suspicions concerning the current threat of post-mining deformation in Miedzianka.

The project aims to create a comprehensive database (geodatabase) which contains information about changes in Miedzianka as a result of the historical mining of copper ore. The purpose of the above geodatabase was:

- 1) creation of a low-budget land development plan that will be useful, among others, for town planners in the revitalization of the Miedzianka area,
- 2) data archiving and presentation of land use changes over time,
- 3) creation of a public application that will allow information about Miedzianka to be easily viewed.

The created geodatabase will be published using a web application. This will make the collected information available to the project team over the internet. The developed application will also be used to present information obtained from terrain deformation measurements, which will be carried out using several different techniques: GPS, remote sensing and surveying.

4. Application for geodata presentation

One of the project goals was to create a functional application that will serve as a tool to assist people involved, for example, in the study of land use changes. What is more, the application should allow maps based on various types of spatial data to be displayed and simple operations to be performed on these maps, i.e. distance and surface measurements, dynamic printouts, address search, or displaying multiple thematic layers at the same time. In the context of working with data from many sources and topographic and thematic maps (mining, geological), this last functionality seemed particularly important.

The second important assumption was the minimization of the amount of work due to the short time span of the project and the low budget. The goal was to prove that in a short time it is possible to create a good quality and truly functional tool. From a technical point of view, the aim of this study was to design a WebGIS architecture that requires no programming skills from the user and does not require him to set up a GIS server. Therefore, it was decided to use the WebGIS platform provided by ArcGIS Online (AGOL) technology, with an open academic license.

AGOL supports all the OGC standards such as WFS, WMS, WMTS as well as REST map services. What is more, AGOL provides configurable user-friendly WebGIS application templates that are designed for various map applications. Therefore, the application was generated without writing a line of code.

According to the required IT infrastructure, the solution is based on the Esri SaaS platform, so all the server functionalities (hosting web maps, geoprocessing tools, as well as web application) can be moved to the cloud. Nowadays, cloud-based WebGIS platforms (SaaS model) have moved logic and data layers to the cloud as a single tier. Therefore, it is now possible to develop WebGIS projects more easily with the use of only SaaS. The second tier of our application contains a desktop GIS which is linked to the AGOL app.

The affine method in desktop GIS (ArcMap 10.6) was used to calibrate the collected archival materials, perform digitization, develop graphical map projects, and upload spatial data to a file geodatabase. This kind of file geodatabase functions as a data layer that feeds graphic map projects prepared using the GIS desktop. All these data are subsequently transmitted to the cloud. This 2-tier (SaaS & Desktop) architecture creates new WebGIS architecture possibilities [7]. The main application interface is shown in the figure below (Fig. 2).

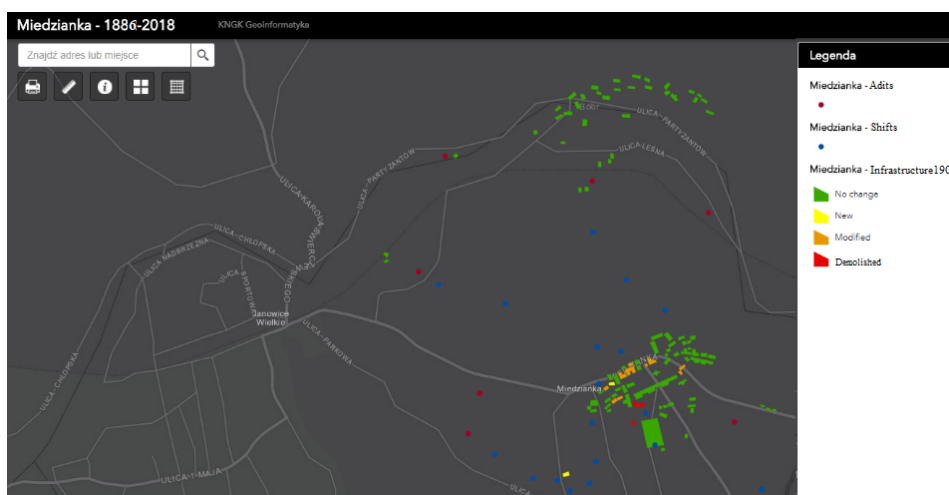


Fig. 2. The main application window

5. Input data

The article uses two types of input data to present both the historical and the current state of the area around Miedzianka:

- historical situation: received from the local geodetic and cartographic documentation center there are 7 archival maps from 1886 to 1951 in the Polish CS92 coordinate system, UTM, and the German Messtischblatt coordinate system on a scale of 1:25 000,
- current state of infrastructure: map of land and building records,
- current surface state: data from the Sentinel 1 satellite mission,
- 80 maps of mining excavations from the archive of the Higher Mining Office (WUG): maps of uranium mines from 1951–1953, drawn up in 1:500 scale; several maps were prepared with descriptions in Russian; some of them are made entirely by hand; some are made by a Polish company based in Stalinogród (currently Katowice).

5.1. Infrastructure change-over

Historical and current documentation in many fields of science is a valuable source of information. In this case, it was used to indicate changes that have occurred in the municipal infrastructure of Miedzianka town. The analysis used 7 archival maps, the first two of which were military maps (year of preparation: 1936, 1951) in the UTM and Poland CS92 coordinate systems. The scale of the maps was respectively 1:100 000 and 1:25 000. The next five maps were topographic maps in the German Messtischblatt coordinate system from 1886 (Fig. 3), 1906, 1913, 1936 and 1939 on a scale of 1:25 000.



Fig. 3. Fragment of the German Messtischblatt topographic map from 1886 on a scale of 1:25 000

Information about the present development was obtained from the current map of land and building records in cooperation with the local geodetic and cartographic documentation center.

5.2. InSAR data

Interferometric Synthetic Aperture Radar is a remote sensing method that allows detection and measurement of dynamic terrain movements. This technology finds particular application in investigating the deformation of mining areas [19, 20]. The present research uses satellite imagery from the Sentinel mission, which is supervised by the European Space Agency “ESA” (website:

www.esa.int/ESA). The Sentinel 1 satellite, which operates under this program, has performed radar imaging of the surface of the Earth since April 2014. Data from the Sentinel 1 mission is obtained through a constellation of identical C-band synthetic aperture radars (two units: A and B), which makes it possible to work on images acquired within a 6-day timespan (reduced from 35 days for ERS-1 and ERS-2 or 30/35 days for ENVISAT) [20].

6. Results

On the basis of the obtained materials, the full interpretation was presented of the changes in Miedzianka from the late 19th century to the present day. The approach included:

- taking into account changes in urban development based on available maps using GIS software,
- obtaining information about the current surface area in Miedzianka by generating a DEM model from interferometric data.

6.1. Urban development

The surface structures in Miedzianka are a perfect example of the impact of mining operations on the land surface. Collected materials from various maps allowed direct identification of changes to buildings. To merge the information from all the maps, the military topographic map from 1936 was used as a reference. The calibration was performed for four adjustment points, with an RMS error of 9.07. Based on the calibrated map in the Poland CS92 coordinate system, further calibrations of 5 topographic maps and 1 military map from 1951 were made. Due to the unusual German coordinate system and the occurrence of both the Greenwich and the Ferro meridians on these maps, it was decided that the calibration would take place on characteristic points in the area such as crossroads, triangulation points, etc. On each map, 8 adjustment points were indicated where the RMS error ranged from 8 to 19.

After the above steps, the urban structure that existed in 1886–2018 was visually analyzed by performing manual vectorization of the buildings on the maps (Fig. 4).

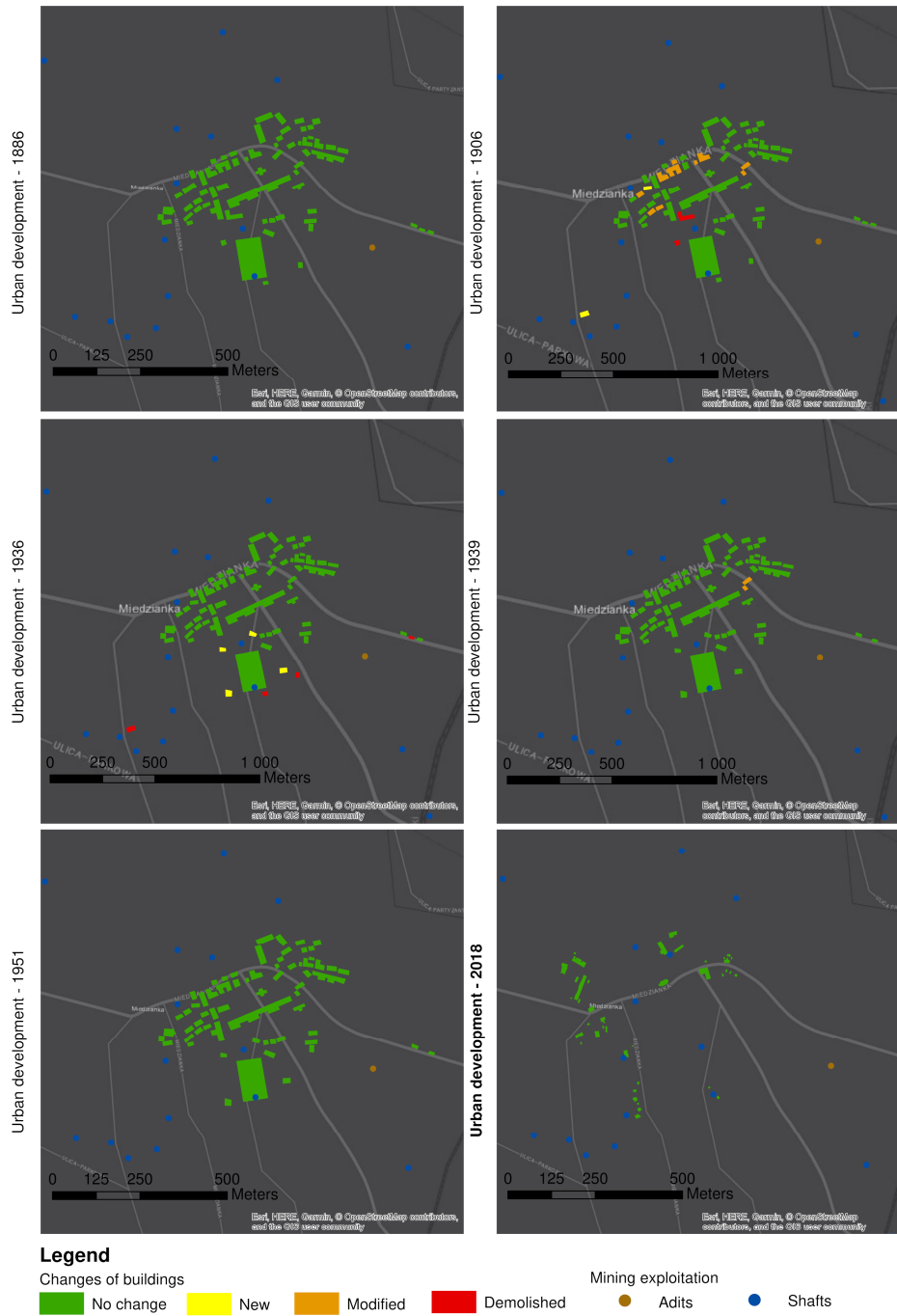


Fig. 4. Changes of urban development in Miedzianka between 1886–2018

Numbers of new, modified or demolished buildings were identified on the maps by comparing them in chronological order, Showing the result of the above analysis in Table 1, the biggest changes took place before 1936. In those years, more than 5% of the total number of buildings were newly built residential buildings (mainly in the upper part of Miedzianka), less than 7% were demolished buildings and about 10% of them were modified (either partially demolished or extended). However, the biggest changes were noticeable when comparing the historical and contemporary data. Only 22% of Miedzianka's current residential buildings are historic. Based on these statistics, it can be concluded that mining exploitation had a huge impact on local development.

Table 1. Characteristics of the urban infrastructure of Miedzianka

Year of information	Number of existing buildings	Number of new buildings	Number of demolished buildings	Number of modified buildings
1886	101	-	-	-
1906	101	2	2	10
1913	100	0	1	1
1936	105	6	1	2
1939	106	2	1	0
1951	106	0	0	0
2018	24	-	-	-

Based on the above analysis, it was found that in Miedzianka during these years there were significant changes in the urban infrastructure. These changes most likely reflected the extensive exploitation carried out during those times. These conclusions can be drawn from information obtained about mining activities such as the exact locations of shafts, adits and buildings that have disappeared, most of which were located near the shafts or adits. In addition, their deterioration was random, as is confirmed by some historical stories about Miedzianka.

6.2. InSAR technique

The indicator of the compatibility level between the phases of two different SAR images is coherence, or more precisely, the correlation coefficient of complex values. Deficiencies in mutual compliance may be the result of technical factors (temporal and perpendicular baseline) or environmental factors (land use and land cover, atmosphere impact, local slope). The coherence value for the area can be read from the coherence map generated on the basis of coregistered SAR images. Lack of mutual correlation of images generates noise and distorts the readability of results [21].

The analysis was carried out on the basis of 12 radarograms, from which 6 coherence maps were generated for different seasons of the year. The temporary baseline between SAR images was 6 days for all cases. The specific pairs of images on the basis of which coherence was examined were analyzed in terms of atmospheric similarity based on archival data from the www.meteomodel.pl portal in order to decrease the variability of conditions. The images with divergent geometrical baseline values were selected to determine whether any coherence deficiencies are caused by this.

The obtained coherence maps were clipped to equal parts of the Miedzianka area (18.58 square kilometers). The mean level of coherence was recorded for each case. The values are similar and do not exceed 0.4 (the threshold value of good readability of interferograms). The collation is shown in Table 2 and views of the coherence maps are shown in Figure 5. The numbers in column 1 correspond to the image numbers.

Table 2. Coherence collation

Number	Date	Min	Mean	Max
1	18.05.2017–24.05.2017	0.012	0.289	0.985
2	29.07.2017–04.08.2017	0.011	0.331	0.977
3	09.09.2017–15.09.2017	0.011	0.330	0.980
4	02.11.2017–08.11.2017	0.012	0.391	0.983
5	13.01.2018–19.01.2018	0.013	0.349	0.979
6	08.03.2018–14.03.2018	0.015	0.327	0.988

On the basis of the obtained values it was possible to state that the coherence for the studied area is weak; this could generate noise that makes it impossible to carry out thorough analyses. All the received coherence maps belong to class 1 (lack of coherence) [21]. Therefore an attempt to perform DInSAR or PSInSAR analysis may turn out to be ineffective [22]. Due to the rejection of the majority of options that may disturb coherence during the analysis, the terrain coverage for the studied area was analyzed.

A significant relationship between the coherence value and the type of land cover was noticed. It was concluded that the best coherence was recorded for arable land (without plants) and buildings; the worst was for meadows and forests. Coherence increases within months when the vegetation is of lower density.

The InSAR technique is often used to create a digital DEM model with an accuracy of up to 1 meter [23]. In this article, radar imagery from the period 14.02–02.03.2018 were used to generate the DEM model. When selecting specific imagery, the maximum possible size of the geometric base was selected.

The generated DEM model (Fig. 6) is characterized by a raster cell size of 0.5 seconds. In relation to the SRTM model, this value is twice as low, which may indicate a much better resolution of the obtained model. However, after

completing the accuracy analysis, it was determined that the accuracy of the DEM model is in the range of 20 to 50 m. For the SRTM model, this accuracy is 1 meter. The low level of accuracy was caused by poor coherence, which was closely related to the type of the studied area: the occurrence of large number of agricultural, forest areas and small number of build-up areas (where the value of coherence is better). Therefore, it can be concluded that the generated DEM model only serves the general visualization of the digital terrain surface.

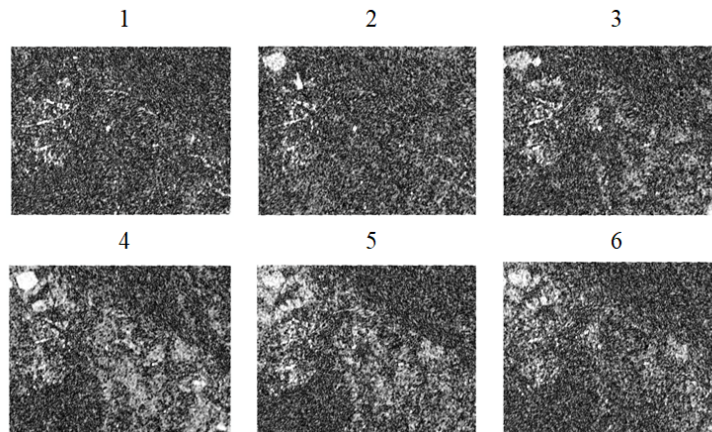


Fig. 5. Images 1-6 showing obtained coherence maps

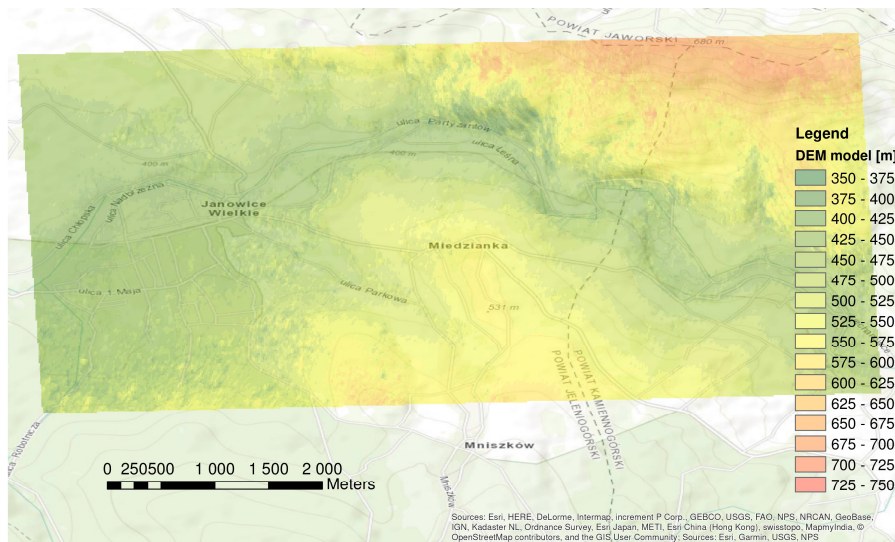


Fig. 6. Generated DEM model from Miedzianka town

7. Conclusions

Spatial planning and revitalization of areas such as Miedzianka require an interdisciplinary approach to the subject. On the basis of archival data and satellite imagery, it is possible to comprehensively present the characteristics of changes taking place in Miedzianka. With the use of tools such as AGOL, the content of the data and its transmission are largely simplified and easily accessible. The created application will be the core of a public database that aims to provide information about changes in land development. This information should be useful for many potential groups of planners. In addition, the great advantage of the created application is the ability to create it without the need for programming. All in all, the development and revitalization of post-mining areas such as Miedzianka will become much easier to manage.

***Acknowledgements:** The research and application presented in this article was carried out as part of the Rector's AGH-UST Grant "Construction of an information system for permanent monitoring of land deformation caused by historical mining in Miedzianka in Lower Silesia with the use of satellite radar interferometry", implemented by a team of students from the KNGK "Geoinformatyka" scientific circle at the Faculty of Mining Surveying and Environmental Engineering.*

Sentinel-1 data were provided by ESA under the free, full and open data policy adopted for the Copernicus program.

The cost of publication of this article was financed by the Chancellor of AGH University of Science and Technology in Cracow from the Geoportal project.

References

- [1] Zalewski W.: History of mining and metallurgy in Upper Silesia until 1806, Publishing house Towarzystwo im. Romana Dmowskiego, Madrid 1967.
- [2] Akinci H., Cömert Ç.: Geoportals and their role in Spatial Data Infrastructures, 5th International Conference on Geographic Information Systems 2008.
- [3] Tait M.G.: Implementing geoportals applications of distributed GIS, Computers, Environment and Urban Systems, vol. 29, 2005, pp. 33–47.
- [4] https://www.esa.int/Our_Activities/Observing_the_Earth/Copernicus/Overview3 {access 2018 r.}
- [5] <http://inspire.ec.europa.eu/about-inspire/563> {access 2018}.
- [6] Dukaczewski D., Ciołkosz-Styk A., Sochacki M.: Regional geoportals in selected European countries – a comparative study, Annals of Geomatics, vol. 4, 2012, pp. 77–98.
- [7] Lupa M., Leśniak A.: Geoportal as a tool supporting geological and engineering works: the case of ISMOP project, vol. 4, 2014, pp. 411–416.
- [8] Khan Z.A., Adnan M.: Usability evaluation of web-based GIS applications. A comparative study of Google Maps and MapQuest, Master Thesis, 2010.
- [9] Lupa M., Samulowska M., Chmielewski S., Myszkowska D., Czarnobilska E.: A concept of WEBGIS pollen allergy mapping, 17th International Multidisciplinary Scientific Geoconference: Informatics, Geoinformatics and Remote Sensing, vol. 17, 2017, pp. 1–7.

- [10] Springer F.: Miedzianka. History of disappearance, Publishing house Czarne 2017.
- [11] Borucki J., Głowadzki Z., Masłowski W., Uberna J., Zajączkowski W.: Evaluation of prospecting prospects for uranium ore deposits in Poland, Publishing house Geologiczne, Warszawa 1967.
- [12] Kaczmarek A., Adamski W., Bareja J., Głowacki Z.: Evaluation of the uranocosity of the Sudetes. Industrial Works R-1, Geological Institute, 1959.
- [13] Bareja E., Jęczmyk M., Kanasiewicz J., Lis J., Miecznik J.B., Sałdan M.: Radioactive elements in Sudetes, Bulletin of the Polish Geological Institute, vol. 341, 1982, pp. 259–272.
- [14] Siuda R., Borzęcki R., Gołębiowska B.: Huts of the former mining industry in the Miedzianka-Ciechanowice region as documentations for the unique hyperergenic mineralization, Wrocław 2010.
- [15] Madziarz M.: "Czarnów", "Miedzianka" and "Stara Góra" mines in the search for uranium minerals and metal ores in the 1940s and 1950s, Wrocław 2009.
- [16] Report: Activity of Sudeckie Zakłady Górnicze in 1952–1955. Unpublished.
- [17] Wojciechowski A.: A map of the gold-bearing capacity of the Western Sudetes in the scale of 1: 100 000, State Geological Institute, 1995.
- [18] Makuch M., Stolarczyk T.: Miedzianka. 700 years of the mining town's history, Publishing house Muzeum Miedzi w Legnicy, Legnica 2013.
- [19] Krawczyk A., Grzybek R.: An evaluation of processing InSAR Sentinel-1A/B data for correlation of mining subsidence with mining induced tremors in the Upper Silesian Coal Basin (Poland), Baltic Geodetic Congress 2017.
- [20] Perski Z.: Applicability of ERS-1 and ERS-2 InSAR for land subsidence monitoring in the Silesian coal mining region, International Archives of Photogrammetry and Remote Sensing, vol. 32, 1998, pp. 555–558.
- [21] Grzybek R.: Identification and analysis of mining areas subsidence with using InSAR technique based on Sentinel-1 SAR imagery, Geoinformatica Polonica, vol. 16, 2017, pp. 53–67.
- [22] Ferretti A., Prati C., Rocca F.: Permanent Scatterers in SAR Interferometry, IEEE Transactions on Geoscience and Remote Sensing, vol. 39, 2001, pp. 8–20.
- [23] Porzycka S., Leśniak A.: Radar image processing using permanent scatterers technique, Archives of Photogrammetry, Cartography and Remote Sensing, vol. 17b, 2007, pp. 661–669.

Przesłano do redakcji: 28.02.2018 r.

Przyjęto do druku: 31.03.2018 r.

Magdalena SĘP¹
Anna SIKORA²

THE VALIDITY OF THE BDOT10k DATABASE ON THE EXAMPLE OF THE TOWN OF TARNOBRZEG

Up to date issue of cartographic studies is a complex problem. The content of the BDOT10k database is particularly important from the user's point of view, which should be updated on a current basis. The authors carry out an analysis of the database's validity along with the assessment of changes in spatial topography based on available non-standard topographical studies and an orthophotomap. The research was carried out in the town of Tarnobrzeg, which due to its specificity (a town with high dynamics of development) allows for a clear picture of the essence of the problem.

Keywords: Tarnobrzeg, BDOT10k, topographic maps, urban structure, development of the city

1. Introduction

Since the 1990s, in Poland, official topographic maps have been made in digital technologies, until 2003 the main tools for their implementation were CAD. In 1999, experimental and pilot works in the field of building a modern topographic database began at the Head Office of Geodesy and Cartography. Test projects "Dunajec and Wisła" in 1999, and "Kujawy" in 2000 became the basis for the development of "Technical guidelines of the TBD topographic database". Initially, the database was called the "topographic database", before the publication of guidelines it was changed to the "topographic database", leaving the TBD abbreviation [1].

The guidelines were issued by the Head Office of Geodesy and Cartography in 2003. In 2008, their updated version was marked with the number 2.0. In the guidelines, the topographical database (TBD) is defined as "uniform in terms of

¹ Corresponding author: Magdalena Sęp, The Faculty of Civil and Environmental Engineering and Architecture, Rzeszow University of Technology, Powstańców Warszawy 12, 35-959 Rzeszow, tel. 178651658; msep@prz.edu.pl

² Anna Sikora, The Faculty of Civil and Environmental Engineering and Architecture, Rzeszow University of Technology, Powstańców Warszawy 12, 35-959 Rzeszow, tel. 178651049; sikora@prz.edu.pl

the conceptual model, an official nationwide system for collecting and sharing topographic data, which besides data consists of an appropriate financing system, organization, IT tool and necessary technical guidelines and instructions". The guidelines set out the rules for the organization of the TBD system, the development of a 1:10,000 topographic map, specification of the basic resource and TBD data exchange standards [2]. The legal basis for the creation of the topographic database was the Geodetic and Cartographic Law [3] and the Regulation of the Minister of Regional Development on detailed rules and procedures for establishing and maintaining the national system of information on land [4].

In the Regulation of the Minister of Internal Affairs and Administration regarding the database of topographic objects and databases of general geographic objects, as well as standard cartographic studies, the names "topographical database" (TBD) and "general geographic database" (BDO) were replaced by the names "database of topographic objects"(BDOT10k) and "general geographic objects database"(BDOO) [5].

2. Database of Topographic Objects – BDOT10k

2.1.Objective of development and legal basis of BDOT10k

The database of topographic objects, BDOT10k, is a spatial database of a reference nature corresponding to the detailed topographical map in scale 1:10,000. The basic task of its creation is to collect and share data for use in various information systems created by public and private institutions. The creation of BDOT10k is intended to prevent unnecessary repeated collection of the same data by various institutions.

The need to create a database of topographic objects for the whole country with details ensuring the creation of standard cartographic analyzes at scales 1:10,000 – 1:100,000, was written in the Spatial Data Infrastructure Act [6]. Guidelines for the creation of BDOT10k were included in the Regulation of the Minister of Interior and Administration [5]. The ordinance together with attachments defines the scope of data collected in BDOT10k and BDOO databases, organization, mode, creation standards, updates and sharing of both databases, also contains information on the joint objects catalog for BDOT10k and BDOO, three-level object classification, UML application scheme and GML scheme for both databases, guidelines for entering objects into databases, technical standards for creating standard mapping surveys are defined on scales from 1:10,000 to 1:1,000,000 [5].

2.2. Structure of BDOT10k

BDOT10k collects information about topographic objects, which include the spatial location of objects, their characteristics, cartographic codes and object metadata. Objects are grouped on three levels: on the first there are categories of object classes, on the second – object classes and on the third, most detailed one there are objects themselves.

The BDOT10k database is created and updated on the basis of data from various sources. The basic materials are public data registers constituting the State Geodetic and Cartographic Resource (PZGiK):

- land and building register – EGiB – is a source of information about the location, geometry, function, purpose of land and buildings,
- geodetic record of the utilities network – GESUT – it collects data on cables, their housings, technical devices related to networks,
- state register of boundaries and areas of territorial division units of the country – PRG – this database contains information on the borders of the state and territorial division units of the country, the boundaries of the coastal belt, the maritime coastline, surface areas of the divisions of the country and sea areas,
- the state register of geographical names – PRNG – is a source of information on the names of towns and physiographic objects,
- register of towns, streets and addresses – EMUiA,
- orthophotomap, aerial and satellite imaging – are a source of information about the most-real condition of coverage and land development,
- numerical terrain model – is a source of geometric data of watercourses and reservoirs, as well as the main data source for BUZM object classes (excavation, flood embankment, dam), OIPR (rock, boulders, rock threshold, etc.).

Sometimes, when the content is useful, other registers are used, such as:

- road data bank – BBD – relational database of the General Directorate for National Roads and Motorways, containing information on geometry, numbering, classes, road technical parameters, lane management, engineering facilities,
- data of the General Directorate for Environmental Protection – to the extent of protected areas,
- data of the National Heritage Institute – to the extent of immovable monuments,
- data of the National Water Management Authority and the Institute of Meteorology and Water Management – to the extent of water network,
- the national official register of the territorial division – TERYT – kept by the Central Statistical Office – is the source of information on the identifiers and names of the territorial division units of the country,
- data from town and community councils – to the extent of institution registered offices.

Field inspections complement and verify data from registers [5].

3. General functional and spatial characteristic of the research area – city of Tarnobrzeg

The city was founded in 1593, with visible development of buildings in the 1770s. Initially, the city developed concentrically around the centrally located market. With time, the center of gravity of the system has been moved south. Even in the mid-19th century, the building structure was mainly single-family residential buildings, free-standing or creating frontages, and several service facilities: the town hall, the monastery of Dominicans and small basic services.

After Poland regained its independence, the city accelerated its development. First, under the Four Year Plan, Tarnobrzeg was included in the Central Industrial District project, choosing Mokrzyce (currently a district of the city) as the place for development of metallurgical plants with a refinery, foundry and copper forge which was to become a driving force for the growth of the urban tissue [7].

The most important event affecting the dynamics of Tarnobrzeg's development was the discovery, in 1953, of rich deposits of native sulfur (it was defined as one of the largest deposits of native sulfur in the world). The new industrial unit – Sulfur Mine of Tarnobrzeg became the reason for the increase in the number of inhabitants, which led to the dynamic development of the city's residential structure, with particular emphasis on the multi-family block building [8]. Similarly to other units of the region, the urban tissue of Tarnobrzeg, based on the location of the main industrial plant, is largely residential and service structural units of multi-family housing and basic public utilities. As a result of the administrative reform of Tarnobrzeg, in 1975, it became a province and this state lasted until 1998. It was a time of dynamic development and investments. The period after the loss of the provincial city's status coincided with technological changes that made sulfur mining unprofitable and the mine was put into a state of liquidation, which significantly contributed to limiting and weakening the construction movement.

4. Current state of BDOT10k along with an analysis of the degree and type of investment in the area of the city of Tarnobrzeg

4.1. Method of analysis

The research method is a comparative analysis of basic cartographic studies, a digital orthophotomap and the BDOT10k database. The analyses were performed using the QGIS program. It is a free and open software, which tools are commonly used to carry out spatial structure analysis [9;10]. Materials for research were collected data from the Regional Center for Geodetic and Cartographic Documentation in Rzeszów. The database of BDOT10k topographic objects and topographic maps in scale 1:10,000 in 1965 and 1992

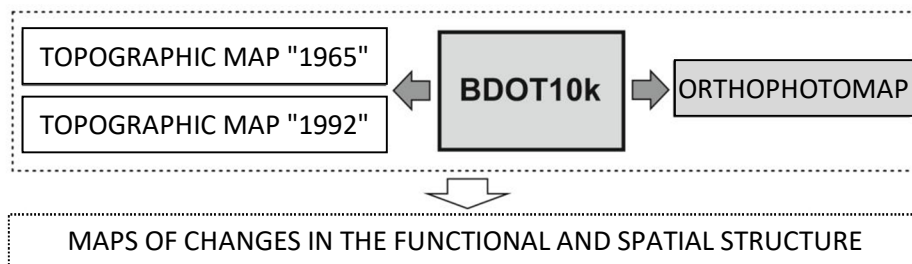


Fig. 1. Diagram of the structure of the comparative analysis (own study)

layouts were used, with maps in the 1965 layout from 1989 and 1999 in the 1992 layout. Orthophotomap (current status in 2017) was downloaded from the Geoportal (geoportal.gov.pl) thanks to the WMTS service (Fig. 1.).

The main analysis is a comparison of the BDOT10k database contents with a digital orthophotomap, which will allow determine the approximate current status of the database. Secondary analysis includes comparison of the database with the topographic map scans. A summary of the results will enable a graphical presentation of maps of functional and spatial changes in the city.

4.2. Updating of the BDOT10k database

The update was started by checking the changes that occurred in the studied area, by comparing the BDOT10 data with the orthophotomap. Thanks to the WMTS service, the orthophotomap was loaded, then vector layers were applied to it. Due to the content of a large number of layers and information in the BDOT10k database, we tried to give the layers appropriate styles, so that they are legible. Database layers often come in contact or overlap, so it is important to have a clear picture of each layer, because the introduced changes could cause topological errors. The city area was analyzed by searching for places where the vector layers did not coincide with the orthophotomap view. An appropriate update of the object classes in these areas has been made. During the analyzes, layers containing new building objects were created. 95 new buildings were created (Fig. 2.), they were mainly single-family residential buildings with accompanying buildings (garages, outbuildings) (in Figure 3 marked as A). Locations where the office buildings (company headquarters) and the health care facility were demolished were also located (in Figure 3 marked as B.).

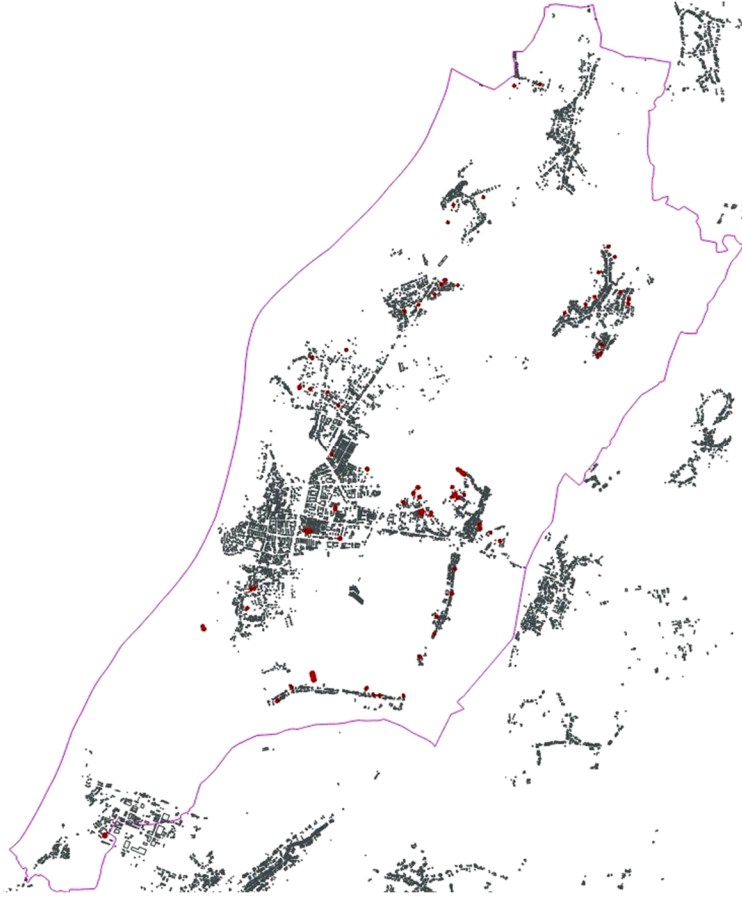


Fig. 2. BDOT10k update. The red color indicates the buildings entered into the base as part of the update based on the orthophotomap (own study)

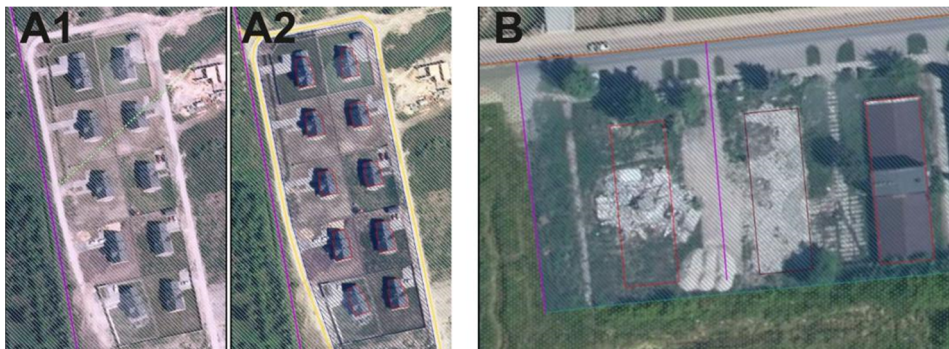


Fig. 3. BDOT10k update. A – introduction of new buildings, improvement of the existing road and introduction of a new one (A1 – view before the update, A2 – after the update), B – demolished buildings visible on the orthophotomap (own study)

After the quantitative update, the dates of introducing the objects to the database were checked. In the attribute tables, all layers contain information about the date of creating the object (*x_dataUtworzenia*) and information about the date of the geometry of the object (*x_aktualność*). For all facilities in the city area, the date of the geometry of the object is 15/10/2012, while the date of creating the object is 15 November 2012, the date of creating the database. The attribute of the buildings was also analyzed and the buildings that had the value "Bud" were selected, which means that at the end of 2012 they were buildings under construction, which were not being used. 242 of such buildings were selected

4.3. Comparison of BDOT10k content and available non-standard cartographic studies

Additional, somehow side-by-side analyzes are the comparison of BDOT10k with topographic maps in the "1965" (from 1989) and "1992" (from 1999) systems. Thanks to the raster map in the "1965" layout, we managed to create a new layer in the base, containing buildings visible on the rasters, due to which you can determine the time of construction of buildings before 1989. Number of such buildings identified is 6,874. The last analysis was made by comparing objects from BDOT10k with topographic maps in the "1992" layout. The analysis did not take into account the previously selected buildings. 3,435 buildings have been identified (Fig. 4.).

In the separate analyzed time intervals, it can be seen that the largest number of single-family residential buildings and farm buildings were built (including, garages). In the years 1989–1999 there were 1,203 single-family buildings built, i.e. 39.5% of all constructed buildings at that time, and 1,501 utility buildings, i.e. 49.5% of all buildings constructed in that period. In the next time interval (1999–2013) the construction pace in Tarnobrzeg decreased, however, the most numerous building groups among the newly-created were single-family residential buildings – 312 and utility buildings – 219, which was respectively 52.5% and 37% share in new buildings in this period. During the construction of the base, 280 buildings were under construction, 86.5% of which were single-family houses (242 buildings).

Apart from the number of buildings, the analysis also covered the building area. Based on data from BDOT10k, it was established that from 1989 to 2013, the area of Tarnobrzeg development increased from 1,069,591 m² to 1,658,410 m², i.e. it increased by 55% (buildings under construction were included in the calculations). The fastest growth in building space is in the years 1989–1999, it was 43%. The Table 1. shows the detailed distribution of surfaces depending on the function.

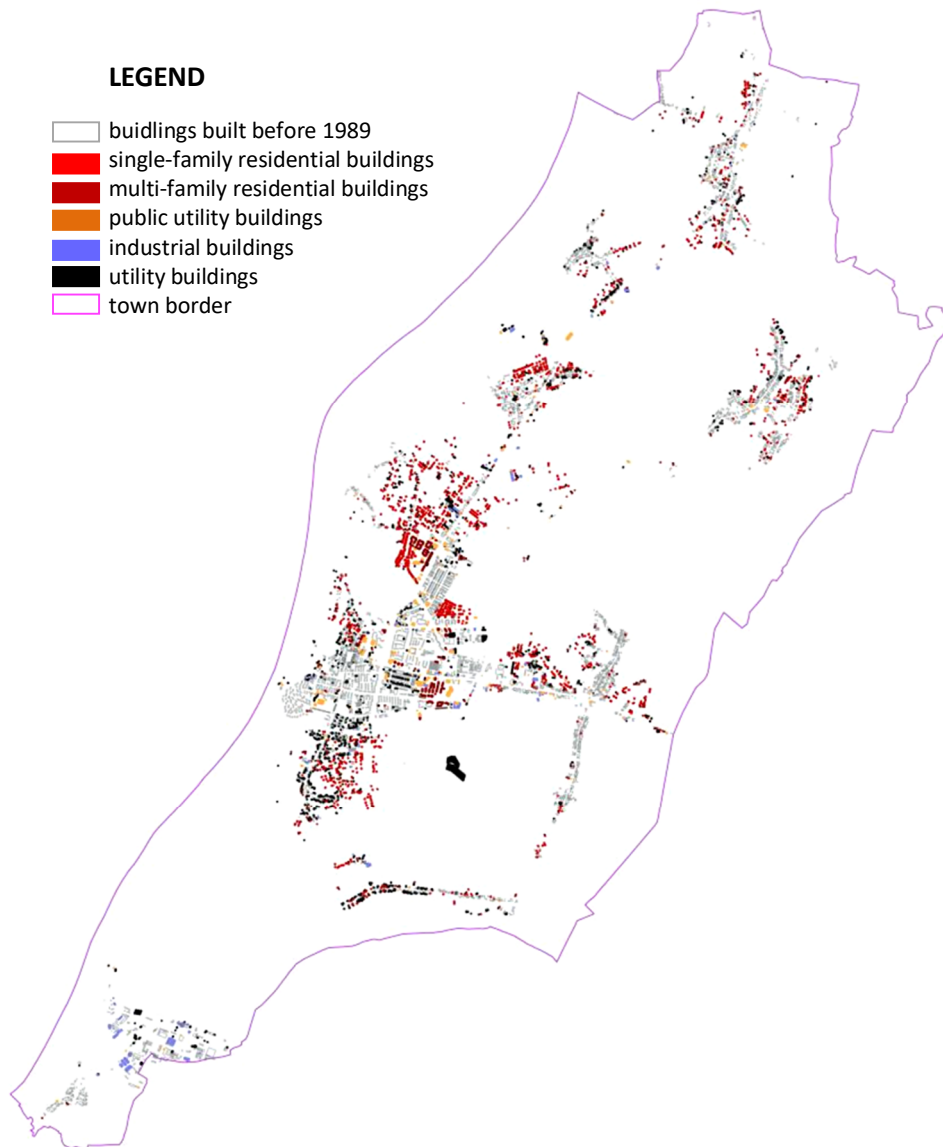


Fig. 4. Analysis of spatial and functional changes in 1989–2013 (own study)

Table 1. Change of building area in the analyzed time intervals (own study)

Buildings Years	Single-family	Multi-family	Residential buildings in total	Utility buildings	Public utility building	Industrial	Σ
	[m ²]						
to 1989	296,135	155,784	451,919	251,880	187,088	178,704	1,069,591
1989–1999	140,775	33,913	174,688	174,908	66,029	47,259	462,884
1999–2013	39,479	2,057	41,536	20,159	10,783	10,361	80,786
under construction	31,310	1,786	33,096	2,053	5,450	4,550	45,149
Σ	507,699	193,540	701,239	446,947	269,350	240,874	1,658,410

5. Conclusions

As part of the research, the Database of Topographic Objects (BDOT10k) was compared with other sources of data, an orthophotomap and topographic maps from the late 1980s and 1990s. In the research area - the city of Tarnobrzeg, after the update based on the orthophotomap, discrepancies were found and 95 new buildings were added to the database. The estimated time of creation of 9,699 objects from the BUBD layer was also determined. The area of development in the city of Tarnobrzeg increased by 55%, i.e. 0.25 km², with the increase of 0.19 km² by 1999. Conducted analyses show that the city was developing most dynamically until 1999, when a reform was introduced changing the administrative division of the country and the unit lost the status of the province.

On the basis of the performed research, it can be argued that the amount of data contained in BDOT10k is sufficient to carry out spatial and statistical analyses, both by using the functions and creating spatial queries in the database, as well as by performing analyses on the layers themselves or between them, and by comparing vector data with raster data. Comparing vector layers with raster layers of topographic maps is much simpler and more transparent than comparing rasters of topographic maps. Furthermore, BDOT10k has a wider range of information about objects than traditional topographical maps. In the database, we can search for information, including about the data source, category of existence, general and detailed function of the object, cartographic codes for the appropriate scales of topographic and general geographic maps, number of storeys, we can also obtain information about geometry (e.g. surface, dimension) due to GIS program functions. The Database of Topographic Objects contains information that did not appear on topographic maps because it would affect their legibility.

Despite the functionality and many attributes that BDOT10k has, the drawback is its out-of-date status. The database that has been used since its inception on 15 November 2012 is not valid, although the Regulation of the Minister of Interior and Administration of 17 November 2011 regarding the database of topographic objects and databases of general geographic objects, as well as standard cartographic studies (Journal of Laws of 2011 No. 279 item 1,642, as amended) says that "updating of data contained in BDOT10k takes place immediately after obtaining new data".

References

- [1] Olszewski R., Gotlib D. i inni, Rola bazy danych obiektów topograficznych w tworzeniu infrastruktury informacji przestrzennej w Polsce. Główny Urząd Geodezji i Kartografii, Warszawa, 2013.
- [2] Wytyczne techniczne Baza Danych Topograficznych (TBD), Główny Urząd Geodezji i Kartografii, 2008.
- [3] Ustawa Prawo geodezyjne i kartograficzne z dnia 17 maja 1989 r. [Dz.U.1989 Nr 30 poz. 163, z późniejszymi zmianami].
- [4] Rozporządzenie Ministra Rozwoju Regionalnego i Budownictwa w sprawie szczegółowych zasad i trybu założenia i prowadzenia krajowego systemu informacji o terenie z dnia 12 lipca 2001 r. [Dz.U.2001 nr 80. poz.866, z późniejszymi zmianami].
- [5] Rozporządzenie Ministra Spraw Wewnętrznych i Administracji w sprawie bazy danych obiektów topograficznych oraz baz danych obiektów ogólnogeograficznych, a także standardowych opracowań kartograficznych z dnia 17 listopada 2011 r. [Dz.U. 2011 nr 279 poz. 1642, z późniejszymi zmianami].
- [6] Ustawa o infrastrukturze informacji przestrzennej z dnia 4 marca 2010 r. [Dz.U.2010 nr 76 poz.489, z późniejszymi zmianami].
- [7] Gołębiowski J., Stosunki społeczno-ekonomiczne w Tarnobrzegu i powiecie tarnobrzekim w okresie drugiej Rzeczypospolitej, Kraków 1992.
- [8] Krasuska J., Wygoda B. i in. 60 lat Tarnobrzekiego Zagłębia Siarkowego, Wydawnictwo Kopalni Siarki Machów SA w Likwidacji, Tarnobrzeg 2014.
- [9] Leń P., Głowienka E., Zastosowanie metod GIS w analizie struktury przestrzennej obszarów wiejskich gminy Sławno w powiecie opoczyńskim, Czasopismo Inżynierii Lądowej, Środowiska i Architektury – Journal of Civil Engineering, Environment and Architecture, JCEEA, t. XXXIII, z. 63 (3/16), 2016, p. 227–238, DOI: 10.7862/rb.2016.205.
- [10] Salata T., Prus B., Gawroński K., Ocena rozwiązań planistycznych z wykorzystaniem przestrzennych baz danych w aspekcie skalowalności rozwoju zabudowy, Czasopismo Inżynierii Lądowej, Środowiska i Architektury – Journal of Civil Engineering, Environment and Architecture, JCEEA, t. XXXIII, z. 63 (3/16), 2016, p. 399–411, DOI:10.7862/rb.2016.223.

Przesłano do redakcji: 17.01.2018 r.

Przyjęto do druku: 31.03.2018 r.

Karol KRUPA¹
Piotr GLEŃ²

THE COMPLEX OF ST. FLORIAN AND ST. CATHERINE CHURCH IN GOŁĄB AS A UNIQUE EXAMPLE OF MILITARY ART OF LUBLIN VOIVODESHIP

With the development of the civilization and the need to ensure safety for the next generation and cultural material, it became more and more vital to provide defence in case of danger. That is why, the character of residential space and historical architecture was influenced by the conflicts, which had various forms. Aside from the buildings, which were fulfilling visible and explicitly defined military function like e.g. fortresses or defence walls, there were also others that have been subjected to the process of incastellation to respond to the needs of the society. Giving the defensive character to the buildings that had originally completely different purpose, especially religious, had been developed since the Roman times. Military art was purely functional at the beginning. Later it was intertwined with decorations and other architectonic elements that were occurring e.g. in churches and conventual complexes. The aim of this article is to analyse the expression of the late Renaissance architecture with the elements of military art (*ars militaris*) in the discussed church, the Loreto Chapel and the wall, which together constitute the religious complex of St. Florian and St. Catherine in Gołęb in Lublin Voivodeship. Referring to functional and architectural-construction solutions of the subject of our research, the author discusses the topic of giving defensive character to religious buildings while keeping their functional layout, decorativeness and rich architectural expression typical for the architecture of the Lublin Renaissance.

Keywords: defensive architecture, church, the Loreto Chapel, the Renaissance, the Lublin Renaissance, Mannerism, military art (*ars militaris*), Jan Zaor, Piotr Likkell

1. Military art (*ars militaris*) in the religious architecture

The need of defence is one of the most natural elements of our behaviour. Human psyche has created several defensive mechanisms functioning on many levels in order to provide safety. Over the centuries, people have created the

¹ Corresponding author: Karol Krupa, Lublin University of Technology, Independent Architectural Lab, Nadbystrzycka Street 38d, 20-618 Lublin; tel. (81) 538 44 54; k.krupa@pollub.pl

² Piotr Gleń, Lublin University of Technology, Independent Architectural Lab, Nadbystrzycka Street 38d, 20-618 Lublin; tel. (81) 538 44 54; p.glen@pollub.pl

techniques and conditions to defend themselves physically. The necessity to protect the most precious and valuable things has triggered the development of technology, engineering, construction and military architecture. "The buildings [...], are the architectural mirror of the dangers of their times" [1]. Over the thousand years, the warfare had a great impact on the forms of the buildings of various sizes and functions. Military architecture (*architectura militaris*) presented in non-uniform form was one of the factors determining the civilization and cultural evolution [2]. The constructors and engineers were basing their projects not only on the experience from the previous periods, but also on the analysis of the military technology progress and theoretical layer of this progress. Summing up all the points above: the architecture and technology, warfare and its time and space – military art (*ars militaris*) is the starting point of the whole subject.

During the Middle Ages, when Romanesque style started to evolve, religious buildings started to have also defensive character, providing shelter and the chance to organize the defence of the population from the area. The Polish name of the church – *kościół* comes from the Latin word *castellum*, which literally means a stronghold, meanwhile in Old-Polish it has the roots in the word *kasztel* (in En. castle) [3]. The area around the religious buildings was used for gatherings and everyday life activities. The use of stone as a construction material and thick walls of the building made these buildings a perfect shelter for the urban population. Defensive function of the temples was often chosen due to its location, which had strategic importance. Places of strategic importance such as hills and elevations near vast grounds, river meanders, marshes, overflow areas or dense forests facilitate observation and limit the risk of invasion by the enemy. A fence in the form of thick walls helping to organize the military defence has enclosed the area. The architecture of churches was not an example of typical defensive constructions though, as opposed to some conventual complexes. They were only adjusted to fulfil the defensive function. However, there are some examples of religious buildings of typical defensive character in Poland and abroad. The elements that reveal the purpose of the building are the body of the building, central situation and adding the storage to the main religious function. With the reserves of food and arms, the population of the area could defend themselves much longer. Examples of such buildings are churches in Bornholm built in the shape of rotunda coming from 12th century. Currently, the four churches demonstrating authentic military art (*ars militaris*) might be visited in Nyker, Nylars, Olsker i Osterlar [4]. In Poland one of the most distinctive example of religious building with military art (*ars militaris*) character is St. Andrew Church in Kraków built around 1079. The church had very important defensive function of the Okole barbican at the foot of Wawel [5].

Over the periods of time, the role of churches as defensive structures has been changing and becoming less and less important. However, incastellation of the religious buildings has been both made originally and on already existing buildings. Giving the defensive function to already built churches was triggered

by numerous political and religious conflicts that were tearing Poland apart in 15th century. The first phase of incastellation was most often encircling the church with fortifications. Next phases were equipping the church with food magazines, ovens and wells taking example from the churches – fortresses of the Romanesque period.

This article is the part of the discussion and analysis concerning the church complex in Gołęb in Lublin Voivodeship, its architecture and functional organization of the church, the Loreto Chapel and the brick fence, which indicated defensive character of the complex. The topic of military art (*ars militaris*) raised in this article is just the beginning of the discussion about the defensive function of the Loreto Chapel in Gołęb, which is a unique example of this architecture in Poland. The questions posed in this article will find their answer during wider historical and architectural analyses of the building.

2. The religious complex in Gołęb

The religious complex in Gołęb is the complex of buildings of great artistic and architectural value, which is an example of the exceptional attractiveness of the art of construction of the late Renaissance with the typical elements of the local architecture. The history of art calls this style *the Lublin Renaissance* intertwining the forms and details characteristic for the Renaissance, Mannerism and early Baroque with the elements of local decorations. The church (1628–1638) and the Loreto Chapel in Gołęb (around 1636) are unique because of their individual aesthetical and ideological saturation, which attract attention and encourage making more thorough analysis (Fig. 1 and 2). The history of the complex is connected with the foundation activity of the outstanding personality of his times, chancellor George Ossoliński, a true statesman and diplomat and the Gołęb's parson of the day, Szymon Grzybowski, who was simultaneously the king's secretary. This unique complex has been constructed by Piotr Likkel coming from Italy, well-known thanks to his architectural achievements in Kazimierz Dolny and Jan Zaor, who has finished decorations of Loreto Chapel [6]. The co-authorship of the church is often attributed to the constructor Jan Wolff, but this is not proven information. Most likely, if he really took part in the construction process, he was dealing with the decorations and stuccos. The body of the church by itself is very different from the ones supposedly designed by Wolff at that time.



Fig. 1. The view of the church from the south-west (Author's picture)



Fig. 2. The view of Loreto Chapel from the south-west (Author's picture)

2.1. Location

An important factor that impacts warfare activities concerning both military and organizational actions is the location of Gołąb village. Most probably one of the main arguments for the construction of the church in this place was the possibility to cross the Vistula River by the ford which was used by travellers, traders and military. The scheme below shows the change of the shape of the Vistula flume over the years. We can see the old meander, which is the remnant of the river course from 10th century. When the church was built, the river already took the different course, which with the meander has limited the accessibility of the complex. What it more, these natural surroundings have created both the good conditions to built the facility with the function of the shelter and the possibility to defend the local population and the goods of the parish. (Fig. 3)

It's worth mentioning that Gołąb village was the background of some important historical events. If it comes to military and defensive activities, Gołąb was the witness of one of the most important battles of the period of the Swedish Deluge. In 1656, Polish troops led by Stefan Czarniecki confronted Swedish Army under the command of Charles X Gustav. Substantially smaller Polish Army was crushed by 11 thousand of Swedish soldiers [7]. Next historical event that was recorded in history books was Gołąb confederacy signed in September 1672. The aim of this arrangement whose leader was Stefan Stanisław Czarniecki was to protect the king Michał Wiśniowiecki [9]. Due to political and historical reasons, the area of Gołąb was the place where the armies were gathered and stationed. As a result of Tarnogród Confederation, in 1716, the fields surrounding the village were used for the Saxon army. In 1791, the Gołąb area was again the warfare theatre, because of the manoeuvres of the national army. During World War 2, the church was seriously destroyed.

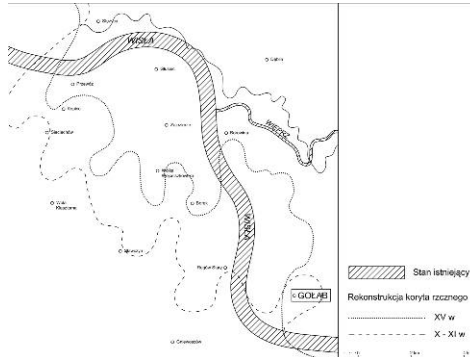


Fig. 3. The scheme of the change of course of Vistula river in the past (own elaboration on the basis of H. Maruszczak, 1997)



Fig. 4. The view of the nave of the church with inside galleries (own photography)

2.2. The Church

The church in Gołęb is oriented, single-nave with two towers on the front. From the east, the sanctuary is finished with semi-circular apse of the same width as the nave, separated with an arc. Single-nave body has hollow niches between the pillars with side altars, the chancel and the pulpit. Because of the outside arcades, the church seems to be three-nave constructed in the form of basilica. This effect was achieved by putting the corridor above the arcades separated with a wall from the main nave. The oblong proportions of the projection stand out from the other realisations of this period, e.g. St. Trinity Church in Radzyń Podlaski or St. Stanislav Church in Czemierniki constructed by famous Jan Wolff. The form of the church demonstrates the strong Dutch influences, because of the exposed, brick façade with clear, distinctive ornamentation.

There are many arguments for taking the church in Gołęb as the perfect example of military art (*ars militaris*). The most important are the forms and architectural details, which exist to these days, and its functional layout. Its defensive character is determined not only by thick walls and windows located high, but also by the above-mentioned corridors over the arcades with battlements in the outside wall of the church (Fig. 5). There are also many battlements in the towers (Fig. 6) in the staircase leading to the chancel and the lanes along the main nave. These elements have been skilfully blended into the ornamentation and architectural detail in the façade. It is possible that the towers were built later onto the already existing building [9]. This applies definitely to the buttresses from the east, but it is not certain regarding the towers. Michał Baliński wrote in 1845: "There is a parish brick church with two towers in Gołęb". We can assume that Gołęb's church has undergone the secondary incastellation, because of the military conflicts and warfare in the area.

Other solution that determines the defensive character of the church is inside gallery (Fig. 4) at the height of second level of windows on the both sides of the

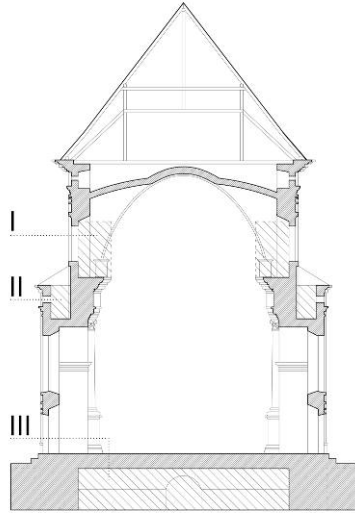


Fig. 5. Schematic cross-section of the church:
I – inside gallery; II – corridor with
battlements; III – halls of underground
level (own elaboration on the basis of [10])



Fig. 6. The corridor with battlements over the arcades
(on the left) and battlements in the church tower
(on the right, the Author's photography)

nave and behind the chancel. The access to the gallery is from the staircase in the tower. It is the element that doesn't exist in the churches built in the similar period and style. Other important argument that supports the thesis of incastellation of the church is underground level. The surface of basement was divided into three main halls (Fig. 7) located under the nave, the smaller crypts under the sanctuary and last arch of the nave and under the vestibule and the towers. Because of the size of the main space of the basements (4.5×10 m, the height of the vault ceilings 2.1 m), we can assume that their original function was storage and defence of the population of the village, but not for the crypts. This is typical layout of the churches of the military art (*ars militaris*) character, which the author has mentioned in the introduction. Unfortunately, the access to the basement is limited and current knowledge about their shape was obtained due to the research made with the use of the minicamera [10]. The basement was immured already in 19th century after numerous floods, which have substantially weakened the construction and technical condition of the temple.

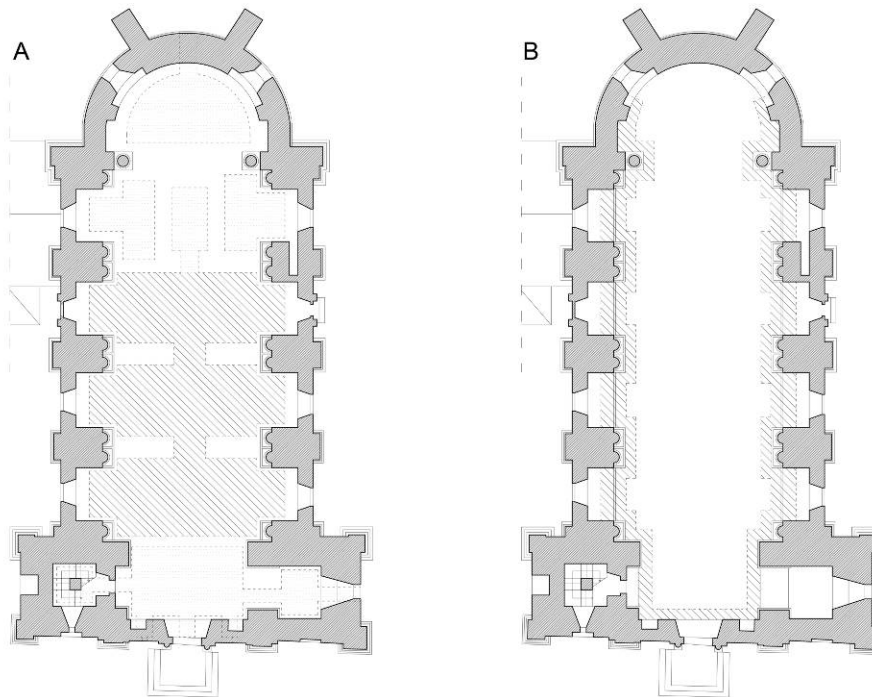


Fig. 7. The scheme presenting the projection of the A – the space on the underground level;
B – inside gallery (own elaboration on the basis of [10])

2.3. The Loreto Chapel

The architecture of the Loreto Chapel is unique. It is closely related to the program of the Holy Mary cult that was animated in 17th century. The Chapel in Gołab is the first example of the religious building of this type in Poland. It was built just like the church, on the initiative of the founder, who learned about the cult of Holy Mary of Loreto during his trips to Italy. The prototype of the Loreto Chapel goes back to 13th century. However, the architectural design created in Loreto in 1507 by the renowned architect Donato Bramante and the sculptor Jacopo Sansovino, acting at the directions of Pope Julius II, has become popular and found many followers no sooner than after 1575. Architectural form of the outside and functional layout of the inside divided into east sanctuary part and west part for the people became the canon for this type of buildings. The rule of architectural housing of the simple, brick building was in force. The building had to have defined size and keep the lane in the walls. According to the scheme, the Loreto Chapel in Gołab was built in 1634–1638. Just like in the Italian prototype, the internal building was surrounded with representational architectural form from the outside. It corresponds to the original building in Loreto, but it has an individual artistic and iconographic touch under the architecture of 17th century Lublin area and iconography basing on Polish tradition. Other innovation

is situation of the chapel. The original chapel and similar buildings in Poland (in Warsaw – in the Church of Our Lady of Loreto from 1645, in Głogówek – in St. Francis Church from 1630–1634) are located inside the other building, whereas the Loreto Chapel in Gołąb was constructed outside. It's worth mentioning that the Loreto Chapel was not finished by Piotr Likkel, but by an architect from Kraków who was most probably Jan Zaor (Zaur or Zaurowicz). Despite the fact that there are no records of the name of the architect who finished the works, it is possible to infer from the style and the process of work of the architect. One could notice many similarities in decoration and composition elements of the façade of the Loreto Chapel and the church in Tarłów (1650) or the St. Peter and Paul Church in Vilnius (from 1668). Additional clue, which would need confirmation with thorough archaeological research, is the use of kiln for ceramics by the associate of Zaor, named the Master of Tarłów. Kilns for some decoration elements like sculptures, capitals or other details were situated usually beside the constructed buildings. Dariusz Włodarczyk in his paper analysing the results of archaeological excavations in 2014 describes the uncovered part of the wall of the width of one brick of non-linear profile. He doesn't define its function, but supposedly it is the part of the kilns used by the associate of Zaor [6].

The elements that define the Loreto Chapel as the example of military art (*ars militaris*) are not as numerous and obvious like in the church. A comparative analysis of such buildings, especially of the prototype of Loreto, gives rise to a presumption that the holes under the hollows with the sculptures of the prophets were also rifle battlements just like those in the lane over the arcades in the church. The places where the holes were located are most probably not a coincidence. They were put in east and west façade, at the end of the lanes. Additionally, one hole is in the north façade from the side of the church. On the façade, from the side of the walls surrounding the complex, there are no holes. One of the elements that might prove that the chapel had the defensive character is the occurrence of embrasures (Fig. 8) used normally for this kind of solutions [11]. Other argument supporting this thesis is the fact that the chapel was built outside in the area of this religious complex. What is more, the corridor between external and internal walls of the Loreto Chapel could be also used for defence. The entrance to the roofing from the lanes gave access to the windows in the upper part of the façade. It was possible that the reason for the incastellation of the chapel was valuable equipment stored in the Loreto Chapel and vicars living in small buildings at the corners of the fence. The crypt in the basement was not used for storage like in the church, because of its volume and access from the outside.



Fig. 8. The hole in the lane of the Loreto Chapel with visible embrasure (the Author's photography)



Fig. 9. The rifle battlements in the church wall (the Author's photography)

2.4. The fence

The church wall was built in 17th century. To this days there are only parts of the original fence from the north and the west remaining. Originally there were the little houses for the vicars who were serving and taking care of the Loreto Chapel until 1845. On the Site Plan of the Gołęb Parish [12] vicar houses were no longer indicated. Thus, it is possible that they were dismantled between 1852 and 1866. The same document reports that there was parish cemetery at three corners of the fence. Nowadays, there are little shrines built in the walls in these places.

The church wall in Gołęb might be classified as wall defensive system with key rifle battlements located in the hollows in the spans of the wall (Fig. 9). With such complex program of the defensive solutions regarding the body and the function of the church, it is completely justified and logical to use the rifle battlements in the fence.

3. Conclusions

The religious buildings in Gołęb are characterized by wide spectrum of cultural values, which to this day are the part of the heritage of more than local importance. They truly deserve to be called unique. Layers and numerous modifications appearing throughout the course of history in the area of Gołęb have partly blurred the difference between original and secondary incastellation of this religious complex. The analysis of the elements that determine the features of military art (*ars militaris*) from the historical fabric of the church allows us to put forward the hypothesis that the Loreto Chapel was constructed the similar way. It might be confirmed if more detailed and complex archaeological research of the area around the church is conducted. Despite lack of homogeneousness of the individual ties, which joins many architectural notes, the religious complex in Gołęb presents wide spectrum of valuable aesthetical solutions. The architects and the masters of the art of construction have skilfully built-in military art (*ars militaris*) making the complex truly unique.

References

- [1] Agnieszka Kłopotowska, *Czynniki „obronności” we współczesnej architekturze zespołów mieszkalnych*, Budownictwo i Architektura, Vol. 6 (1) 2010, Politechnika Lubelska, Lublin 2010, p. 51.
- [2] Janusz Bogdanowski, *Architektura obronna w krajobrazie Polski od Biskupina do Westerplatte*, Warszawa-Kraków 1996, p. 11.
- [3] Zenon Klemensiewicz, *Historia języka polskiego*, Warszawa 2002, p. 30.
- [4] Artur Rok, Sławomir Pytel, Uszula Myga-Piątek, Grzegorz Jankowski, Gabriel Korbut, *Ocena wartości i stanu zagrożenia ufortyfikowanych obiektów sakralnych województwa śląskiego*, „Raport merytoryczny z wykonania projektu”, Będzin 2012.
- [5] Bonawentura Maciej Pawlicki, *Ze studiów nad relikiami domniemanego palatium Sieciecha w Krakowie*, „Czasopismo techniczne Politechniki Krakowskiej”, volume 23, year 108, Kraków 2011.
- [6] Mariusz Karpowicz, *Barok w Polsce*, Warszawa 1988, p. 296.
- [7] Teodorowicz J., *Bitwa pod Gołębim*, Wojna polsko-szwedzka 1655-1660, edited by J. Wimmer, MON, p. 286–295.
- [8] Michał Baliński, Tymoteusz Lipiński, *Starożytna Polska pod względem historycznym, jeograficznym i statystycznym opisana*, Warszawa 1845.
- [9] Bożena Opiłło, Małgorzata Mrzygłód-Tomasik, *Wyciąg z programu prac konserwatorskich elewacji Domku Loretańskiego w Gołębim*, Kraków 2008.
- [10] Wiesław Nawrocki, *Inwentaryzacja podziemi kościoła pw. Św. Floriana i św. Katarzyny w Gołębim*, Kraków 2011.
- [11] Janusz Bogdanowski, *Sztuka obronna*, Kraków 1993, p. 116–117.
- [12] 190 Centralne Władze Wyznaniowe Królestwa Polskiego, Akta Komisji Rządowej Wyznań Religijnych i Oświecenia Publicznego dotyczące się Funduszków Kościoła Parafialnego w Gołębim, 1852-1866, sygn. 553.

Przesłano do redakcji: 25.02.2018 r.

Przyjęto do druku: 31.03.2018 r.

Iveta BULLOVÁ¹

ANALYSIS OF THE AIR FLOW IN SELECTED BUILDINGS

Airflow properties are most apparent adjacent to the surface of the building, because there take place any reactions between liquid and solid object. Air exchange rate is associated with air flow through a building by natural – through small openings and cracks in the structure. Due to leakages in the building construction, opening and closing of windows, the air in the building shifts. The value of air exchange rate is hard to predict and depend of several variables – wind speed, difference between outside and inside temperatures, the quality of the building construction. The paper analyzed the air flow in selected buildings and quantified the value of air pressure differences and the air exchange rate with the emphasis on specification of aerodynamic coefficients.

Keywords: air flow, aerodynamic coefficients, wind speed, air exchange rate

1. Introduction

The interior of the building allows prevailing comfortable climate, whereas the outside is determined by the weather. Building envelope - façade - protects the internal environment from external adverse climatic factors - temperature, sun, water, snow, wind. From these climatic factors is the wind most variable meteorological element in the surface layer of the atmosphere. The article analyses factors influencing the air flow and quantified the air pressure difference and the air exchange rate for selected buildings types.

2. Analysis of air flow in the building

An important component is analysis of the air flow in a building which influences: decrease (increase) in energy use for heating, sizing of the heating system, hygienic comfort, studying the movement of smoke.

Buildings and the building façade forms in real environment the interface between the internal and external environment as a result are formed air pressure differences. Air flow in buildings is complex, time dependent and multi-directional.

¹ Corresponding author: Iveta Bullová, Institute of Architectural Engineering, Faculty of Civil Engineering, TU of Košice, Vysokoškolská 4, 04200 Košice, Slovakia, +421 55 60246, iveta.bullova@tuke.sk

Air flow through and within buildings has been based on the requirement for continuity of mass and momentum caused by wind forces and thermal effects and these two components operate concurrently. Total air pressure difference is expressed:

$$\Delta p_C = \Delta p_\theta + \Delta p_v = \pm h_0 \cdot g \cdot (\rho_e - \rho_i) + C_p \cdot \frac{\rho v^2}{2} \quad (1)$$

where: h – height from the the Neutral Pressure Plane - NPP (m),
 ρ_e, ρ_i – outside and inside air density (kg/m³),
 C_p – overall aerodynamic coefficient (-),
 v – air velocity (m/s).

Due to the fact that the wind is the most variable meteorological element in the surface layer of the atmosphere and the building with its properties - shape, surface, air permeability - affects the air flow in the surface layer, is the quantification of the pressure difference from the wind effects Δp_v quite difficult.

2.1. Air flow – wind

Wind flow is substantially influenced by pressure differences - in weather maps depicted by isobars. In real conditions are isobars curved, because an air flow operates the centrifugal force and with respect to the movement of the earth around the vertical axis there is also some deviation - so-called Coriolis force. Wind power is expressed by a gradient wind speed v_G , which is considering the influence of temperature gradient, Coriolis force and centrifugal force.

Air velocity - wind speed - depends on factors operating in the boundary layer which are: change of height above ground, terrain roughness - expressed by the vertical gradient b , dependent on the type of locality. Change of wind speed with height change is expressed mostly in the form of power law:

$$v_z = v_{10} \cdot \left(\frac{z}{z_{10}} \right)^b \quad (2)$$

where: v_{10} – wind speed at 10 m above ground (m/s),
 v_z – wind speed at a height of above ground (m/s),
 b – exponent characterizes the locality - roughness of the terrain,
 $b = 1/4 - 1/7 = 0,25 - 0,14$ (-).

2.2. Interaction wind – building

For assessing of natural ventilation it is necessary the knowledge of distribution of air pressure on the buildings facades. Wind effects on buildings (pressure, respectively suction) and their size are expressed using the aerodynamic coefficients of external pressure C_{pe} [-], the internal pressure C_{pi} [-] and the overall pressure C_p [-].

Aerodynamic coefficients of external pressure C_{pe} [-] can be expressed by: calculations according to national standards, experimental measurements in-situ, experimental measurements in the aerodynamic tunnel, simulation using CFD calculation software.

Aerodynamic coefficient of external pressure can be affected by a large number of parameters – geometry of the building, details on facade, positions on facade, wind speed and wind direction.

2.3. The air permeability of the facade

Facade and openings show a certain degree of the air permeability which causes the changes of external and internal pressure. Therefore, by the wind effects, the size of the internal pressure coefficient must be taken into consideration.

For engineering practice is very important knowledge of the value of the internal aerodynamic coefficient, because it can cause result in increased values at leeward and lateral sides, because infiltration may cause alteration of aerodynamic coefficients of positive total pressure (pressure) to negative (suction) value.

To determination of the internal aerodynamic coefficient it is important to know the modification of the building changes in the interaction of internal and external pressure.

We distinguish 5 different modifications of buildings [3]:

a) buildings without the internal partitions and:

- without openings,
- with the openings located in one peripheral wall,
- with openings situated on two opposite peripheral walls,
- with openings situated in all external walls,

b) buildings with internal partition walls and with openings situated in all external walls.

Given that in the current period there are no legislative requirements for the quantification of the air permeability of all separating structures of buildings (partitions, doors, etc.) it is possible to deal with aerodynamic coefficients of internal pressure only for buildings without internal dividing by partitions.

For the building without internal dividing by partitions and with window construction of the same dimensions and of the same air permeability coefficient of joint i_{LV} [$m^2/(s.Pa^n)$] will by values of internal aerodynamic coefficient C_{pi} expressed from the graphical [2,5] as a function $f(a)$ and a determined from equation:

$$C_{pi} = f(a) (-), \quad a = \frac{S_{(+)}}{S_{(-)}} \quad (3)$$

where: $S_{(+)}$ – total surface of the openings on the windward side of a building, (m^2),
 $S_{(-)}$ – total surface of the openings on the leeward sides and lateral sides of a building (m^2).

3. Air pressure difference and air exchange rate in the reference building

Values of external and internal aerodynamic coefficients - for different mutual ratio of openings and for the selected reference building – simple building with 8 floors – $h = 22.4$ m, rectangular ground-plan, middle plate-type building, with spatial proportionality: $0.5 \leq h/b = 1.25 \leq 1.5$ and with the surface area proportionality: $1.5 \leq l/b = 2.8 \leq 4.0$ are in Table 1.

Table 1. Values of external and internal aerodynamic coefficients

	Windward side - longer side			Windward side - shorter side		
	$C_p = C_{pe}$	$C_p = C_{pe} - C_{pi}$		$C_p = C_{pe}$	$C_p = C_{pe} - C_{pi}$	
		2:1	3:1		2:1	3:1
Windward side	+0.7	+0.9	+0.85	+0.8	+1.4	+1.6
Lateral side	-0.5	-0.3	-0.35	-0.5	+0.1	+0.3
Leeward side	-0.3	-0.1	-0.15	-0.1	+0.5	+0.7

Based on the updated values of aerodynamic coefficients were calculated the pressure differences from the temperature and wind effect and air exchange rate. The values are shown graphically in Figure 1 and 2 for the selected day - January 06, 2017 in Kosice - wind direction 360° acts on the longer side, with considering of the impact of openings with a mutual ratio 2:1 and 3:1 ($C_p = C_{pe} - C_{pi}$) and without considering the impact of openings ($C_p = C_{pe}$) on windward and lateral side.

Figure 1 shows that the pressure difference from the differences of temperature Δp_θ (Pa) is relatively uniform (from 8.7 to 10.1 Pa), but the pressure difference from the wind effect Δp_v is considerable (15.5 ÷ 126.6 Pa – pressure on the windward

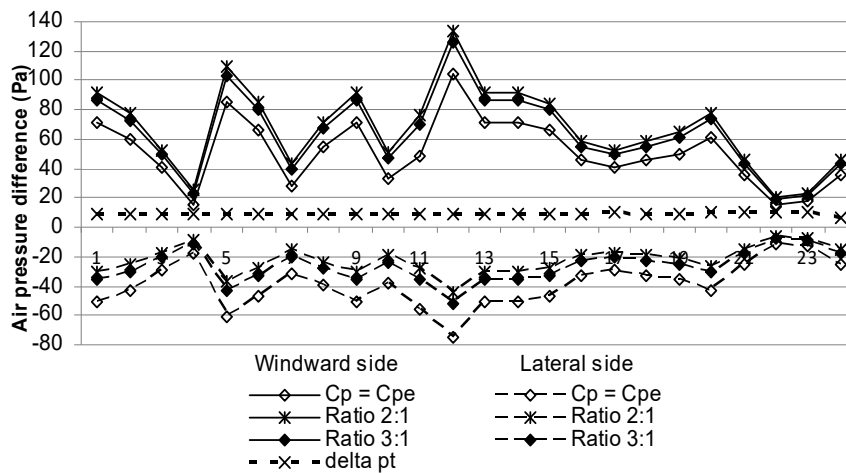


Fig. 1. Comparison of the air pressure difference for windward and lateral side with considering and without considering the impact of openings – open terrain

side, -6.6 to -74.5 Pa - suction on the lateral side), which ultimately influences the overall pressure difference and air exchange rate.

As shown in Figure 1 on the windward side are values of the pressure difference from the wind without considering of openings significantly higher than in the lateral side. Influence of openings on the windward side increases the wind effects and on the lateral side vice versa - reducing.

The air exchange rate in the reference room can be generally defined by calculation and measurement. Is developed the methodology for determining of the air exchange rate based on experimental measurements of carbon dioxide [6]. The values of air exchange rate can be calculated from the equation:

$$n = 3600 \cdot \frac{V_{inf}}{V_m} = 3600 \cdot \frac{[\sum(i_{l,v} \cdot l) \Delta p_c^m]}{V_m} \tag{4}$$

where: V_{inf} – volume of infiltrated air in the room with natural airflow, (m³),
 V_m – room volume, (m³),
 $i_{l,v}$ – gap permeability coefficient, [m³/(m.s.Pa^{0,67})],
 l – length of the gap, (m),
 Δp_c – overall air pressure difference, (Pa).

Values of air exchange rate are calculated by the formula (4) for reference room oriented to windward and the lateral wall with the volume $V=53 \text{ m}^3$, $i_{l,v}=0,4 \cdot 10^{-4} \text{ m}^3/(\text{m.s.Pa}^{0,67})$ and length of joint 14 m.

As can be seen from Figure 2, on the windward side are the values of air exchange rate without considering the impact of openings higher than the specified standard value - $n = 0.5 \text{ 1/h}$. When considering the impact of openings, these values increase. On the lateral side are the values without considering of the openings lower and, due to the influence of the holes, are even more reduced.

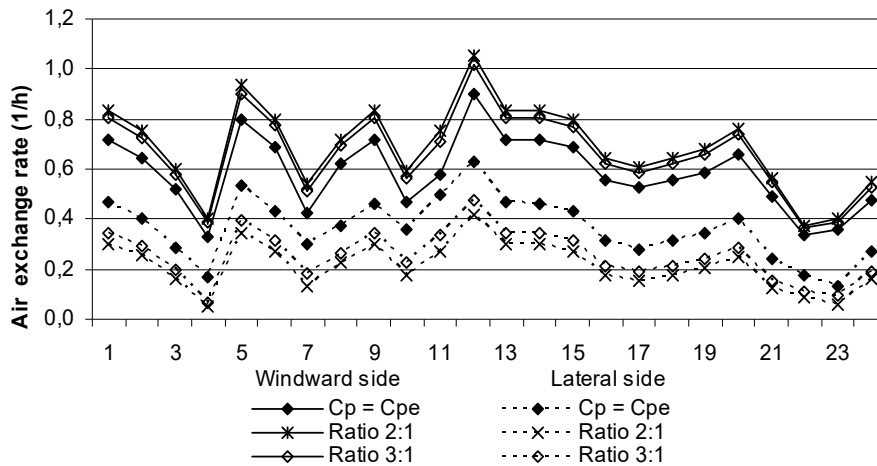


Fig. 2. Comparison of the air pressure difference for windward and lateral side with considering and without considering the impact of openings – open terrain

4. Conclusion

The theoretical analysis and the exact results of the values of the air pressure differences and air change rate for selected building show that acceptance of the air permeability of the façade affecting the pressure conditions in the interior is very important.

Pressure difference from different temperatures Δp_θ is relatively uniform, but pressure difference from the wind effects Δp_v is very variable during the day, significantly influence the air exchange rate and therefore is necessary already in urban planning accurately know and define the type of climate data and the expected urban form.

Redistribution of air pressure inside the building is influenced by the layout and orientation of openings towards the direction of the applied wind, as well as their size and mutual ratios on every side of the building. Due to this fact, the consideration of the air permeability of building envelope is very important, especially because significantly influence the redistribution of pressure in the interior resulting in high variability of the air pressure difference and consequently the air exchange rate.

Acknowledgements: This article was elaborated within the framework of the project VEGA 1/0835/14.

References

- [1] Amin, J. A., Ahuja, A. K. Effects of side ratio on wind-induced pressure distribution on rectangular buildings. *Journal of Structures*, 2013.
- [2] Bielek M., Bielek B. Interakcia budova – vietor v teórii energetickej potreby budov, In: 6. vedecká konferencia Budova a energia 2005, Podbanské 12-14.10.2005, pp. 64–69.
- [3] Bielek M., Bielek B. et al. Vplyv stavebných materiálov a konštrukcií na kvalitu života. Parametrizovanie energeticko-environmentálneho hodnotenia stavebných konštrukcií a budov. *Aerodynamika budov pre kvantifikáciu ich prirodzeného vetrania*. Bratislava: PROFING, spol.s.r.o., 2005.
- [4] Bielek M., Černík, P., Tajmír, M.: *Aerodynamika budov*, Alfa, Bratislava, 1990.
- [5] Holmes, J. D. Mean and fluctuating internal pressures induced by wind. Colorado: *Proceedings of 5th international wind engineering conference*, 1979.
- [6] Kapalo P., Voznyak O. Experimental measurements of a carbon dioxide concentration for determining of a ventilation intensity in a room at pulsing mode. In: *Czasopismo Inżynierii Łądowej, Środowiska i Architektury – Journal of Civil Engineering, Environment and Architecture*, JCEEA (ISSN 2300-8903), t. XXXII, z. 62 (4/2015), p. 201–210, DOI:10.7862/rb.2015.189.
- [7] STN EN 1991-1-4:2007, Eurokód 1. Zaťaženie konštrukcií. Časť 1-4. Všeobecné zaťaženia. Zaťaženie vetrom. Bratislava: Slovenský ústav technickej normalizácie, 2007.

Przysłano do redakcji: 24.03.2017 r.

Przyjęto do druku: 31.03.2018 r.

Irena ICKIEWICZ¹
Piotr KODA²

THE INFLUENCE OF THE ENVIRONMENT ON OBJECTS OF HISTORICAL VALUE

The result of the environment's influence on objects of historical value is the ongoing process of their deterioration. The main cause for the deterioration process is the flow of heat and moisture which also brings salinary solutions. The correct diagnosis on the causes of adverse effects affecting buildings of historical value serves as the basis for further activity which can result in protecting an object of value against further deterioration. Dampness issues which occur in buildings are usually caused by the lack of proper anti-dampness insulation and an incorrect micro-climate inside (temperature and air humidity outside). In order to evaluate the influence of a micro-climate on dampness processes, the selected buildings of historical value had air temperature and relative air humidity monitors installed, each having the capacity for continuous data retrieval. Every month, examinations of wall dampness are being carried out using a PWM-3 hygrometer. Based on the measurements from the first two months, initial conclusions were drawn. Deeper analyses and the conclusions stemming from these will be drawn after the entire cycle of measurement ends at the end of 2018 (after one, full year of measurements).

Keywords: buildings of historical value, partition microclimate, humidity measurements, wall dampness measurement, microclimate measurement

1. Introduction

Sustaining (survival) of objects of historical value depends on regular conservation efforts which should focus primarily on the correct building exploitation, maintaining the conditions of interactions with the surroundings on a natural level, and quick prevention of destructive actions.

The concept of the natural level is in other words a system of external physical parameters such as: temperature, relative humidity, ground moisture content, salinization of walls [1].

¹ Corresponding author: Irena Ickiewicz, Politechnika Białostocka, Katedra Gospodarki Przestrzennej i Budownictwa Energooszczędnego, ul. Wiejska 45 E, 15-351 Białystok ; tel.797995993; i.ickiewicz@pb.edu.pl

² Piotr Koda, Politechnika Białostocka, Zakład Budownictwa Ogólnego, doktorant Wydziału Budownictwa i Inżynierii Środowiska Politechniki Białostockiej, koda-koda@wp.pl (*the examination was carried out a part of statutory work S/WBiŚ/3/2016 from the science fund of the Ministry of Science and Higher Education*)

The main factors affecting the durability of historically significant buildings are varied forms of moisture and salts which are diluted in it and which move inside the capillary tubes. A diverse internal surface of the buildings materials used in those times which are porous-capillary contributed to the specific properties of such materials, as well as mechanisms of their destruction [2–4]. Dampness appears initially on external walls, which are the primary cause of visible damage. It is both the water originating in acidic rain as well as capillary tubes rising damp from subsoil. This form of damp is dangerous in the winter due to the cycles of freezing and unfreezing of free moisture. In the water present in the capillary tubes there are salinary solutions originating in the subsoil or flushed out of the ceramics and plasters. The most commonly present are: chlorides (CaCl_2 , MgCl_2), nitrates (NO_3) i sulfates (K_2SO_4 , MgSO_4), these are hygroscopic easily soluble in water. Salts precipitated from the solution damage both plasters and brick layers [6, 7].

2. Description of the phenomenon of how buildings of historical value are impacted

The main phenomena causing the processes of degradation of objects of historical value are:

- heat flows,
- diffusion of moisture,
- salinary solutions flows.

2.1. Heat flow

The distribution of heat flow in the wall forces the place of moisture condensation, freezing of water into ice, and as a consequence the damaging of protective layers. Analyzing one-dimensional heat flow (Fourier's law), distribution of temperatures inside a partition can be determined, and next based on such distribution water vapor pressure in capillary walls can be evaluated. Comparing real distribution of pressures in walls with limit values, when condensation of water vapor in capillary tubes occurs, an area of partition dampness can be determined.

On this basis, a scope of dampness with condensation damp can be determined, which as a consequence can lead to the development of molding fungi on the wall surface. The basic dependencies for a single layer wall is presented below. The heat flow is described by the Fourier law of heat conductivity [3, 4].

$$q = -\lambda \frac{\Delta T}{d} \quad (1)$$

On the border, q flux is the same.

$$q_1 = -\lambda_1 \left(\frac{T_1 - T_0}{d_1} \right) \quad (2)$$

where: q – heat flux [W/m²];
 λ – heat conductivity rate, [W/m·K];
 d – layer thickness [m];
 $(T_0 - T_2)$ – temperature increase from the initial state T_0 [°C];
 ΔT – temperature difference [°C].

2.2. Moisture diffusion – moisture condensation zones

The diffusion process is described by the diffusion equation, which stems from the balance of diffusing mass inside the partition (Fick's law) and initial-boundary condition. In the simplest case (stationary, one-dimensional) this equation is: [3, 7];

$$D = \frac{d^2 c^\alpha}{dx^2} = 0 \quad (3)$$

where:

$$c^\alpha = \frac{\rho^\alpha}{\sum_\alpha \rho^\alpha}, \quad \rho = \sum_\alpha \rho^\alpha \quad (4)$$

c^α – mass participation of the diffusing component of the solution in capillary tubes;

ρ^α – mass density of the unit of volume for component α , $\alpha=1,2..n$;

ρ – density of the entire body.

Moisture flow inside the wall are more complex than heat flow. The cause for this is a multi-element composition of the diffusing solution, phase shifts and component reactions. Stationary distribution of temperature and damp on wall thickness make it possible to relatively easily determine the scope of the zone that is subject to dampness. The obtained results make it possible to establish approximate real values. Determining the zone of condensation depends on the distribution of temperature and subsequently partial pressure of water vapor in the subsequent layers [3, 6].

3. Wall dampening based on buildings of historical value in northern-eastern Poland

Issues with dampening in buildings which occur are usually caused by the lack of appropriate anti-dampness insulation and inappropriate microclimate of the interior (temperature, air humidity) [1].

The cause of dampness in construction objects is not only capillary damp but also condensation damp. The state of partition dampness caused by condensation damp has significant impact on the state of the object's usage. In un-utilized buildings or buildings used periodically (such as places of worship), the temperature of interior air is on average $\pm 5^{\circ}\text{C}$ (depending on exterior temperatures). For that reason, the wall surface temperature on the inside is relatively low. Such a state is very „conductive” to precipitation of surface and internal condensation damp (the wall surface temperature is lower than the dew point) [4]. For that reason, an un-utilized (unheated) building is more quickly subject to damage from wall dampness. The accumulated damp (free moisture) during periods of negative temperatures is subject to freezing, and as a result, to bursting the subsequent sub-surface layers.

To sum up, the phenomenon of partition dampness in buildings can occur as:

- damp penetration via hygroscopic water input,
- damp penetration due to lack of proper anti-damp insulation (capillary water rising),
- damp condensation of cold wall surfaces.

3.1. Buildings selected for examination

In order to determine the influence of interior microclimate on the level (state) of dampness of partitions in buildings of historical value, 3 example churches were selected. The selected objects have been struggling with the increasing issue of the deterioration of substance in historically significant walls are:

- St. Andrew's church in Barczewo,
- St. Anna's church in Barczewo,
- A church under the invocation of St. Mary's Immaculate Conception – Wigry.

At the beginning of the examination, the history of the building, history of repairs and renovations, with the emphasis on materials used, as well as whenever possible archival documentation were all analyzed. Interviews were held with the current users and administrators of the buildings.

A historical church in Barczewo under the invocation of St. Andrew the Apostle was erected in XIV century as a single-nave, gothic church made of ceramic bricks. The scale of damage caused by damp is very significant (fig. 1).



Fig. 1. St. Andrew's church in Barczewo - a) main entrance b) damaged side elevation
c) multiple traces of damp visible on the walls from the inside

A historical St. Anna's church in Barczewo

The church was erected in XIV century; gothic. The church's vaulting were designed as arch and stellar vault. The church is made of full ceramic brick, plastered interior (fig. 2).

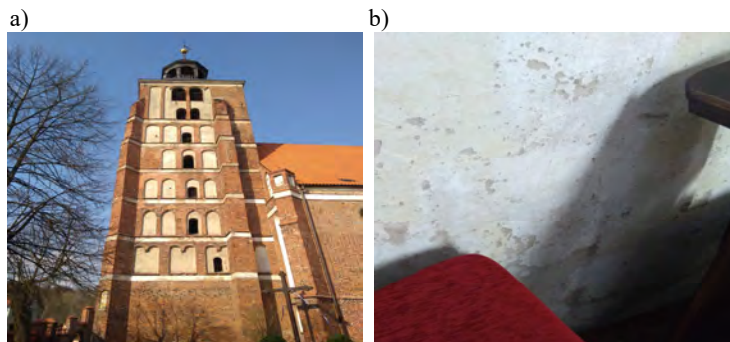


Fig. 2. St. Anna's Church in Barczewo- a) general view of the elevation, b) visible signs of damage cause by capillary and condensation damp

A historically significant church under the invocation of St. Mary's Immaculate Conception in Wigry, erected in XVII century, a baroque, single-nave design made out of full ceramic bricks, plastered on the inside (fig. 3).



Fig. 3. A church under the invocation of St. Mary's Immaculate Conception - Wigry, a) general view of the building complex b) and c) visible outer layer damage caused by damp

3.2. Examination – interior microclimate and wall dampness

In order to carry out a precise analysis of the conditions occurring inside of the selected buildings, wireless Efento recorders were utilized. These recorders make it possible to register temperature and humidity in buildings with the option of saving data. These recorders also have the capacity for notifying when safe levels of temperature and humidity are being exceeded and generating automatic reports.

The recorders that were used are powered by batteries (2 years of continuous operation). The recorders were mounted on the objects between January and February 2018. With the goal of correctly interpret the conditions present in the churches, the recorders were mounted on 2–3 places in equal distances from each other. The recorders mounted in 3 churches are shown in fig. 4.

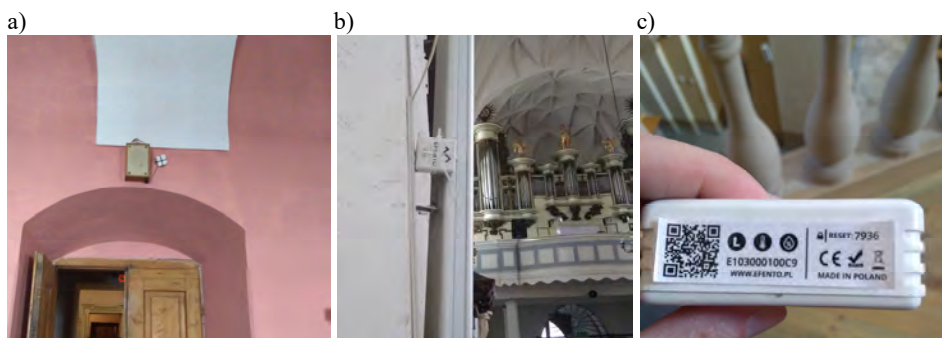


Fig. 4. Mounted sensors for measuring the temperature and humidity of the interior air a) in a church in Wigry over the entrance b) in the St. Andrew the Apostle's church in Barczewo c) in St. Anna's church in Barczewo d) general view of the mounted sensors

The recorders were mounted on 7.01.2018 in the church in Wigry and on 9.03.2018 in both churches located in Barczewo. In the St. Andrew the Apostle's church, 3 sensors were mounted, in the side nave, in the main nave and at the matroneum.

Apart from continuous measurements of the microclimate, once a month measurements of wall dampness are performed using the PWM – 3 hygrometer. This gauge is used to investigate the mass dampness levels of construction elements via the measurements of the difference in electrical capacitance of the condenser built out of a measurement electrode and the examined element; depending on its water content. The range of the gauge is 0÷25% with the margin of error at 0.5%.

Dampness measurements are carried out at the floor level, for all objects, and at the level of 1.2 m and 1.8 m. The values recorded in measurement points in the selected points are compiled in table 2.

In order to interpret the measurement results, a table specifying the level of mass dampness of walls made of ceramic bricks (Table 1).

Table 1. Recommended level of wall dampness by [5]

Dampness level	Mass dampness [%]	Wall
I	0÷4	of acceptable dampness
II	4÷5	of elevated dampness
III	5÷8	medium damp
IV	8÷12	highly damp
V	>12	wet

Sorption dampness of a full brick in room temperature should not exceed 4% of the material mass value [8].

4. Results and analysis

The results of wall dampness measurements for the selected churches are compiled in table 2.

The results of the air temperature and humidity measurements between 07.01.2018 and 09.03.2018 from the church in Wigry, the St. Andrew the Apostle's church in Barczewo and St. Anna's church, also in Barczewo, are shown in graphs (fig. 5a–d).

Table 2. The results of wall dampness between 07.01.2018 and 09.03.2018 for the church under the invocation of St. Mary's Immaculate Conception – Wigry and between 09.03.2018 and 09.04.2018 for St Andrew the Apostle's church in Barczewo (1) and St. Anna's church in Barczewo (2)

Measurement date	Location	Mass dampness [%] (level of wall dampness)		
		at floor level	at 1.20 m	at 1.80 m
07.01. – Wigry	Wigry	17% (wet)	17% (wet)	15% (wet)
09.02. – Wigry	Wigry	18% (wet)	17% (wet)	16% (wet)
09.02. – Barczewo	Barczewo (1)	22% (wet)	19% (wet)	16% (wet)
	Barczewo (1)	22% (wet)	18% (wet)	17% (wet)
09.03. – Barczewo	Barczewo (2)	19% (wet)	18% (wet)	16% (wet)
	Barczewo (2)	18% (wet)	17% (wet)	16% (wet)

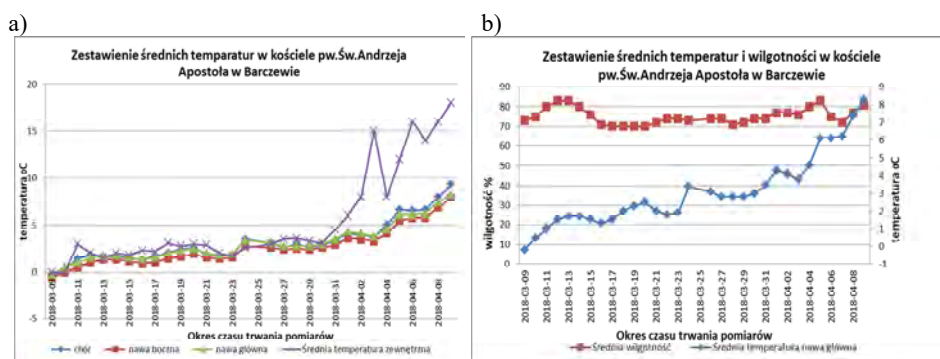


Fig. 5. Temperature and dampness levels as a function of time; 5a) levels of interior air temperature in 3 measurement points + the temperature of exterior air, 5b) temperatures and humidity of interior air – Barczewo (1)

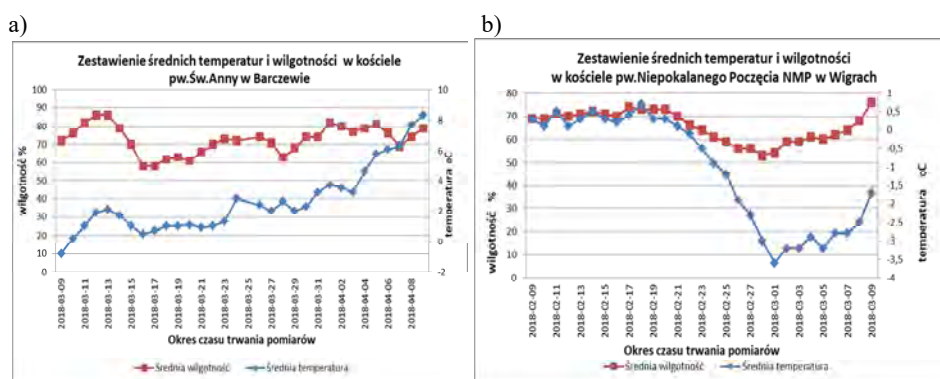


Fig. 6. Temperature and dampness levels as a function of time) a) temperatures and humidity of interior air - Barczewo (2) b) temperatures and humidity of interior air – Wigry

4.1. Results analysis

Diagrams of air temperature and humidity values included in fig. 5–6 pertain to 3 churches (Wigry and 2 Barczewo churches). In order to determine whether the location of gauge placement in the building had influence on the levels of temperature and humidity (fig. 5a), the gauges in St. Andrew the Apostle's church were located in the side-nave and at the matroneum. It turned out that the differences in temperature values are insignificant and amount to between 0.8°C and 1.5°C. The highest temperatures were recorded at the matroneum but a significant influence of the exterior temperature on the interior temperatures.

Measurements from both Barczewo churches were included for the period of 9.03.2018 and 8.04.2018. Diagrams 5b and 6c show the dependence of the relative air humidity on interior air temperature in Barczewo churches. Due to low temperature fluctuations (max. 3°C) in the period of 15.03 and 4.04. the air humidity values were also not significantly different and remained at the level of ~70% in St. Andrew the Apostle's church and in St. Anna's church between 60% and 70%. Noticeable differences in humidity occurred in the first week of measurements and in the last couple of days, where the exterior air temperature has increased significantly. In the Wigry church, measurement results were included for the period between 9.02. and 9.03.2018, which causes the distribution of temperature and humidity values to be significantly different (fig. 6d). A conspicuous dependence of interior air humidity on temperature was observed. It was also noticed that the decrease in interior air temperature happened when interior air temperature was negative. Despite the interior temperatures in St. Anna's church being relatively stable, a noticeable spike of ~ 30% in relative air humidity values within a few days was noticed. This phenomenon poses a challenge to be interpreted (fig. 5a). Based on wall dampness results, it was concluded that in all the analyzed cases, the walls are wet within their entire measured height (from 0.2 m to 1.80 m). The dampness of walls exceeded the allowed value of 4% and was recorded at between 17% and 22%.

5. Summary and conclusions

The analysis presented initial results of microclimate measurements from the interior of 3 building of historical value (a Wigry church and two Barczewo churches) and the results of wall dampness measurements.

For the purpose of wall dampness analysis, a theory of heat and humidity flow, presented in p.2.1 i 2.2 was used, as well as the results obtained during the microclimate and partition dampness measurements.

Based on the analysis of the obtained data (measurement results), it can be concluded that:

- 24h temperature fluctuations on days when service is being held exceed the recommended value of 1°C and are above 2.0°C, and relative air humidity

- increases by 6÷7% with the recommended value being 5%. Such a state can be the cause for the excessive humidity being precipitated out of the air on cold walls, windows, stained glass and the floor.
- Wall dampness level measurements indicate that they are wet and exceed by over 4 times the recommended value of up to 4%.
 - It is difficult to conclude, based on the analysis of wall dampness from one month only, whether the influence of the environmental microclimate has a significant impact on wall dampness levels. The results from 1 month (March), where their differences amounted to 1% indicate that in the winter (February – March) this impact was insignificant.
 - The correct interpretation of these results can take place after the analysis of phenomena recorded at least after a 1-year cycle.
 - Such analysis will allow us to notice how the cycle of building dampness in the summer and winter periods occurs and how construction partitions behave and how the microclimate which can be significantly influenced by exterior temperature, rainfall, atmospheric pressure, insolation or wind is structured.
 - In the analyzed objects, especially on St Andrew the Apostle's church in Barczewo, with walls being wet to such an extreme degree, (22% on the floor level and between 17% and 18% at 1.80 m) the analyzed walls should be without a doubt subject to dynamic drying, using the most efficient drying method.
 - It has to be taken into consideration, however, that the protection of the analyzed objects against the damaging influence of dampness and adverse influence of the environment can pose a significant challenge and would require an in-depth analysis of the phenomenon.

References

- [1] Borusewicz W.: Konserwacja zabytków budownictwa murowanego, Arkady, Warszawa 1971.
- [2] Klem P.: Budownictwo ogólne T 2 Fizyka Budowli, Arkady, Warszawa 2001.
- [3] Kubik J.: Fizyka budowli zabytkowych, Opole 2013 (na prawach rękopisu).
- [4] Pogorzelski J A.: Fizyka cieplna budowli, PWN, Warszawa 1976.
- [5] Trochonowicz M. : Budownictwo i Architektura 7 (2010).
- [6] Wesołowska M.: Ochrona murów licowych przed wpływem środowiska. Wydawnictwo Uczelniane UTP w Bydgoszczy, 2016.
- [7] Wyrwał J.: Ruch wilgoci w porowatych materiałach i przegrodach budowlanych. Wydawnictwo WSI, Studia i Monografie z.31, Opole 1989.
- [8] Instrukcja WTA. Merkblatt 2-9-04/D Sanierputzsystem, Neues WTA-Merkblatt Sanierputzsysteme 2-9-04/D, 2006.

Przesłano do redakcji: 28.03.2018 r.

Przyjęto do druku: 31.03.2018 r.

Informacje dodatkowe

1. Lista recenzentów współpracujących będzie opublikowana w czwartym numerze *Czasopisma Inżynierii Lądowej, Środowiska i Architektury*: 64(4/18) oraz na stronie internetowej:
www.oficyna.prz.edu.pl/pl/zeszyty-naukowe/czasopismo-inzynierii-ladowej-s/
(dotychczasowa nazwa: *Zeszyty Naukowe Politechniki Rzeszowskiej, Budownictwo i Inżynieria Środowiska*), strona internetowa:
www.oficyna.prz.edu.pl/pl/zeszyty-naukowe/budownictwo-i/
2. Zasady recenzowania są udostępnione na stronie internetowej:
www.oficyna.prz.edu.pl/zasady-recenzowania/
3. Informacje dla autorów artykułów są udostępnione na stronie internetowej:
[oficyna.prz.edu.pl/informacje-dla-autorów/](http://oficyna.prz.edu.pl/informacje-dla-autorow/)
4. Formularz recenzji jest udostępniony na stronie internetowej:
www.oficyna.prz.edu.pl/pl/zeszyty-naukowe/czasopismo-inzynierii-ladowej-s/
5. Instrukcja dla autorów omawiająca szczegółowo strukturę artykułu, jego układ, sposób przygotowywania materiału ilustracyjnego i piśmiennictwa jest zamieszczona na stronie internetowej:
[www.oficyna.prz.edu.pl/pl/instrukcja-dla-autorów/](http://www.oficyna.prz.edu.pl/pl/instrukcja-dla-autorow/)
oraz
www.oficyna.prz.edu.pl/pl/zeszyty-naukowe/czasopismo-inzynierii-ladowej-s/ w zakładce „Instrukcja dla autorów”
6. Dane kontaktowe do redakcji czasopisma, adresy pocztowe i e-mail do przesyłania artykułów oraz dane kontaktowe do wydawcy są podane na stronie internetowej (Komitet Redakcyjny):
www.oficyna.prz.edu.pl/pl/zeszyty-naukowe/czasopismo-inzynierii-ladowej-s/

Zasady recenzowania, informacje dla autorów, formularz recenzji, instrukcja dla autorów i dane kontaktowe do redakcji czasopisma i wydawcy będą również opublikowane w czwartym numerze *Czasopisma Inżynierii Lądowej, Środowiska i Architektury*, z. 65 (4/2018).

Ark. wyd. 10,5. Ark. druk. 11,25.

Oddano do druku w czerwcu 2018 r. Wydrukowano w czerwcu 2018 r.

Zakład Poligrafii Politechniki Rzeszowskiej, al. Powstańców Warszawy 12, 35-959 Rzeszów
Zam. nr 89/18